25

HAMBURGER WASSERBAU-SCHRIFTEN

Herausgegeben von Prof. Dr.-Ing. Peter Fröhle

2023

Robert Lepper

A contribution to understanding the recently enhanced coastal siltation in the German Wadden Sea

WASSERBAU
River and Coastal Engineering

A CONTRIBUTION TO UNDERSTANDING THE RECENTLY ENHANCED COASTAL SILTATION IN THE GERMAN WADDEN SEA

Vom Promotionsausschuss der
Technischen Universität Hamburg

zur Erlangung des akademischen Grades

Doktor-Ingenieur

genehmigte Dissertation

von
Robert Lepper (geb. Hagen)

aus
Wolfsburg

2023

Gutachter: Prof. Dr.-Ing. Peter Fröhle
Prof. Dr. rer. nat. Christian Winter
Dr. rer. nat. Frank Kösters
Tag der mündlichen Prüfung: 10. August 2023

DOI https://doi.org/10.15480/882.8712

ORCID Robert Lepper (https://orcid.org/0000-0002-8446-2004)

SUMMARY

The German Wadden Sea on the Northwestern European Shelf is world's largest channel-shoal system that comprises broad coherent intertidal flats, islands, shoals, and several estuaries. Coastal management (e.g., land reclamation, diking, channel closure, coastal construction, or channel deepening) has shaped the German Wadden Sea's coastline and its estuaries for centuries. As a consequence, navigational channel dredging and coastline maintenance have become routine coastal engineering tasks. Since the 2010s, German coastal stakeholders reported further enhanced coastal siltation which resulted in increased dredging efforts, muddy recreational areas, or habitat loss. The scope of this dissertation was therefore to (1) scientifically quantify changes in coastal siltation and to (2) investigate the evolution of driving mechanisms. The overarching objective was to assess to what extent and why enhanced coastal siltation occurred at the study site during a chosen recent study period of 1996 to 2016.

I deployed a baroclinic numerical model of the North Sea to assess changes in the German Wadden Sea during this period. A novel data aggregation approach was developed to translate these extensive modeling data into representative samples for trend assessment. These processed data were then merged with bathymetry and surface sediment data to estimate the observed evolution of area, height, water volume, and sediment volume in the subtidal and intertidal zones.

The bathymetry data analysis revealed notable lateral intertidal expansion and vertical accretion at the cost of a retreating and deepening subtidal zone. The respective sediment and water volumes confirmed this observation. Interestingly, the total coastal (i.e., subtidal and intertidal) sediment volume was mostly balanced with few exceptions; hence, local sediment redistribution from the subtidal to the adjacent intertidal zone was likely dominant over sediment import. Decadal surface sediment distributions furthermore suggested that the coverage of mudflats in the southern and southeastern German Bight increased gradually.

Research on the accretion of sediments in the coastal zone emphasizes the dynamical equilibrium concept which was followed closely in this dissertation. Equilibrium may be assumed whenever the transverse profile of a channel-shoal environment remains more or less constant on morphological time scales. As this was not the case at the study site, changes in the tidal and non-tidal drivers affecting the dynamical equilibrium were investigated. Results were ambiguous at first because no noteworthy changes in non-tidal forcing aside from minor sea level rise and more frequent landward-facing waves were found. There were, however, changes in tidal forcing. Significant trends in principle and shallow water tidal constituent's amplitude and phase were found in modeled and observational data. This development resulted in an overall increase in tidal range by several $mm\ yr^{-1}$, declining tidal duration and flow velocity flood dominance, and increasing flood and ebb slack duration. Local changes in tidal asymmetry were found to be correlated with subtidal deepening and increasing relative intertidal storage.

In conclusion, reports about enhanced coastal siltation were considered plausible as recent

bathymetry evolution and an increasing mudflat coverage were found. Changes in tidal forcing and asymmetry initially suggested that the sediment import into the coastal zone should be hampered which is counterintuitive considering the observed bathymetric development. An increase in mean flood and ebb slack duration could, however, enhance the deposition of fine material which would fit the scope of coastal siltation. Furthermore, reduced tidal and wave energy from broader, higher tidal flats is reasonable to suspect which should also facilitate more sediment deposition. I hypothesized that observed bathymetry evolution resulted from a morphological disequilibrium that was initiated by sea level rise. Future research was recommended on the interaction of sea level rise, bathymetry changes, tidal dynamics, and sediment transport.

Abstract

The Wadden Sea on the Northwestern European Shelf is world's largest channel-shoal system that comprises broad coherent intertidal flats, islands, shoals, and several estuaries. Coastal management has shaped the Wadden Sea's coastline and its estuaries for centuries which is why navigational channel dredging and coastline maintenance have become routine coastal engineering tasks. Since the 2010s, German coastal stakeholders reported further enhanced coastal siltation. My research objectives were (1) to identify whether there was quantifiable evidence of enhanced coastal siltation and (2) to find the driving processes behind this development. An analysis of bathymetry data confirmed that intertidal flats accreted and that lateral expansion and subtidal deepening occurred. Balanced subtidal and intertidal sediment budgets suggested a redistribution of local subtidal sediments to intertidal flats. In addition, surface sediment data indicated a gradually increasing mudflat coverage over time. Based on this information, numerical modeling and observational data were used to quantify changes in tidal and non-tidal forcing: I found near-constant wind-wave and storm surge conditions which indicated that event-driven phenomena were an unlikely driver. Spatial tidal analysis and observational data revealed amplitude and phase shifts of principle and shallow water tidal constituents which reflected in increased tidal amplitude, and reduced flood dominance. Furthermore, diminishing flood flow velocity and increased slack duration were noted. These phenomena were related to increased relative intertidal storage and to subtidal deepening from bathymetry evolution. Hence, the reduction in channel volume and the intertidal accretion likely decreased tidal and wave energy on the tidal flats and enabled the deposition of more fines. Longer flood and ebb slack duration should add to this effect. The import of sand into the coastal zone was likely reduced as flood dominance diminished at the entire study site.

Acknowledgement

I am deeply grateful for the outstanding professional, personal, and generous financial support of the Federal Waterways Engineering and Research Institute, Germany (BAW) and of the Hamburg University of Technology (TUHH) that made this dissertation possible. First and foremost, I want to acknowledge my mentor and friend Dr. Andreas Plüß who has sparked my interest in the North Sea with countless technical discussions and who has always provided the encouragement I needed. I am equally grateful to Dr. Frank Kösters for always granting exceptional technical and professional advice and for never failing to identify logical gaps in my argumentation. Same goes for Prof. Dr. Peter Fröhle who patiently helped me numerous times to (re-) design this dissertation's guiding theme and for motivating me to think outside of the box. I furthermore appreciate the time, thought, and feedback every co-author invested to improve my manuscripts. All of you have made important contributions and taught me to view my work from different perspectives. Another great acknowledgment goes to the PROGHOME department at BAW for always providing excellent, sophisticated, and professional software solutions. My modeling effort would not have been possible without your support. Finally, I must express my deepest gratitude for the exceptional support of my parents Gudrun Hagen and Dr. Sebastian Groth, their spouses, and my wife Mira Lepper. You were always at my side and I would not have succeeded without you and your encouragement. Thank you.

CONTENTS

List of Figures

List of Tables

ABBREVATIONS

AufMod	Aufbau eines Modellierungssystems zur Morphodynamik in der Deutschen Bucht (in German)
ALS	airborne laser scanning
BAW	Federal Waterways Engineering and Research Institute, Germany
BODC	British Oceanographic Data Centre
BSH	German Federal Maritime and Hydrographic Agency
COSMO	consortium for small-scale modeling
EasyGSH-DB	Erstellung anwendungsorientierter synoptischer Referenzdaten zur Geomorphologie, Sedimentologie und Hydrodynamik in der Deutschen Bucht (in German)
FDA	flow duration asymmetry
FES	finite element solution
FVA	flow velocity asymmetry
HN-Model	hydrodynamic, numerical model
HW	high water
IPCC	intergovernmental panel on climate change
LW	low water
MAE	mean absolute error
ME	mean error
MSL	mean sea level
MUA	morphological unit averaging approach
NHN	«Normalhöhennull» i.e., German chart datum
SLR	mean sea level rise
RMSE	root mean square error
SHOM	Service Hydrographique et Océanographique de la Marine (in French)
SPM	suspended particulate matter
SpHW	spring tide high water
SpLW	spring tide low water
SSC	suspended sediment concentration
SSH	sea surface height
TDA	tidal duration asymmetry
T_E	ebb duration
T_e	ebb current duration
T_F	flood duration
T_f	flood current duration
T_T	tide duration
T_t	tide current duration
TUHH	Hamburg University of Technology

UKHO	United Kingdom Hydrographic Office
UNESCO	United Nations Educational, Scientific and Cultural Organization
UnTRIM	unstructured, tidal, residual, intertidal, mudflat model
UnK	unstructured k-model
WI	water-injection dredging
WSV	German federal water and shipping administration

CHAPTER 1
INTRODUCTION

CONTENTS

1.1 Motivation and Relevance

In theory, constant sediment supply under stationary tidal and wave forcing in the absence of river runoff would result in a near constant morphology over time so that no artificial sediment management would be required whatsoever. This state is defined by the *dynamical equilibrium* concept whereby sediment import and export remain more or less constant over time (Pritchard and Hogg, 2003). However, such conditions are rarely found at coastlines in the 21^{st} century as changes in forcing (e.g., climate change or mean sea level rise), on the one hand, and coastline management, on the other hand, are constantly affecting the morphology. The drawbacks of artificial coastal and estuarine management, e.g., by channel deepening, channel closure, channel straightening, land reclamation, sand mining, or construction, are increased sediment import through tidal pumping, channel and tidal flat siltation, or local and remote scour. The unrelenting threat of mean sea level rise (SLR) is likely to amplify such unfavorable phenomena as a higher mean sea level (MSL) must ultimately be compensated by sediment redistribution and import (Khojasteh et al., 2021).

The coastline along the southern North Sea on the Northwestern European Continental Shelf is not only an area of economic activity, harbors, and offshore wind farms but also a site with strict coastal protection measures. The Dutch, German, and Danish coasts are connected by the world's largest coherent tidal flat system, i.e., the Wadden Sea, which extend over more than 450 km in length and covers 11,000 km^2. The Wadden Sea comprises a large variety of landscapes such as broad tidal flats, offshore shoals, barrier islands, islands, estuaries, and branched tidal channels with shallow embankments. Its unique biodiversity and unspoiled intertidal flats have been protected as UNESCO world heritage site since 2009 regardless of heavy coastline modification.

Although most areas in the Wadden Sea remain natural, maintenance of navigational channels and shipping routes near large ports, e.g., the German port of Hamburg, increases. German port authorities and coastal stakeholders reported further enhanced channel and harbor siltation since the 2010s. This claim reflected in dredging volume records of German estuaries that attained record levels in the 21^{st} century (Table 1.1 and Figure 1.1). Arguably, major deepening projects in the Weser and Elbe estuaries in the period of 2007 to 2017 contributed to the observed increase and the linear growth will be limited by sediment availability in the future. It should also be noted that dredged sediment cannot be removed entirely when convenient dumping sites within or in the mouth of the estuaries are used.

Nevertheless, the dredged hopper volume increased by more than 50 % in the Jade and Weser estuaries and by approximately 10 % in the Elbe estuary in the period of 2000 to 2018. Even higher increase rates were recorded for water-injection dredging (WI) with increases in the Jade, in the Weser (each more than 75 %), and in the Elbe estuary (15 %). Reports about

TABLE 1.1: Dredged sediment volume from all German estuaries in the year 2018

	Outer Ems in 10^6 m^3	Jade in 10^6 m^3	Weser in 10^6 m^3	Elbe in 10^6 m^3
Hopper	5.9	5.3	7.5	14.1
WI	–	0.17	1.7	1.5

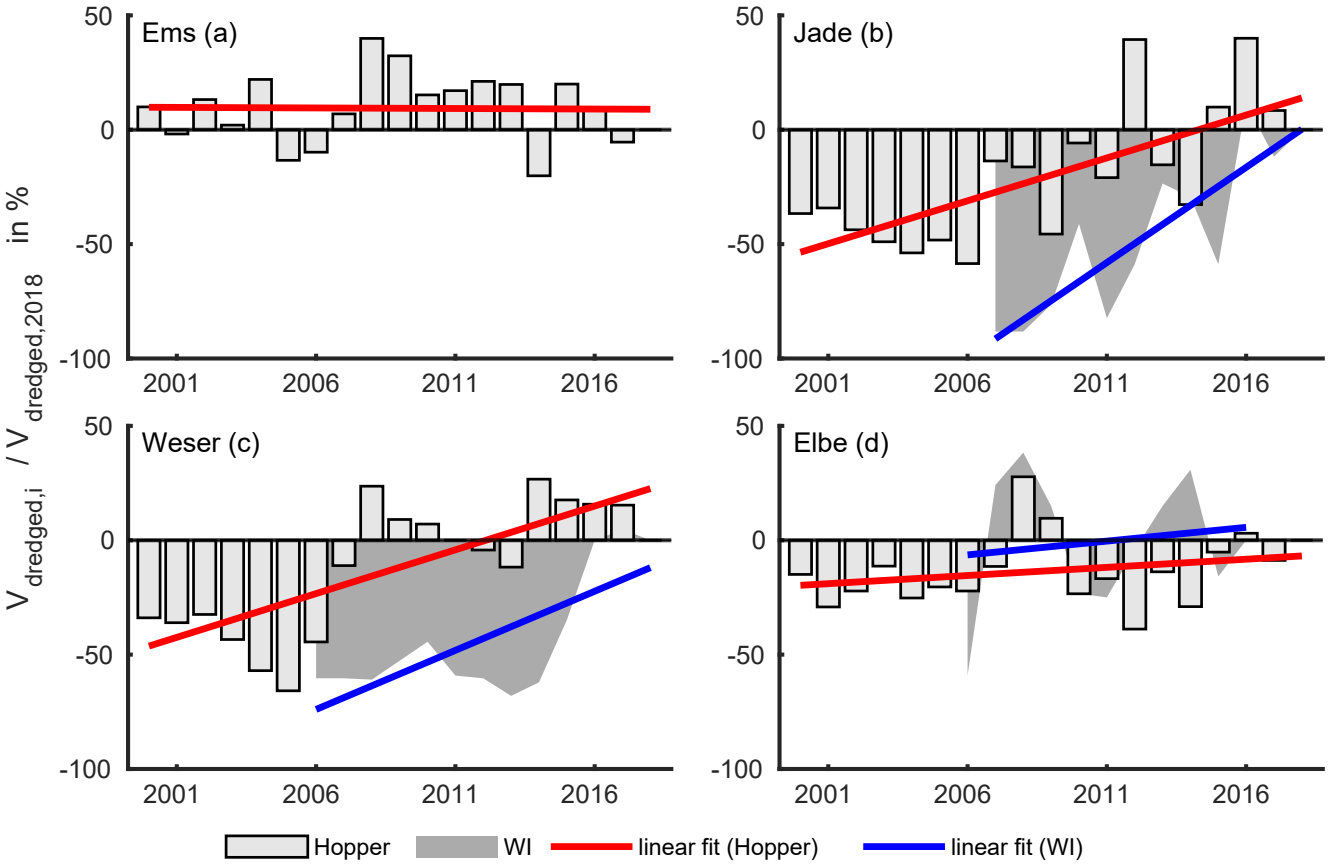

FIGURE 1.1: The evolution of the normalized dredged sediment volume in the Ems (a), Jade (b), Weser (c), and Elbe (d) fairways in the period of 1996 to 2018. The annual volume was normalized by the dredged volume of the year 2018.

enhanced navigational channel siltation hence seem reasonable at first glance although no scientific quantification was conducted, yet. The unknown implications of climate change, «likely» mean sea level rise (SLR) of 0.43 *m* to 0.84 *m* by the year 2100 relative to the period of 1986 to 2005 (Oppenheimer et al., 2019), the increasing demand for green energy, and the unremitting desire for economic growth will intensify the need for efficient and sustainable sediment management strategies in the future. This requires a better understanding of drivers and effects at the study site.

1.2 Research Objective

Local port authorities and coastal stakeholders reported intensifying channel and harbor siltation in the German Bight since the 2010s. Dredging records (Figure 1.1) in the fairways of Jade, Weser, and Elbe support their claims at first glance.
Consequently, my main research objectives are (1) to quantify recent coastal (subtidal and intertidal) sediment accretion, (2) to identify changes in the drivers for coastal siltation, and (3) to analyze recent changes in morphology, tidal forcing, and non-tidal forcing (effects) connected to enhanced coastal siltation in the German Bight.

1.3 Research Questions

(1) Is there evidence of enhanced coastal siltation in the period of 1996 to 2016?

(2) What are the forcing change(s) that facilitated enhanced coastal siltation?

1.4 Thesis Structure

After a brief introduction to the study site in Section 1.5, I conduct a literature review in Chapter 2 on the drivers of intertidal siltation (Section 2.1) before focusing on recent changes in morphology, sediment composition, and forcing (Section 2.2). Afterward, I outline the research gaps from my literature review in Section 2.3.
The theoretical thesis framework (Section 3.1) outlines in detail how I addressed these research gaps. Chapter 3 describes the data which I created to answer my research questions (Sections 3.2 to 3.3) followed by an introduction to the novel and established frameworks for tidal, morphology, and surface sediment analyses (Sections 3.4 to 3.9).
The first result chapter (Chapter 4) presents recent changes in coastal morphology (Section 4.2) and surface sediments (Section 4.3) to answer the first research question. The second result chapter (Chapter 5) explores the development of the non-tidal (Sections 5.2 to 5.3) and tidal forcing (Sections 5.4 to 5.5) with respect to the second research question.
Chapter 6 begins by revisiting the research questions in Section 6.1 before introducing and outlining the relevance of my results in a practical context (Section 6.2). A critical discussion of limitations and assumptions (Section 6.3) and an outlook to future research questions (Section 6.4) conclude the thesis.

1.5 Study Site Description

1.5.1 General Description

The North Sea is located in the North Atlantic Ocean on the Northwestern European Continental Shelf (Figure 1.3, top left). It is dominated by tidal and meteorological forcing from the North Atlantic Ocean and has micro to macro tidal range at a mean water depth of only 90 m (Quante and Colijn, 2016). The surface area covered by the North Sea was estimated at 575,300 km^2 and its water volume to 42,300 km^3 (Otto et al., 1990).
The coastal zones in the Dutch, German, and Danish administrative zones consist of coherent flat-channel systems, barrier islands, islands, shoals, and estuaries. This unique environment is commonly referred to as the «Wadden Sea» and was inscribed on the UNESCO world heritage list in 2009 for its ecological richness and natural dynamics. The Wadden Sea covers an area of 11,500 km^2, or a length of 450 km extending from the West Frisian barrier island Texel to the southwestern tip of Denmark near the island Fanø (Figure 1.3). The Dutch Wadden Sea (also West Frisia) extends from Texel in the central North Sea to the Ems estuary. Texel is bordered to the East by further barrier islands (Vlieland, Terschelling, Nes, and Schiermonnikoog) until the Ems estuary near the island Borkum. East Frisia inherits more barrier islands eastwards of Borkum (Juist, Baltrum, Norderney, Langeoog, Spiekeroog, and Wangerooge). The Jade estuary (until Jade Bay) is located east of the barrier island Wangerooge and west of the Weser

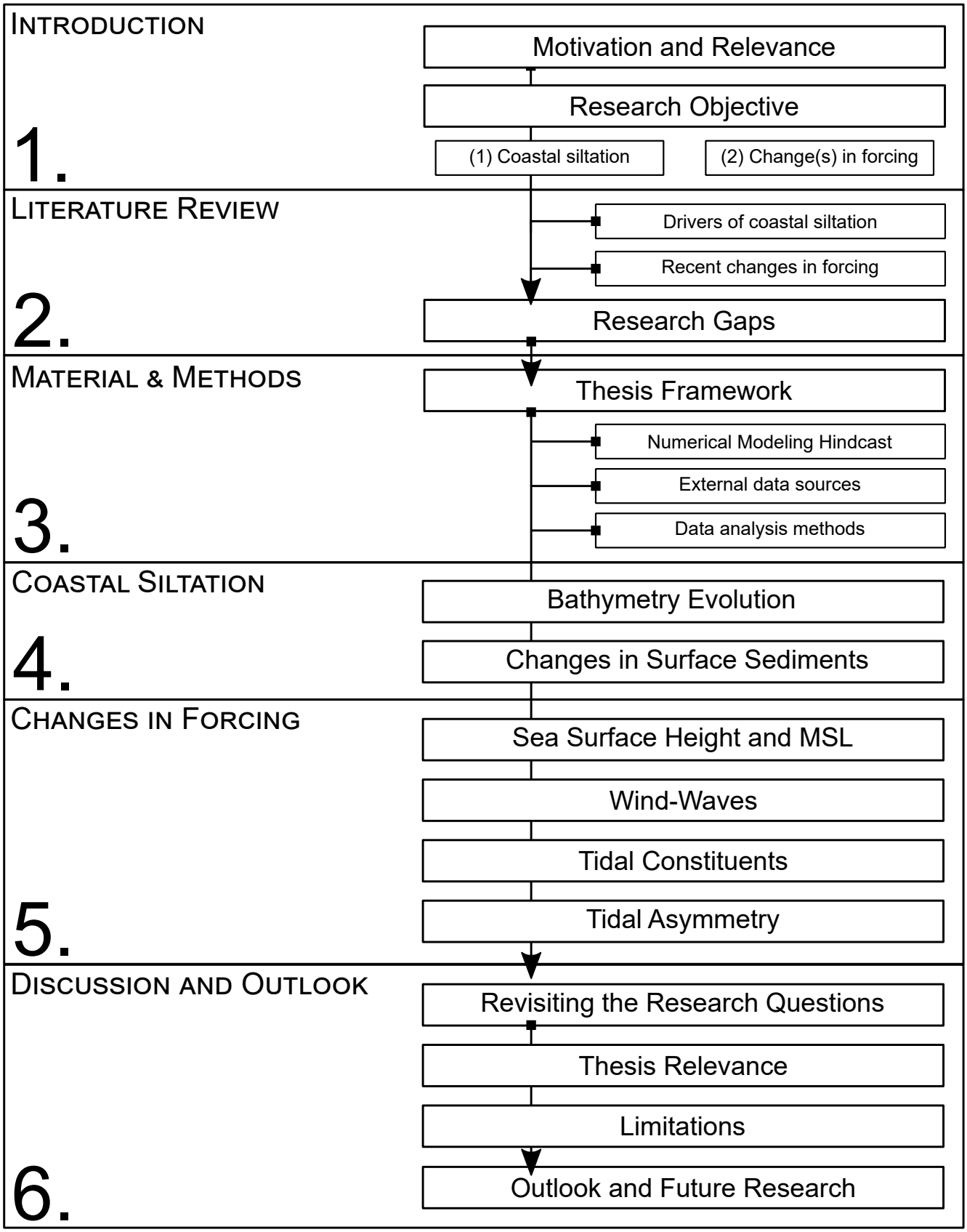

FIGURE 1.2: Thesis structure presented as flow chart.

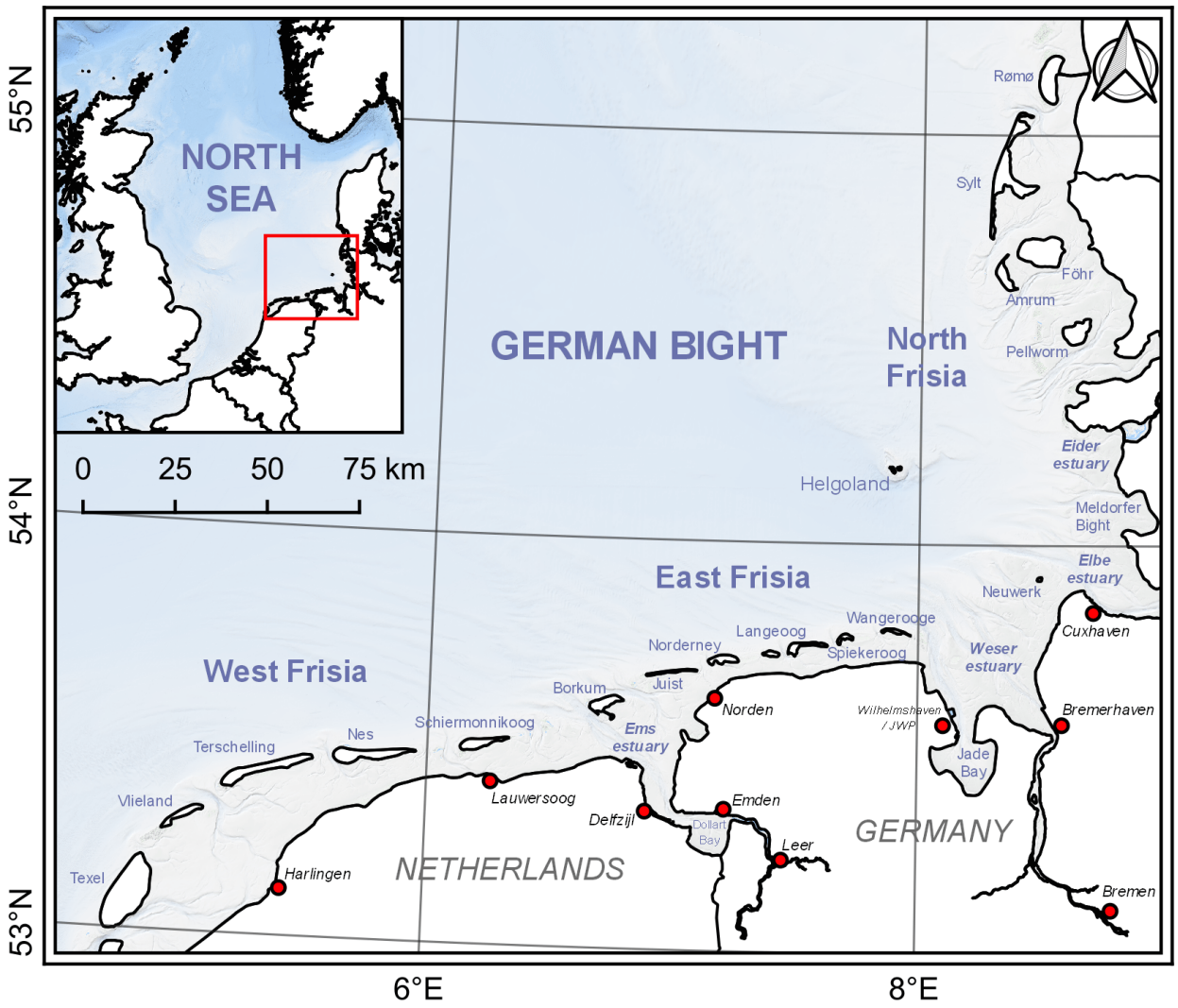

FIGURE 1.3: Map of the North Sea (top left), and the Wadden Sea area (right). Regional areas such as West Frisia, East Frisia, North Frisia, and the German Bight are highlighted as well as names of islands, rivers and main cities.

estuary. The Weser estuary connects the German Bight to the ports of Bremerhaven and Bremen and the northeastern adjacent Elbe river connects the port in Hamburg and the entrance to the «North Sea - Baltic Sea Channel» to the North Sea. North Frisia begins north of the Elbe estuary in the Meldorfer Bight near Büsum. The Eider estuary is situated north of the Meldorfer Bight and is protected by a tidal barrage. North Frisian barrier islands and islands (Pellworm, Langeness, Amrum, Föhr, and Sylt) extend into the Danish Wadden Sea with the islands Rømø and Fanø.

1.5.2 Forcing

Currents in the North Sea (long-term average: Figure 1.4) are subject to strong seasonal wind-driven and wave-driven variability (e.g., Stanev et al., 2019). Most of the water from the North

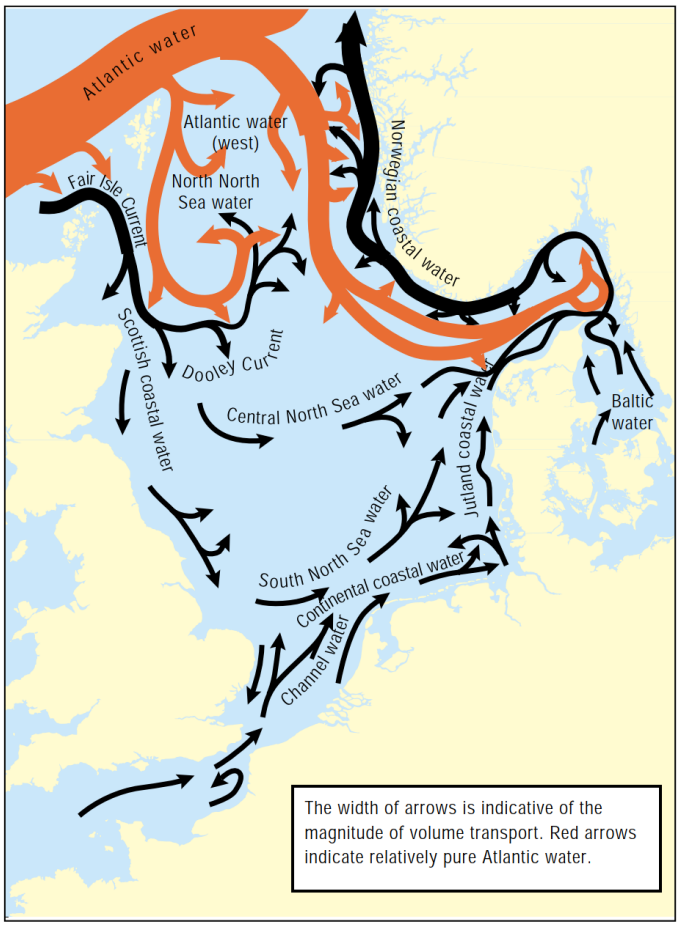

FIGURE 1.4: Water circulation in the North Sea from the North Atlantic near in Scotland and the English Channel towards Norway and the Baltic Sea (adapted from OSPAR Commission, 2000; Turrell, 1992).

Atlantic Ocean bypasses the North Sea to the Northeast. The flux from the North to the Wadden Sea results from the mixing of Scottish coastal and continental coastal water in the southern North Sea (Figure 1.4). From here, currents continue parallel to the Dutch and German coasts before approaching the Danish Coast. The hydrography in the Wadden Sea is therefore dominated by the interaction of counterclockwise rotating tidal currents from the North Atlantic. Tidal ranges in the southern North Sea vary between micro to macrotidal ranges with three M_2 amphidromes in Portsmouth (UK), the northern English Channel, and northwest of the German Bight (Otto et al., 1990). The annual freshwater discharge from all rivers was estimated within the range of 295 km^3 to 355 km^3 including melt water from Norway and Sweden (OSPAR Commission, 2000). Additional freshwater from the Baltic Sea outflow was determined at «around» $15,500\ m^3\ yr^{-1}$, i.e., 445 km^3 (Quante and Colijn, 2016). Waves in the southern North Sea occasionally reach a fully arisen sea state as wave build up in some areas is neither fetch nor wind limited. In the storm season from September to April, frequent strong west and east wind events cause severe storm surges. The latest, severe storm surges in the German Bight were *Tilo* in 2007 (also known as *Kyrill*), *Xaver* in 2013, and *Nadia* in 2022 which resulted in sea surface heights of 2.8 m, 3.1 m, and 2.8 m above mean high water. Sudden large-scale air pressure changes over the North European Shelf can furthermore trigger water level fluctuations (i.e., «external surge») of up to 1 m in the German Bight (Gönnert, 2003).

1.5.3 Bathymetry and Surface Sediments

Storm surges, tides, and waves have shaped the bathymetry and coastline of the German North Sea coast into a highly complex system of deep channels with steep slopes, intertidal flats, and shallow embankments. An example of the bathymetry in the German Bight (Figure 1.5) shows peak depths of more than 80 m at the northwestern tip. The German Wadden Sea coast can be distinguished between narrow channels in East Frisia and broad channels in North Frisia. North Frisia comprises complex tidal systems of barrier islands, dams, and islands while East Frisian inlets are classical shoal-channel-flat systems between barrier islands. Inlet systems are disrupted by estuaries which carve further broad and deep channels to the German North Sea coast.

The «Figge Map» from the early 1980s resulted from the first complete field campaign that mapped marine surface sediments in the German Bight (Figge et al., 1980). Further efforts were undertaken by Meyer and Ragutzki (1997) who classified the geology of intertidal flats in East Frisia until 1997 and published data on surface sediment distributions. They found that 81 % of the tidal flat area was predominantly sandy, 13 % was equally muddy and sandy (i.e., mixed flats), and 6 % was muddy (i.e., an area of roughly 1,400 km^2). The Dutch Wadden Sea is also dominated by fine to medium sands (Elias et al., 2012; Postma, 1981; Wang and Townend, 2012) with nearshore mud accumulation in shallow wave-sheltered areas.

The median grain diameter (i.e., d_{50}) distribution from the EasyGSH-DB data collection (Sievers et al., 2020b) synthesized existing surface sediment data (Figure 1.6). Fine to medium sands were estimated in the shoal and ebb delta area of the East Frisian barrier islands (c), coarse

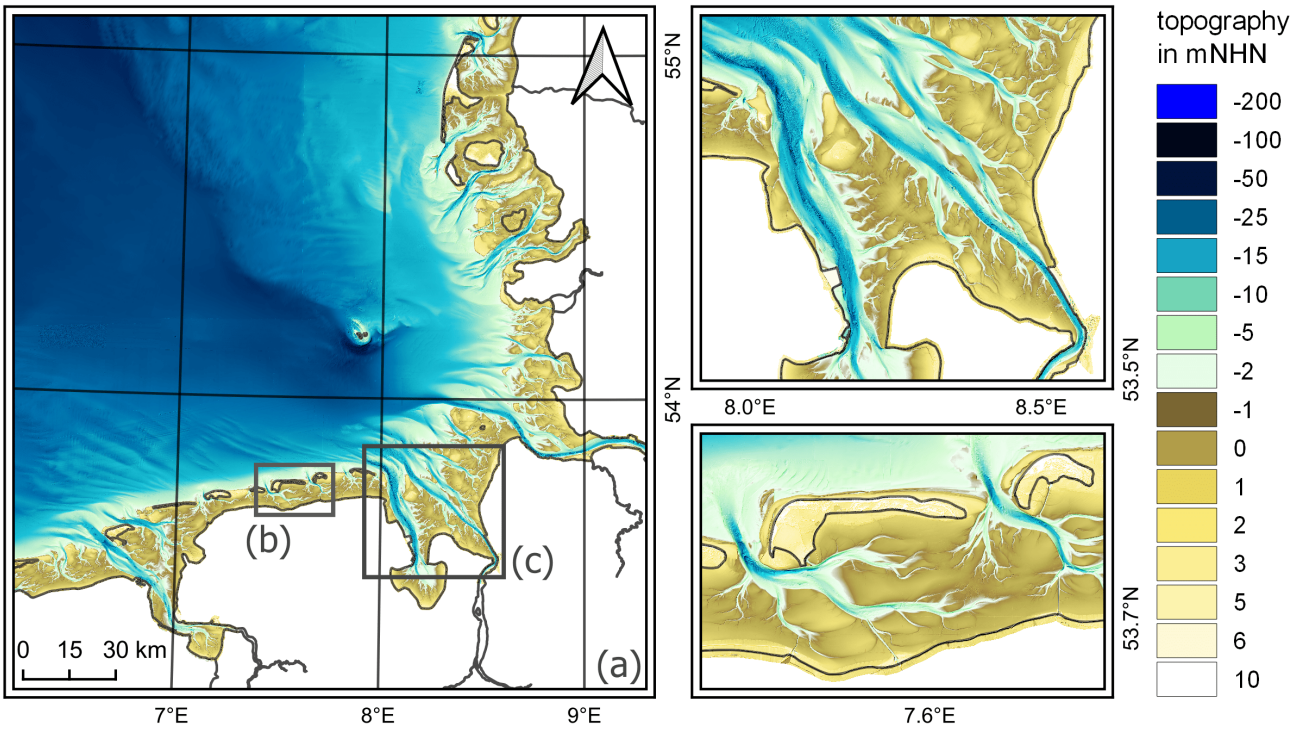

FIGURE 1.5: Topography of the German Bight (a), in the outer Weser estuary (b), and Spiekeroog / Wangerooge inlet (c) in the year 2015 from the EasyGSH-DB data collection (Sievers et al., 2020a).

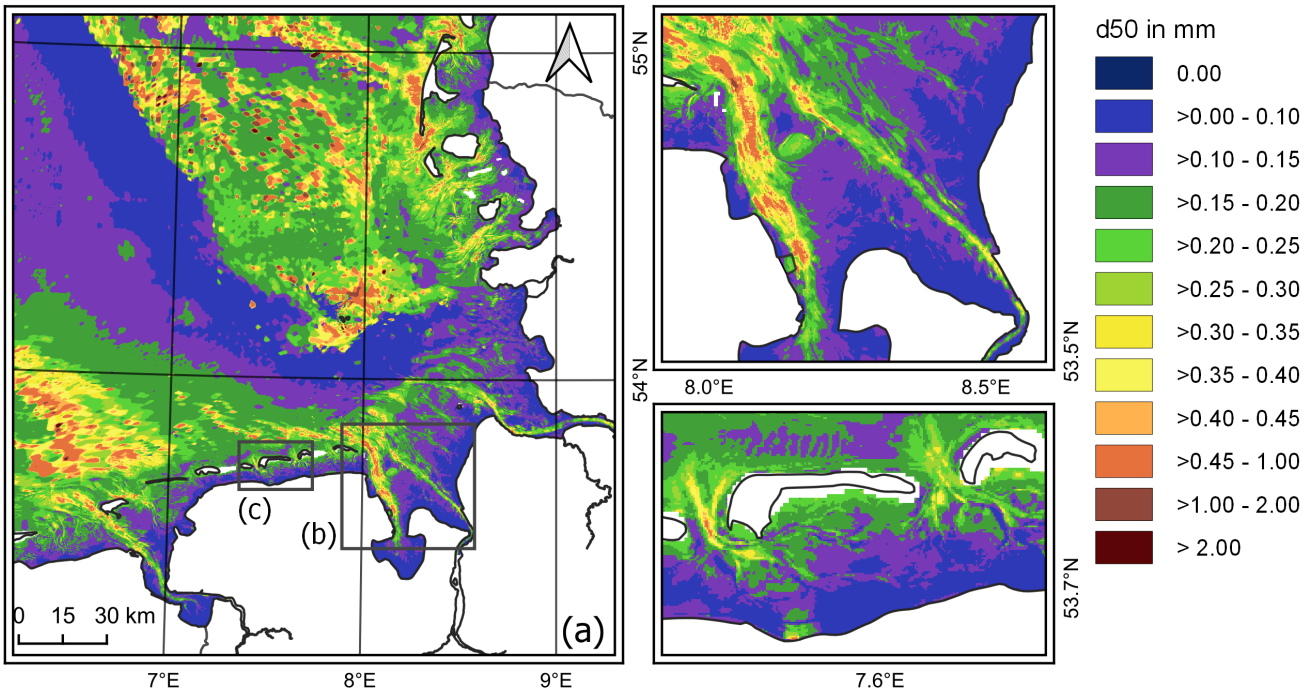

FIGURE 1.6: The median grain size diameter d_{50} in the German Bight (a), in the outer Weser estuary (b), and Spiekeroog / Wangerooge inlet (c) in the year 2016 from the EasyGSH-DB data collection (Sievers et al., 2020b).

to medium sands in tidal channels (a, b), and very fine, muddy sediments in shallow wave-sheltered areas of the Ems, East Frisia, the Jade, the outer Weser and Elbe, and in most parts of North Frisia (b, c).

CHAPTER 2
LITERATURE REVIEW

CONTENTS

2.1 The Drivers of Coastal Siltation

Tides and waves dominate suspended and bedload sediment transport in coastal waters. Wetting and drying of intertidal flats, storm surge activity, grain grain interaction, flocculation, hindered settling, turbulence damping through seasonal and haline stratification, limited sediment availability, biological potential, etc. further influence the erosion, settling, and transport behavior of sediments.
For all subsequent considerations, the term «siltation» refers to the accretion of cohesives and fine sands (i.e., «fines») in the coastal zone. The coastal zone is defined by the subtidal and intertidal zones until the -20 mNHN (German chart datum) height isobath. Mark that coastal siltation often coincides with the formation of mud which is a mixture of cohesives, organics, minerals, and water (Winterwerp et al., 2021).

2.1.1 Sediment Transport Processes

Tides and waves induce shear stress τ on the seabed. The shear stress magnitude depends on near-bed current velocity magnitude, wave height, wave period, and wave breaking considering the respective water depth. Most sediment transport formulae define a critical shear stress τ_{crit} to estimate the initiation of sediment movement (i.e., erosion). The eroded particle trajectory depends on grain properties (e.g., grain size, porosity, and density) as sediment can either be suspended into the water body (i.e., suspended or SPM-transport) or dragged along the sea floor (i.e., bedload transport). Most sand fractions are transported as bedload while fine to very fine sands and cohesive sediments ($d \leq 0.16\,mm$) suspend into the water body (van Rijn, 2007). A suspended sediment particle moves with the water body and its vertical displacement is determined by molecular diffusion and turbulent mixing. When the energy is insufficient to keep sediment particles in suspension, grains sink to the sea floor at a sinking velocity w_s. Numerous flume and laboratory experiments have shown that assuming a constant sinking velocity for sandy sediments is a reasonable simplification. In contrast, the cohesive sediment sinking velocity varies due to grain grain interaction and flocculation. High concentrations of cohesive particles can either accumulate near the seabed (hindered settling, lower w_s), interact at high concentrations to form fluid mud (Winterwerp et al., 2017), or aggregate in flocs in brackish water to increase their sinking velocity. The stability of flocs is closely linked to turbulence in the water body as high turbulence dissolves floc aggregates. Laboratory flume tests showed that cohesive sediments were deposited when τ_{crit} was below 0.1 N/m^2 to 0.2 N/m^2 and were eroded above 0.4 N/m^2 to 0.5 N/m^2 (Holt and James, 1999). There is evidence that a constant critical bed shear stress is oversimplified in the field, as e.g., consolidated beds require much higher bed shear stress for erosion (e.g., van Prooijen and Winterwerp, 2010).

2.1.2 The Dynamical Equilibrium Theory

The following section takes a deeper look at the interaction between morphodynamics, tides, and waves in coastal environments under infinite sediment availability and without river runoff. Tides generate low periodic magnitudes of bed shear stress during flood and ebb while waves induce large episodic magnitudes of bed shear stress. Shallow water effects weight the

tidal shear stress and advection towards flood or ebb (i.e., tidal asymmetry or tidal distortion). Friedrichs (2011) synthesis on mudflat morphodynamics incorporated these processes in the Eulerian and Lagrangian tidal asymmetry framework (based on the work of Pritchard, 2005; Ridderinkhof, 1997). The Eulerian frame of reference describes the ratio of flood- and ebb-related parameters of the tide at a location, e.g., a tidal gauge, while the Lagrangian framework outlines the equilibrium of wave and tide-induced energy in intertidal environments, e.g., a tidal basin. Eulerian tidal asymmetry descriptors can be applied as *indicators* for residual sediment transport in tidal systems (e.g., Dronkers, 1986) while Lagrangian asymmetry cannot be quantified directly. The dynamical equilibrium of an intertidal flat is reached when its trajectory «remains more or less constant over some characteristic period of natural forcing» (Friedrichs, 2011). Another definition stated that a system reaches its dynamical equilibrium if the balance between sediment import and export «in the order of decades or more» (Pritchard and Hogg, 2003) is nearly zero. In other words, stationary tide and wave forcing on morphologically relevant time scales eventually result in some form of steady state (for an overview see Friedrichs, 2011), provided that the system is not influenced artificially (e.g., by dredging), that river runoff is absent, and that sediment supply is infinite. The Wadden Sea, however, is a known sediment sink (Stive et al., 1990) and exhibits notable morphodynamic variability, both recently (Benninghoff and Winter, 2018, 2019) and in the past (Vos and Knol, 2015), which raises questions as to the existence of a dynamical equilibrium at the study site.

2.1.3 Lagrangian Tidal Asymmetry

An energy gradient between a tidal channel and an intertidal flat is a precondition for Lagrangian asymmetry (Friedrichs, 2011): If wave shear stress or a high flow velocity magnitude (high-energy) cause sediment erosion in a tidal channel, flood advection transports sediments landward to tidal flats where the particles settle as a result of the low energy environment (Figure 2.1, a). If the energy of the subsequent ebb is insufficient to resuspend the previously accommodated sediment (Figure 2.1, b) a residual landward transport occurs. High-energy events on intertidal flats (e.g., waves during storm surges) reverse this effect: The advection of the withdrawing water after a high-energy event then results in net seaward transport. Lagrangian asymmetry therefore always requires a spatial gradient in sediment concentration or energy in combination with sufficient tidal advection (Friedrichs, 2011). A common feature in natural tide-dominated flat-shoal environments is a decreasing median grain size diameter from the tidal channel towards the dike from decreasing levels of energy (Flemming and Nyandwi, 1994). This feature was observed in the Elbe estuary near Neuwerk (Reineck and Siefert, 1980) and Cuxhaven (Albers and von Lieberman, 2010), in the Dutch Wadden Sea (Janssen-Stelder, 2000; Postma, 1961), and in the Danish Wadden Sea (Madsen et al., 2010) among many others. Postma (1961) furthermore found in a variety of measurements in the Dutch Wadden Sea that Lagrangian driven sediment import affected fines only (64 μm to 128 μm).

Several authors distinguished Lagrangian asymmetry descriptors in settling or scour lags (Gatto et al., 2017; Postma, 1961; Pritchard and Hogg, 2003). For example: A suspended sediment fraction with a sinking velocity of 1 $mm\ s^{-1}$ sinks 3.6 m in one hour. If the flood slack period is extended by just 10 minutes, settling of 4.2 m occurs and the possible area for the accretion of fine sediments on the tidal flat would increase as a result assuming constant water depth (i.e.,

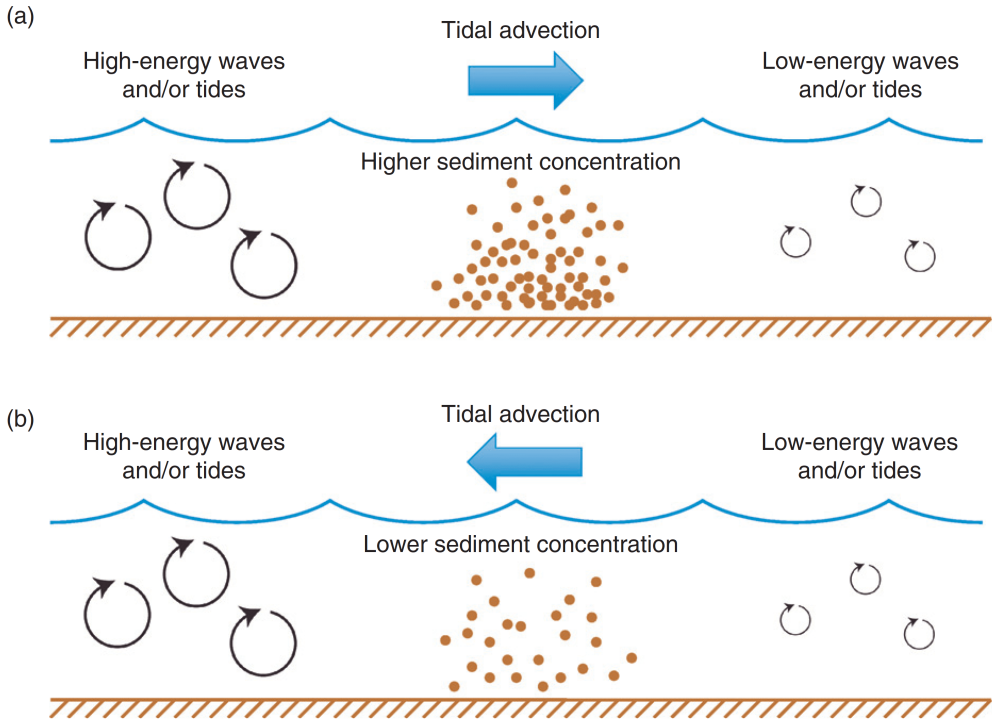

FIGURE 2.1: Calm-weather Lagrangian tidal asymmetry (adapted from Friedrichs, 2011) during flood (a) and ebb (b).

enhanced settling lag). Slack duration also determines the erosion threshold lag until erosion from the bed becomes possible (i.e., scour lag). Hence, longer slack periods lead to a longer residence time of sediments on the tidal flat and facilitate siltation.
Siltation from Lagrangian asymmetry thus depends on the (erosive) tidal or wave energy magnitude, slack water duration, and particle settling velocity (de Swart and Zimmerman, 2009; van Maren and Winterwerp, 2013). Lagrangian-induced net transport during calm-weather was related to the (Eulerian) peak velocity asymmetry (Postma, 1961), critical shear stress for erosion τ_{crit}, the sinking velocity of sediment particles (van Maren and Winterwerp, 2013), and the duration of slack water (Dronkers, 1986).

2.1.4 Eulerian Tidal Asymmetry

The flood and ebb properties of an ideal symmetric tide are equal. When symmetric tides enter shallow water, bed friction distorts the tidal signal and weights it towards flood or ebb. This is defined as Eulerian tidal asymmetry. The degree of tidal distortion depends on the amplitude of the incoming tidal signal, local and regional bathymetry (water depth), surge, spring-neap variability, and the interannual (Gräwe et al., 2014; Müller et al., 2014) and perennial (Pugh, 1987) modulation of tidal constituents. Systems are regarded as flood dominant if their flood duration (T_F) is shorter than their ebb duration (T_E) which usually results in higher flood than ebb flow velocity (Aubrey and Speer, 1985; Friedrichs and Aubrey, 1988; Speer and Aubrey, 1985). A greater flood than ebb current velocity also means that a system is flood dominant. Gong et al. (2016) defined the ratio of flood and ebb duration as tidal duration asymmetry (TDA), the ratio of flood and ebb slack duration as flow duration asymmetry (FDA) (also slack water asymmetry; Gatto et al., 2017), and the ratio between peak flood and peak ebb

flow velocity magnitude as flow velocity asymmetry (FVA). Dronkers (1986) hypothesized that the residual sediment flux of coarse sediments is limited by flow velocity magnitude (i.e., FVA) while fines are more dominated by the duration of flood and ebb slack (i.e., TDA & FDA) because of different sinking velocities and critical shear stress for erosion. Conceptual studies in a 2D depth-averaged model found that the Eulerian flow velocity asymmetry (FVA) is the dominant driver behind calm-weather intertidal sand accretion provided that critical shear stress for erosion and particle settling velocity are in a favorable range (van Maren and Winterwerp, 2013) which is in line with Dronkers (1986) ideas.
TDA and FVA can also be estimated by tidal constituent phase relations (e.g., $\theta(2M_2 - M_4)$) of the sea surface height (SSH) or current velocity in combination with relevant amplitude ratios such as M_4 to M_2 (Friedrichs and Aubrey, 1988). Other authors also defined other tidal constituent phase relations (for an overview see Guo et al., 2019) which may be more appropriate for tides along branched estuaries (Zhang et al., 2018). It is also possible to estimate Eulerian tidal asymmetry by evaluating the SSH or velocity distribution skewness (Nidzieko, 2010) to obtain a qualitative indication about flood or ebb dominance (Gong et al., 2016; Song et al., 2011). The drawback of this method is the lack of quantitative information about the described SSH or flow velocity signal.
Eulerian tidal asymmetry can furthermore be estimated by estuarine bathymetry, geometry, and tidal amplitude (i.e., stability criteria) based on continuity and momentum (for overview see Friedrichs, 2010). Flood and ebb dominance in shallow, convergent estuaries (comparable with short tidal channels with tidal flats) correlates with intertidal width changes $\Delta b/b$, intertidal storage V_s, and with the relative tidal amplitude expressed by the water depth ratio a/h. Systems with a large V_s are usually ebb dominant because the rising tide needs to overcome a higher frictional resistance than the falling tide. Without V_s, flow resistance during flood is low which favors flood dominance (Friedrichs and Aubrey, 1988; Pethick, 1980). Intertidal flats are always flood dominant as they are dry during ebb and inundated during flood. This inevitably favors sediment import (Friedrichs, 2010). A review of stability criteria criticized the sensitivity of the relative tidal amplitude a/h to the hydraulic depth h, their dependence on bathymetry data resolution and quality, the simplified theoretical background of the schematic channel cross section, and oversimplified 1D approaches (Zhou et al., 2018).

2.1.5 Calm vs. Rough Weather Conditions

The dynamical morphological equilibrium of the German Wadden Sea is determined by the balance of calm- (May to September) and rough-weather (October to April) conditions. Calm-weather spells can be characterized by low suspended sediment concentration (SSC) and sediment accommodation, while rough-weather spells enhance erosion and SSC in the coastal zone following the Lagrangian asymmetry framework (see Section 2.1.3). Several studies agreed that seasonal wave-induced coastal erosion and enhanced mixing contribute to an overall higher SSC in the entire southwestern North Sea in the rough-weather period (Dyer and Moffat, 1998; Fettweis and van den Eynde, 2003; Gayer et al., 2006; Stanev et al., 2009; Staneva et al., 2009). Low flow velocity, low river runoff, and less wave activity during calm-weather periods was found to promote flocculation of fines (Chang et al., 2006a,b).
Local studies confirmed these observations: A numerical modeling study on the short-term morphodynamics in the outer Weser indicated that sand transport on sheltered tidal flats and

channels was tide-dominated, while exposed tidal flats were wave-dominated (Herrling et al., 2017). Similar modeling studies also found that the morphology of outer sands, shoals, and tidal flats in the German Wadden Sea were mixed-energy or wave-dominated than that of the protected flats in the hinterland (Herrling and Winter, 2018; Kösters and Winter, 2014). Long-term bed level observations in the Dutch Scheldt estuary established that calm-weather accretion can be reversed or even permanently disrupted by storm surges (de Vet et al., 2020). Similar observations were made in the Elbe estuary where enhanced mud erosion was documented during onshore wind directions (Albers and von Lieberman, 2010; Reineck and Siefert, 1980). Another study in the Dutch Wadden Sea confirmed that the suspended sediment concentration on an intertidal flat was significantly higher during rough-weather than during calm-weather conditions (Janssen-Stelder, 2000). Yet another recent five-month measurement campaign in the Dutch Vlie basin found that wind speed and direction directly affected the suspended particulate matter (SPM) transport. The authors measured high SPM concentrations after a change in wind direction from calm conditions to moderate landward winds that exceeded concentrations during rough weather conditions. This phenomenon was related to the erosion of non-consolidated fine sediments on low-lying tidal flats (Colosimo et al., 2020). These results agree with a numerical modeling study that showed a dependency of the sediment flux through a tidal inlet on the wind direction in the Dutch Wadden Sea (Sassi et al., 2015). Ridderinkhof (1997) also found that net landwards transport was inverted at an offshore wind speed of approx. 10 $m\ s^{-1}$ in the Dutch-German Dollart bay.

2.1.6 Accommodation Space

On morphological timescales, land reclamation could still influence coastal siltation in the German Wadden Sea. Extensive diking and salt marsh draining in the Dollart bay (Ems estuary) always resulted in enhanced siltation of the salt marshes in front of the dikes (Vos and Knol, 2015). Whenever new areas were reclaimed, the marsh before a new dike silted up and ultimately transformed into a smaller salt marsh which reduced the available accumulation space permanently. Therefore, it cannot be ruled out that coastal siltation in response to past land reclamation is ongoing. A numerical modeling study in the Ems estuary demonstrated that the loss of depositional areas (i.e., the removal of SSC in the Dollart area) led to a 50 % increase in SSC in the Ems River (van Maren et al., 2016). In their discussion, the authors argued that a larger sediment sink in Dollart bay would have the same effect as sediment removal, ultimately reducing SSC, and possibly decreasing coastal siltation in Dollart bay, the Ems river, and adjacent tidal basins. Another study in the English Humber Estuary also linked «exceptionally high SSC concentrations» to land reclamation and artificial estuarine realignment (Morris and Mitchell, 2013).

2.1.7 Stratification

Thermal and haline stratification trap fine sediments in the coastal zone and estuaries (for an overview see Burchard et al., 2018). It is important to note that estuarine circulation and related processes were not addressed in this thesis for the sake of simplicity. Mesotidal range and frequent wave-stirring led me to neglect baroclinic aspects in the following. The detailed numerical modeling or extensive measurements that would be necessary to capture changes in

water column stratification and SSC sufficiently would have involved a disproportionate effort beyond the scope of this thesis. Nonetheless, I recognize that sediment trapping near the coast is correlated with water column stratification and deserves future research.

2.2 Recent Changes

Subsequent sections explore the documented recent changes in (1) morphology, (2) surface sediments, (3) non-tidal, and (4) tidal forcing in the German Wadden Sea with respect to the research questions.

2.2.1 Morphology and Surface Sediments

An analysis of the German Wadden Sea's geomorphology in the period of 1998 to 2016 showed a lateral intertidal expansion by up to 18 % and an increase in mean intertidal flat height with peak accretion in Jade Bay and the Weser estuary (Benninghoff and Winter, 2019, see Figure 2.2). A concurrent subtidal channel depth increase and a subtidal area decline implies

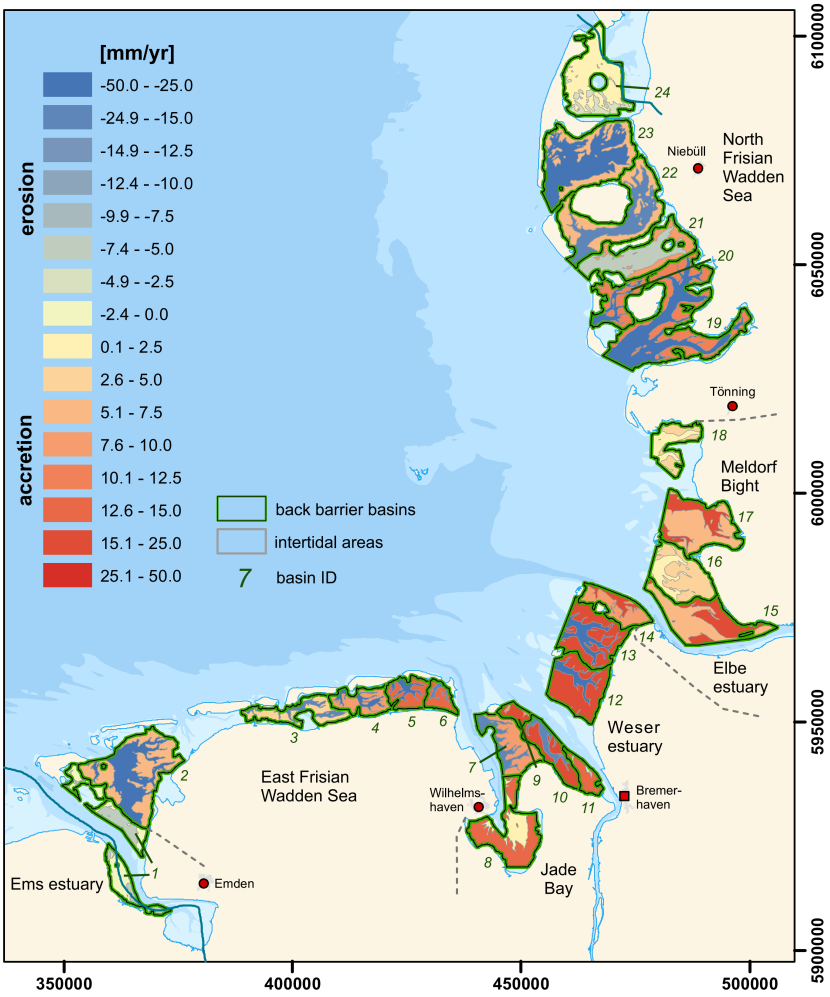

FIGURE 2.2: Annual height changes in the German Bight in the period of 1996 to 2016 (adapted from Benninghoff and Winter, 2019).

that tidal channels in the Wadden Sea have narrowed and deepened. A similar study confirmed vertical intertidal accretion and a subtidal deepening in the outer Weser (Benninghoff and Winter, 2018) although methodology and input data were near-identical in both studies. They emphasized low confidence in their bathymetry data and could not exclude implausible height jumps despite introducing a weighted regression approach based on data confidence in Benninghoff and Winter (2019) and excluding several areas from analysis. Therefore, further research on this subject using more plausible data is required. A similar development of intertidal bed levels was found in the Dutch Western Scheldt estuary (de Vet et al., 2017) and in the Dutch Wadden Sea (Nederhoff et al., 2017) with mean intertidal height increases of 1 $cm\ yr^{-1}$. The bathymetry evolution in the German Bight had implications on the subtidal and intertidal sediment budget in the German Wadden Sea. Benninghoff and Winter (2019) suggested a partial sediment exchange between the subtidal and intertidal zone because intertidal sediment accretion exceeded subtidal loss in most cases. Sediment budget considerations in the Dutch Wadden Sea estimated a similar annual sediment import of 9.4 $10^6\ m^3\ yr^{-1}$ in the period of 1935 and 2005 which was mostly related to the closure of the Zuiderzee in 1957 notwithstanding (Alonso et al., 2021; Elias et al., 2012). Alonso et al. (2021) pointed out that tidal inlets in the Dutch Wadden Sea imported predominantly mud with net sand import being almost nonexistent in the period of 1995 to 2015. This supports partial sediment exchange hypothesis proposed by Benninghoff and Winter (2019). No studies were found that describe the decadal evolution of surface sediments on the intertidal flats in the Dutch, German, or Danish Wadden Sea. This could be related to a lack of reliable observational data for bathymetry and sediments as e.g., stated by Sievers et al. (2021).

2.2.2 Non-Tidal Forcing

Mean sea level

The probable mean sea level rise (SLR) until the end of the 21^{st} century is currently estimated between 0.43 m (RCP2.6) to 0.84 m (RCP8.5) relative to the MSL of the period 1986 to 2005. Annual SLR in the period of 1901 to 1990 was estimated to 1.4 $mm\ yr^{-1}$ globally and has accelerated to 3.6 $mm\ yr^{-1}$ in the period of 2006 to 2015 (Oppenheimer et al., 2019). SSH observations of tidal gauges in the North Sea found a breakpoint in the late 1990s which increased the annual increase from 1.7 $mm\ yr^{-1}$ to 2.7 $mm\ yr^{-1}$ on average (Steffelbauer et al., 2022). The impact of SLR on tidal dynamics in the North Sea was predicted with numerical models although simplifications in model configuration (e.g., lacking baroclinity, coarse grid resolution, bathymetry assumptions) made predictions vulnerable for misinterpretation. The comparison of studies by Pickering et al. (2012) and Ward et al. (2012), for example, yielded opposite projections for the response of the M_2 amplitude to SLR even though the model configuration seemed comparable at first glance. This discrepancy was a direct result of the flooding vs. no-flooding of the low-lying hinterland philosophy (Pickering et al., 2017). Numerical simulations in Chesapeake Bay, Delaware Bay, and San Francisco Bay (US) all indicated decreasing tidal amplitude if the flooding of the low-lying hinterland under SLR was permitted (Holleman and Stacey, 2014; Lee et al., 2017) with similar findings in Bohai Bay, China (Pelling et al., 2013a), and the North Sea (Pelling et al., 2013b). The most recent numerical SLR impact studies on the Northwestern European Shelf (Idier et al., 2017; Jordan et al., 2021; Pickering et al., 2017; Schindelegger

et al., 2018) projected a spatially varying change in tidal amplitude proportional to SLR in the German Wadden Sea with the highest difference in M_2 amplitude in North Frisia. It must be emphasized that the role of bathymetry evolution under SLR is still underexplored and could change the sign of the prediction (as demonstrated by Jordan et al., 2021).

Waves and wind

Only little recent research was conducted on the development of wave heights in the German Bight since the 2000s. An analysis of the wave-climate in the southern North Sea in the period of 1958 to 2002 demonstrated an increase in the 99^{th} percentile of the significant wave height with no further increases towards the end of the studied period. The study furthermore emphasized a high correlation between wind and wind-waves in the southern North Sea (Weisse and Günther, 2007). Changes in the North Atlantic Ocean followed this pattern. A weak linear increase in swell intensity in the northeast Atlantic Ocean was found in the same period; it was related to the increasing storm frequency in the course of the 20^{th} century (Gulev and Grigorieva, 2006). However, this increase in storm frequency ceased in the late 1990s (Krieger et al., 2021; Weisse and Günther, 2007). A 30-year wave hindcast in the Baltic Sea based on the COSMO-REA6 (Bollmeyer et al., 2015) and CoastDat2 (Groll and Weisse, 2017) data indicated that significant wave heights had increased by less than 5 % at westerly wave-exposed locations in the nearby Baltic Sea (Dreier et al., 2020). The absence of other research on trends in wave height and direction led me to focus the remainder of this section on the well-researched development of wind and atmospheric boundary conditions (based on the work of Feser et al., 2015; Quante and Colijn, 2016). I assume that changes in predominant wind direction and wind magnitude translate to a proportional response in regional wave parameters.
A study on geostrophic winds over the German Bight in the period of 1897 to 2018 found below long-term average wind speeds in the 99^{th} quantile and constant wind speeds in the median since the late 1990s (Krieger et al., 2021). Moreover, the study compared wind speeds in the German Bight to the northeastern Atlantic Ocean which has been considerably stormier in the same period. A recent review paper on the long-term (decadal) development of storminess over the North Atlantic and northwestern Europe seemingly contradicts these results, as most studies indicated an increase in storminess over the past few decades (Feser et al., 2015). Still, most studies also found a decrease in storminess in the late 1990s when focusing on the North Sea. It is therefore reasonable to conclude below average wave heights and storm frequency in the German Bight since the late 1990s. Nearly constant median geostrophic wind speeds over the German Bight indicate constant mean wave forcing.
The predominant wind direction is also of interest in the context of intertidal siltation (see Section 2.1.5). No studies were found that analyzed the decadal changes in wind directions. It should be noted that decreasing storminess in the past 20 years directly contradicts current climate projections that support a higher probability for storm frequency, duration, and strength (Feser et al., 2015; Ganske et al., 2016; Quante and Colijn, 2016).

2.2.3 Tidal Forcing

SLR affects tidal dynamics which in turn affect coastal morphology or vice-versa. The link between tidal amplitude and tidal asymmetry to a basin's geometry and bathymetry (Sections 2.1.3 to 2.1.4) creates a chain of relationships. On the one hand, large-scale changes in

forcing (i.e., tidal amplitude and modulation, MSL, or waves) affect the dynamical equilibrium and therefore the morphology of the coastal zone. On the other hand, changes in morphology cause changes in local and regional tidal dynamics. The following review of the changes in tidal dynamics in the German Wadden Sea was partially adapted from Hagen et al. (2022).
MSL increased by roughly 21 $yr \times 3.2\ mm\ yr^{-1} = 6.7\ cm$ in the period of 1996 to 2016. Tidal range has risen by approx. 21 $yr \times 3.3\ mm\ yr^{-1} = 6.9\ cm$ (Jänicke et al., 2020) although a lower increase in tidal range is likely and its increase varies locally (Leon Jänicke, personal communication, 2021). A trend analysis of observed tidal characteristic values revealed increasing high water (HW), decreasing low water (LW), increasing flood duration (T_F), and increasing tidal range in the German Bight (Jensen et al., 2019; Jänicke, 2021). Even though changes in the order of centimeters of MSL and tidal characteristics appear minor in mesotidal conditions, implications on large-scale tidal dynamics are probable (as suggested e.g., by Haigh et al., 2020; Jordan et al., 2021). Interestingly, Jänicke et al. (2020) showed decreasing tidal range at the British east coast along with increases in the Dutch and German Wadden Sea which indicated a moving amphidrome location. While Jordan et al. (2021) suggested that this is related to SLR and mean intertidal flat height, Jänicke et al. (2020) elaborated on changes in water column stratification (i.e., a stronger pycnocline) that stabilized the water column against turbulence for higher tidal range near the coast.
A modeling study on the consequences of local bathymetry changes for regional tidal dynamics found a local and regional impact on M_2 and M_4 amplitudes as well as $\theta(2M_2 - M_4)$ (Jacob et al., 2016). The applicability of the $\theta(2M_2 - M_4)$, however, is disputable in the southern German Bight because the M_4 amplitude is locally more than 50 times smaller than M_2 and baroclinic bias was likely present in their study. Another modeling study illustrated that the changes in flood current velocity and flow velocity asymmetry (FVA) were nearly compensated when intertidal flats were raised and tidal channels deepened with SLR (Wachler et al., 2020). Further modeling investigated the effect of (again uniform) vertical intertidal flat accretion in combination with SLR scenarios and concluded that the M_2 amplitude and the $\theta(2M_2 - M_4)$ respond most if intertidal flats drown under SLR (Jordan et al., 2021). In fact, the representation of the intertidal bathymetry was found to have a noteworthy influence on the impact of SLR on tidal characteristics (Rasquin et al., 2020). This impact was, to date, solely investigated by applying a uniform increase in the intertidal flats' height, instead of varying their elevation and lateral extent. Lateral expansion, however, can be expected based on recent bathymetry evolution at the study site (see Section 2.2.1 Benninghoff and Winter, 2019). A conceptual morphodynamic model of a simplified estuary has shown that SLR enhanced the lateral expansion of tidal flats at increased sediment export (Guo et al., 2021). Still, the feedback mechanisms between SLR and its impact on tidal characteristics and coastal morphology remain underexplored.

2.3 Identified Research Gaps

(1) Enhanced coastal siltation
Benninghoff and Winter (2019) discovered laterally expanding and accreting intertidal flats in the German Wadden Sea. However, they emphasized low confidence in their bathymetric data and, as a result, excluded of parts of the Wadden Sea from their analysis. The use of constant high and low water boundaries for tidal zone estimation furthermore neglects SLR. For these

reasons, an update of their work with more recent and detailed data can provide novel insights into possible accretion hotspots in the German Wadden Sea to answer the first research question. Similarly, the long-term changes in surface sediments have not yet been documented outside of local short-term measurement campaigns and remote sensing classifications in the German Bight. This information would be valuable to quantify changes in coastal siltation.

(2) Changes in non-tidal forcing
Many studies have linked the effect of SLR, storm surges, and waves to coastal morphodynamics and siltation. The Lagrangian tidal asymmetry framework suggests that changes in non-tidal external forces could affect the dynamical equilibrium of long-term coastal morphodynamics. However, no studies were found which investigated the recent development of local MSL, wind-wave activity, and storm surge SSH in the entire German Bight.

(3) Changes in tidal forcing
It is established that SLR must cause bathymetry adaptation to maintain the dynamical equilibrium. Bathymetry changes, however, also provoke feedback in local and regional tidal dynamics. This causes a *chicken-and-egg* problem: Has the recent bathymetry evolution impacted tidal dynamics? Has SLR caused bathymetry adaptation? Either way, there are no data providing a full spatial coverage to confirm or contradict recent local changes in tidal dynamics in the German coastal zone. Knowledge on the development of these parameters is, however, essential to estimate changes in residual sediment transport or coastal siltation.

CHAPTER 3
MATERIAL AND METHODS

CONTENTS

3.1 Thesis Framework

This section describes the theoretical framework of this thesis based on the research questions (Section 1.2) and previously identified research gaps from the literature review (Section 2.3).

3.1.1 Research Question 1: Coastal Siltation

First, it is imperative to translate reports about enhanced coastal siltation into a quantifiable scientific context to unravel if, to what extent, and where sediments deposited. For this purpose, I refine the method of a recent geomorphological analysis of the German Wadden Sea (Benninghoff and Winter, 2019) with novel bathymetry data (Sievers et al., 2020a) and annual tidal high and low water boundaries from a numerical model for the period 1996 to 2016. New bathymetry data provide an improved spatial resolution and contain more airborne laser scanning (ALS) surveys in the intertidal zone, so that they are likely to reveal more information about intertidal accretion. Furthermore, a new geomorphological analysis enables the calculation of the intertidal storage volume V_s, the subtidal channel volume V_c, and the mean subtidal channel depth h (following the definitions of Friedrichs, 2010) to establish a link to changes in tidal forcing (see below).
In addition to the morphological perspective, I use recently published decadal surface sediment data (Sievers et al., 2020b) to estimate representative surface mud content in the intertidal zone based on grain size distribution median and skewness (as defined by Folk and Ward, 1957). I aim to develop a data-driven approach that reproduces the validated remote-sensing tidal flat classification of Meyer and Ragutzki (1997). I follow the sedimentological tidal flat description of Ragutzki (1980) to extrapolate spatially variable changes in mud content on the intertidal flats of the German Bight.

3.1.2 Research Question 2: Recent Changes

Coastal siltation in the absence of river runoff and with infinite sediment supply is driven by the following processes (see Section 2.1): (1) Tides and waves redistribute sand and mud in intertidal systems under calm- and rough-weather conditions (i.e., Eulerian and Lagrangian asymmetry) until a dynamical equilibrium state is achieved. (2) Vertical haline and thermal density gradients dampen vertical mixing and trap SPM. (3) Biological activity, grain grain interaction, and flocculation vary the sinking velocity of sediments. (4) Local seabed properties such as the degree of consolidation, soil porosity, ice-coverage, vegetation density and species, mussel banks, etc. influence the erosion and deposition of sediments.
I chose to focus my work on (1), the changes in non-tidal (i.e., SSH and waves) and tidal forces (i.e., tidal constituents, Eulerian and Lagrangian tidal asymmetry). Nevertheless, I recognize that (2-4) are contributing mechanisms to coastal siltation. The investigation of estuarine and tidal inlet turbidity maxima, thermal and haline stratification changes and implications, or spatially varying erosional or depositional seabed properties would require local, high-resolution modeling in combination with novel numerical model implementations and laboratory experiments which does not concur with my research questions.
Changes in wave, tidal, and non-tidal forcing are investigated with validated modeled data

from a baroclinic numerical hindcast of the North Sea (Hagen et al., 2021b). I chose a hindcast modeling period of the years 1996 to 2016 to include one full nodal cycle (1997-2015), SLR, and the recent bathymetry evolution (Benninghoff and Winter, 2019) as represented in the bathymetry data (Sievers et al., 2020a). I modeled the entire North Sea and assimilated the open boundary to observations because tidal dynamics in the system were shown to be sensitive to coastal bathymetry changes and SLR (see Section 2.2).
Research on the drivers of coastal siltation underlined the importance of wind and wind-wave magnitude and direction (Section 2.1.5). Field surveys and numerical modeling showed that fines accrete during calm-weather (low-energy) while rough-weather conditions (high-energy) promote residual seaward transport following the Lagrangian tidal asymmetry framework (Section 2.1.3). I decided to conduct a review of recent changes in non-tidal forcing to understand if MSL, storm surge SSH, or waves facilitated more coastal siltation. As changes in storminess and MSL are already well researched, my work focuses on a review of the modeled SSH and wave anomaly with the quantile method of Woodworth and Blackman (2004).
Based on this information, I direct my attention to changes in tidal dynamics as the intensity of Lagrangian asymmetry also depends on the local (i.e., Eulerian) tidal properties. The changes of the coastal bathymetry of the German Bight (Benninghoff and Winter, 2019) likely affected local and regional tidal dynamics. First, I investigate changes of the modeled amplitude and phase of the dominant semidiurnal M_2 and its first overtide M_4 in the German Bight to establish the presence of changes in tidal dynamics outside of nodal modulation. Second, I conduct a trend analysis of the relevant main and shallow water constituents with measurements and nonlinear multiple regression (Hagen et al., 2021a) to connect observational data to my model results. Third, I assess the development of Eulerian tidal asymmetry descriptors and slack duration based on modeled data. I follow the tidal asymmetry framing of Song et al. (2011) and Gong et al. (2016) who defined tidal duration asymmetry (TDA), flow velocity asymmetry (FVA), and flow duration asymmetry (FDA) as mentioned in Section 2.1.4. Since changes in Eulerian tidal asymmetry are considered as indicator for the residual sediment transport (following Dronkers, 1986, ideas), analysis results may unravel recent changes.

3.2 External Data Sources and Availability

Observational gauges (locations in Appendix A), annual bathymetries, and decadal surface sediment data (Table 3.1) were used in model validation and trend estimation. Most measurement locations were permanent gauges with varying temporal coverage and their data were always checked visually for plausibility and outliers whenever applicable.
I frequently used bathymetries and decadal surface sediment data from the EasyGSH-DB data collection (Sievers et al., 2020a,b) on regular 10 m and 100 m grids in the period of 1996 to 2016 for numerical modeling and data analysis. It must be noted that these bathymetry data underlay a high degree of uncertainty as they were merged and interpolated from of a high number of individual measuring campaigns with varying instrument accuracy (Sievers et al., 2021). The state-of-the-art airborne laser scanning (ALS) technology, for example, has an estimated horizontal and vertical accuracy of 5 cm to 20 cm. Benninghoff and Winter (2019) assumed a mean survey accuracy of ± 20 cm following the AufMod documentation which I considered

TABLE 3.1: List of external data sources with observational gauge data in the top and bathymetry data in the bottom half.

Name and link	Nationality	Authority
BODC data center	GB	BODC
BSH gauge network	DE	BSH
FINO 1 to 3	DE	BSH
PegelOnline	DE	WSV
SHOM data base	FR	SHOM
WaterInfo	NL	Rijkswaterstaat
ZDM coastal data	DE	WSV
EasyGSH-DB annual bathymetry (Sievers et al., 2020a)	DE	BAW
EasyGSH-DB surface sediments (Sievers et al., 2020b)	DE	BAW
Dutch Bathymetry	NL	Rijkswaterstaat
British Bathymetry	UK	UKHO
French Bathymetry	FR	SHOM
EMODnet Bathymetry Consortium (2018)	–	EMODnet

reasonable for the EasyGSH-DB bathymetries as well. Additionally, different surveying frequency (i.e., high frequency in navigational channels, low frequency on intertidal flats) and surveying technique (ALS, multi-beam, single-beam, etc.) must be kept in mind whenever interpreting bathymetry data and its parameters.
Severe limitations also exist for the EasyGSH-DB surface sediment data. The sediment sample frequency and density was considerably lower than bathymetry data with a notably worse time coverage, as more than 90 % of the underlying sediment sample data base were older than the year 2000. In addition, the interpolation methodology for sediment samples uses modeled bed shear stress to estimate a representative area (Sievers et al., 2021). Modeled shear stress, however, is dependent on model implementation, model validity, and various other uncertainty. From a practical stand point, most available sediment samples were sieved which means that grains below 0.063 mm are captured as remainder. Therefore, sediment fractions $d < 0.063\ mm$ in the EasyGSH-DB surface sediment data cannot be distinguished.

3.3 A 20-Year Numerical Modeling Hindcast

Earth sciences and oceanography apply numerical process-based models to fill data gaps for a user-specified model domain. This section was adapted directly from Hagen et al. (2021b) with minor changes in wording and figure design.
Several other hindcast model data products for the German Bight followed a similar goal but were inapplicable due to insufficient temporal coverage, coarse grid resolution, or data quality. The unstructured CoastDat data (Weisse and Plüß, 2006) and CoastDat2 (Geyer, 2014; Groll and Weisse, 2017) data contain SSH, current velocity, and wave climate products at a regular 1.6 km spatial resolution with hourly time intervals (waves 5.5 km regular grid, 3-hour intervals). Similar to CoastDat2, the ERA-40 data set describes the wind and wave climate. ERA-40 demonstrates higher skill than CoastDat2 when compared to measurements; yet it

covers a shorter time period (Reistad et al., 2011). There are similar data from coastal engineering projects, e.g., the AufMod data collection (Heyer et al., 2015) which provides annual tidal characteristics. Other data products cover the northwest European Shelf region (e.g., https://marine.copernicus.eu/), or the entire globe (e.g., global tides of the finite element solution (FES) by Lyard et al., 2021) and are therefore limited to coarse grid resolution near the coast (minimum 2.5 *km* regular grids on the European shelf).
As pointed out by Groll and Weisse (2017) and Rasquin et al. (2020), a high spatial resolution of data sets is required in the German Bight to properly resolve the morphologically complex nearshore areas (see Section 1.5). Additionally, only few of the hindcasts above considered annually varying bathymetry for numerical model simulations which is crucial in the morphodynamically highly active Wadden Sea (Jacob and Stanev, 2021). Sufficient temporal coverage is also an important criterion because a typical tidal cycle in the North Sea takes about 12.4 *h* and contains two peaks in current velocity (flood and ebb). Hence, a 1-hour temporal resolution would be too coarse to represent peaks in both SSH and current velocity for robust statistical analyses. None of the data products mentioned above reach that spatial and temporal resolution.

3.3.1 Modeling Software

I chose the semi-implicit finite difference / -volume hydrodynamic model «unstructured, tidal, residual, intertidal, mudflat model (UnTRIM)[2]», version February 06^{th}, 2019, with the well-established subgrid approach for high-resolution bathymetry representation to solve instationary flow- and transport problems on unstructured grids (Casulli, 2009; Casulli and Stelling, 2011; Sehili et al., 2014). UnTRIM[2] is based on TRIM-3D (Casulli and Cattani, 1994; Casulli, 1990) and UnTRIM (Casulli and Walters, 2000). Modeling results are SSH, current velocity, tracers, salinity, temperature, turbulence, sediment concentration, or fluid density.
UnTRIM[2] is coupled to SediMorph[1] (Malcherek et al., 2002) for erosion and deposition fluxes, bed discretization, and roughness estimation. Wave parameters and feedback on hydrodynamics are two-way coupled with the spectral unstructured k-model (UnK). Known shortcomings of UnK[2] are the lack of dissipating processes (e.g., white-capping or wave-breaking) and wave-wave interaction (e.g., triads or quadruplets).

3.3.2 Model Setup

A 20-year hindcast requires a computational model setup which (1) is applicable for all years, (2) is sufficiently detailed concerning horizontal and vertical mesh resolution, (3) represents relevant physical processes, and (4) is computationally efficient. Therefore, boundary and initial data for SSH, bathymetry, wind speed, air pressure, and fresh water discharge must be available for the entire hindcast period of 1996 to 2016 to maintain data consistency.
The model considers 3D hydrodynamics, salinity, heat flux, two-way (online) coupled waves, freshwater discharge, wind forcing and air pressure fluctuation, external surge from the North Atlantic Ocean, and SLR. The open boundaries to the North Atlantic were forced with tidal constituents from FES2014b (Section 3.2) for SSH, constant salinity, and a long-term monthly

[1] `http://http://wiki.baw.de/de/index.php/Mathematisches_Verfahren_SEDIMORPH`
[2] `http://http://wiki.baw.de/de/index.php/UNK` (Schneggenburger et al., 2000)

mean temperature from the gauges Lerwick (north) and Roscoff (southwest) averaged over the water column. External surge at the open boundaries was incorporated by adding smoothed differences between calibrated baroclinic simulations and nearby observations to the open boundaries (Plüß, 2003). This approach implies that surge is constant along an open boundary which is not the case in nature. Modeling practice, however, has shown that the predicted SSH agrees well to measurements in the German Bight despite this simplification. Further aspects concerning the numerical model, the calibration procedure, and a thorough validation were published separately (BAW Technische Berichte et al., 2020, in German only).
The model domain (Figure 3.1) covers the North Sea from Norway to Scotland, the English Channel, and the Danish Straits. The model extends approximately 1,400 *km* in north-south and 1,200 *km* in west-east direction. Comparable modeling approaches of the German Bight (Heyer et al., 2015; Plüß, 2003; Putzar and Malcherek, 2015) showed that tidal dynamics and transport in the German Bight can be reproduced well with models of the North Sea or the

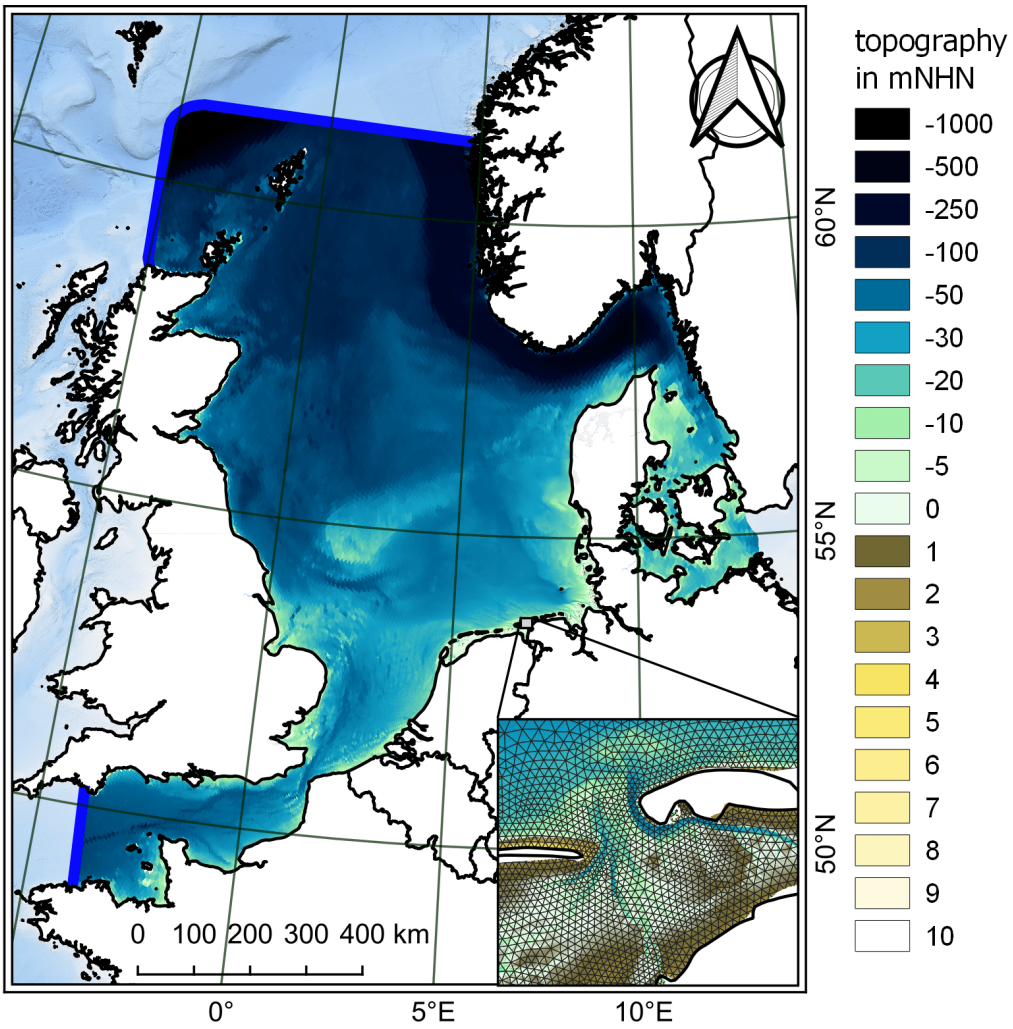

FIGURE 3.1: The domain of the numerical North Sea model with open boundaries represented by blue lines, closed boundaries by black lines, and land by white patches. Topography is shown with negative values indicating depths with respect to «Normalhöhennull» i.e., German chart datum (NHN). A zoom in East Frisia (bottom, right) near the islands Juist and Norderney shows the computational grid (gray triangles). The figure was modified from Hagen et al. (2021b).

European continental shelf (e.g., Zijl et al., 2013) because only large-scale approaches resolve tide-surge interaction and the complex amphidromic system of the North Sea.
The model uses an unstructured grid with a varying horizontal grid resolution of 10 km near the northern boundary down to 45 m in the Ems estuary, with roughly 75 % of all grid nodes located in the German Bight. The German Wadden Sea and the outer estuaries of Ems, Weser and Elbe were resolved until the tidal weir with a typical edge length between 40 m and 500 m (e.g., Figure 3.1, bottom, right). Additionally, a subgrid refinement between 4 (open North Sea) and 12 (within the estuaries) was applied to ensure an accurate water volume approximation of the computational grid throughout the hindcast period (Section 3.3.1). The grid discretization used roughly 202,000 horizontal grid cells and more than 10,000,000 subgrid elements. The vertical resolution utilized 54 fixed z-layers with a half meter delta between $+4$ mNHN and -20 mNHN, gradually becoming coarser downwards.
Wind data and air pressure were extracted from the COSMO-REA6 (Bollmeyer et al., 2015) which provides hourly reanalyzed meteorological data on a regular 6 km grid. Fresh water discharge was considered at the Dutch coast (Rhine, Maas, Western Scheldt, Ijsselmeer, Lauwersoog, and Waal river) and for the major estuaries in the German Bight (Ems, Elbe, Weser, and Eider) together with their main confluents (Leda, Wümme, Lesum, Hunte). Bathymetries (Sievers et al., 2020a) were interpolated annually to the computational subgrid within the German Bight and parts of the Dutch Wadden Sea. The remaining bathymetry of the North Sea was obtained from sources in Table 3.1 and assumed to be constant over time. External data were checked semi-automatically and corrected for outliers and errors in unit or vertical coordinate reference system before usage (exemplary bathymetry given in Figure 1.5 and Figure 3.1). Major groins, dams, and training walls were included in the model grid at their realistic height and extent in the German Bight.
Bottom roughness was calibrated with a spatially varying Nikuradse roughness ranging from 0.08 m in the English Channel to 0.002 m in Northern Frisia. Turbulence closure uses a conventional k-ε model with constant values for horizontal and vertical viscosity. Initial conditions for SSH, depth-averaged current velocity, waves, and the depth-averaged distribution of salinity and temperature were nested from model results of predecessor years. The first year (1996) was started from an astronomically forced simulation from FES2014b using the initial salinity and temperature distribution from a climatology (Janssen et al., 1999).
Waves were computed with UnK which ran on a separate unstructured grid (not included). The wave-grid located more (roughly 80 %) of its elements between the -30 mNHN isobath and the coastline of the German Bight. The horizontal grid resolution for waves varied between 20 km near the open boundary to 150 m in the tidal channels of the German Wadden Sea. The wave spectrum was limited to 32 frequencies between 0.006 Hz and 1.6 Hz with 24 specified directions (steps of 15 degree). UnTRIM^2 and UnK were two-way coupled which implies that current velocity, SSH, and meteorological forcing were communicated between the models at every time step. Wave energy was transferred to UnTRIM^2 as wave radiation stress affecting local currents.

3.3.3 Model Validation

This section provides the model validation against measurements in the hindcast period of 1996 to 2015 with harmonic and tidal characteristic analysis (error metrics provided in Appendix B). Observational data sources were presented in Section 3.2 and their locations are given in Appendix A. A more detailed documentation of model calibration and validation in the years 2006 and 2012 can be found in a technical report (BAW Technische Berichte et al., 2020, in German only). This section uses the harmonic and tidal characteristic analysis from Section 3.4.

Tidal constituents

I chose to validate the modeled semidiurnal tidal constituent M_2 against observations because its amplitude is more than 7 times larger than any other constituent in the German Bight, making it the dominant driving force of tides. An annually varying network of 10 (1996) to 41 (2006) tidal gauges in the model domain was used for validation with most gauges located within the German Bight. The varying number of gauges resulted from data availability and quality restrictions such as extensive data gaps. Observed and predicted SSH were analyzed harmonically and their difference (i.e., error) was used to estimate error metrics. I chose the mean error (ME), the error standard deviation (σ), and a root mean square error (RMSE) for a goodness-of-fit estimation of M_2 amplitude and phase for each year (Table 3.2).
The ME of the M_2 amplitude varied from -3 *cm* to 2 *cm* with a standard deviation between 3 *cm* to 7 *cm*. The largest RMSE was calculated in the year 2006 with 7 *cm* and the lowest in the years 1996, 2003, and 2013 with approximately 3 *cm*. The phase error was between -1.2 degree and -4.9 degree in the years 1998 and 2005 and the standard deviation varied between 1.2 degree to 3.3 degree. The RMSE of the phase was always lower than 5.2 degree (in the year 2005) which would correspond to a M_2 phase lag of 10 minutes. Comparable North Sea models documented M_2 RMSEs between 6.4 *cm* to 20 *cm* for the amplitude and 5.1 degree to 10 degree for the phase (Gräwe et al., 2016; Plüß, 2003; Zijl et al., 2013).

Sea surface height

Observed and predicted tidal signals were validated using the RMSE of tidal characteristics. The RMSE was computed from the difference of observed and predicted tides (i.e., more than 700 tides per year) for each year. No-data values may occur as a result of lacking observational data, data gaps, a high number of suspect values, or outliers. The scale was chosen to a maximum of 5 % and a minimum of 1 % of a peak tidal range of 5 *m* at the study site.
Most tidal range RMSEs (Figure 3.2) were between 10 *cm* and 20 *cm*, except for DWG, CUX, and BAL, usually before the year 2008. The RMSE was lowest at DUK, NOY, and HOH with 5 *cm*, 9 *cm*, and 8 *cm*, respectively, and largest at DWG, BAL, and CUX in the period of 1996 to 2008. Large RMSEs before the year 2008 could be related to uncertainty in model bathymetry, or inaccuracy of measurements caused by older, non-digital measuring instruments.
After the tidal signal was validated for its amplitude (i.e., tidal range and M_2 amplitude), the vertical extent of the signal was checked by comparing the RMSE of the tidal high water in analogy to the tidal range (Figure 3.3). The RMSE distribution of the tidal high water showed margins between 5 *cm* in HEL and ALW to 20 *cm* in BAL. Most RMSE values were in between

TABLE 3.2: The mean error (ME), standard deviation (σ), and root mean square error (RMSE) of the amplitude A and phase g of the predicted vs. observed M_2 tidal constituent in the period of 1996 to 2015 (adapted from Hagen et al., 2021b).

		A in m			g in degree		
year	# gauges	ME	σ	RMSE	ME	σ	RMSE
1996	10	0.00	0.04	0.03	-3.9	2.5	4.5
1997	12	0.00	0.04	0.04	-2.2	2.7	3.4
1998	12	-0.03	0.04	0.05	-1.2	1.2	1.7
1999	19	0.00	0.05	0.05	-2.5	1.8	3.1
2000	25	-0.02	0.03	0.04	-3.0	1.3	3.2
2001	28	-0.01	0.04	0.04	-2.4	1.8	2.9
2002	27	-0.02	0.04	0.04	-1.7	1.7	2.4
2003	23	0.00	0.04	0.03	-1.5	2.0	2.5
2004	27	-0.02	0.03	0.04	-2.3	1.9	3.0
2005	30	0.00	0.04	0.04	-4.9	1.7	5.2
2006	41	0.01	0.07	0.07	-2.3	3.3	4.0
2007	32	-0.02	0.05	0.05	-1.5	1.9	2.4
2008	28	-0.03	0.04	0.05	-1.7	2.5	3.0
2009	25	0.01	0.04	0.04	-2.2	2.7	3.4
2010	30	0.00	0.04	0.04	-1.8	2.2	2.8
2011	27	0.00	0.04	0.04	-3.1	2.3	3.8
2012	26	0.00	0.04	0.04	-2.5	2.2	3.3
2013	31	0.01	0.03	0.03	-2.9	2.2	3.6
2014	23	0.02	0.03	0.04	-3.3	1.7	3.7
2015	25	0.02	0.04	0.04	-3.3	1.9	3.8

7 *cm* and 13 *cm* and the gauges NOY, HOO, ALW, HEL, BKA, and HOH exhibited RMSEs below 10 *cm* except for NOY in the period of 2004 and 2006. The largest RMSEs were computed in DUK, DWG, and CUX which are all tide records located in the mouths of the estuaries of Ems, Weser, and Elbe, indicating that the error in tidal high water increased upstream of the outer estuaries. This was possibly related to insufficient horizontal and vertical grid resolution of the numerical model in the complex bathymetry in the German estuaries. Additionally, the gauge DWG suffered from systematic bias (not included) of 5 *cm* to 8 *cm* throughout all years which may also amplify its tidal high water RMSE disproportionally.

The flood duration (T_F) was chosen as indicator for shape and lag of the modeled SSH (i.e., tidal duration asymmetry). The RMSE of the flood duration (Figure 3.4) was between 10 and 20 minutes at most gauges. BKA, BUS, and HOH deviated with an RMSE of 20 to 37 minutes while BKA and HOH exhibited a constant deviation of 17 to 22 minutes and 20 to 25 minutes. The error of the modeled flood duration at BUS increased over time. The error remained constantly larger than 29 minutes after the year 2010 which may be the result of local bathymetric changes which were not represented in the model's bathymetry.

In addition to the RMSE of tidal characteristics (Figures 3.2 to 3.4), extreme events play a role as the southern North Sea is subject to frequent storm surge events. Storm surge SSH was expressed by the difference of the peak tidal high water of prediction and observation (Figure 3.5). The error was usually lower than 20 *cm* and the lowest error margins were observed

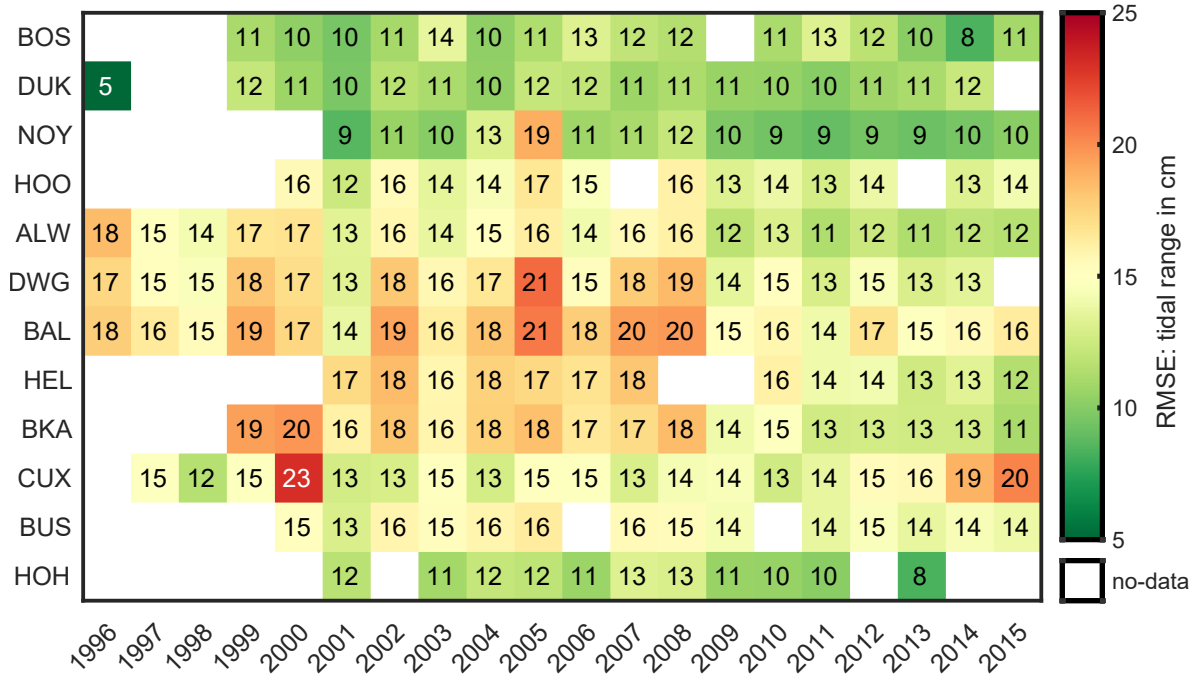

FIGURE 3.2: RMSE of the tidal range in the period of 1996 to 2015 at representative gauges (adapted from Hagen et al., 2021b).

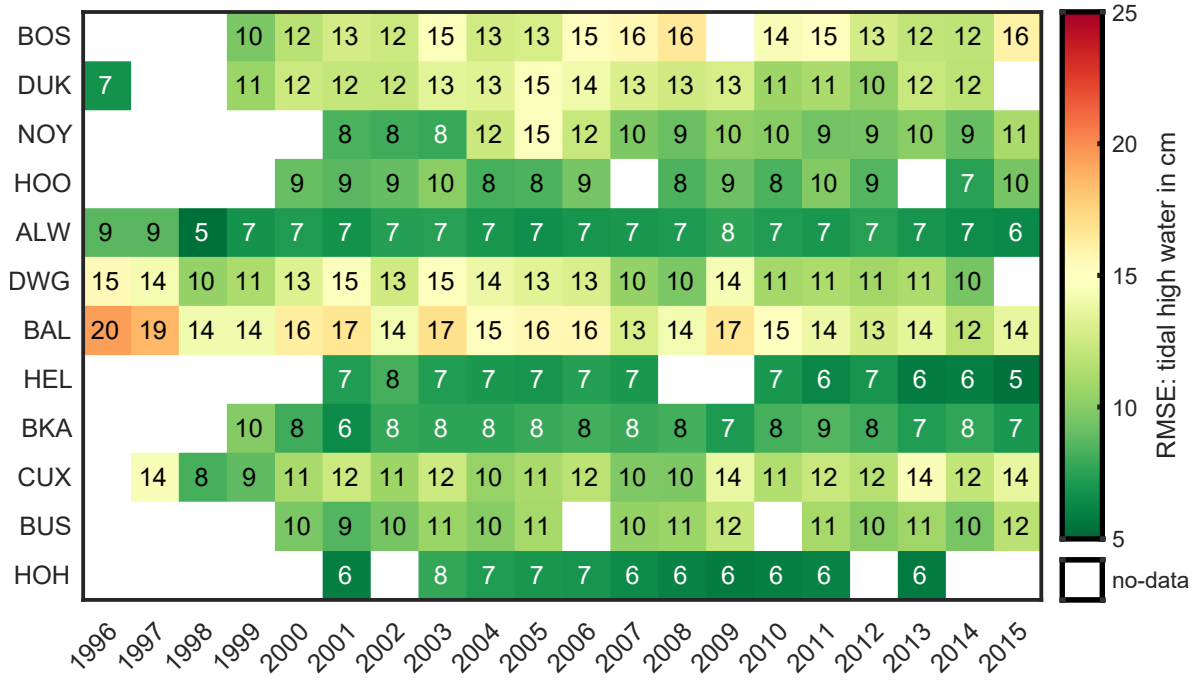

FIGURE 3.3: RMSE of the tidal high water in the period of 1996 to 2015 at representative gauges (adapted from Hagen et al., 2021b).

at ALW, HEL, BKA, and HOH. The model overestimated extreme water levels in the eastern German Bight near the Ems estuary (BOS, DUK, NOY) and in the Weser estuary (DWG, BAL). The peak overestimation of 37 *cm* was noted in DUK and HOH and the minimum underestimation by -37 *cm* at BKA (outliers). Hence, the modeled data may deviate in extreme water levels in the low decimeter range.

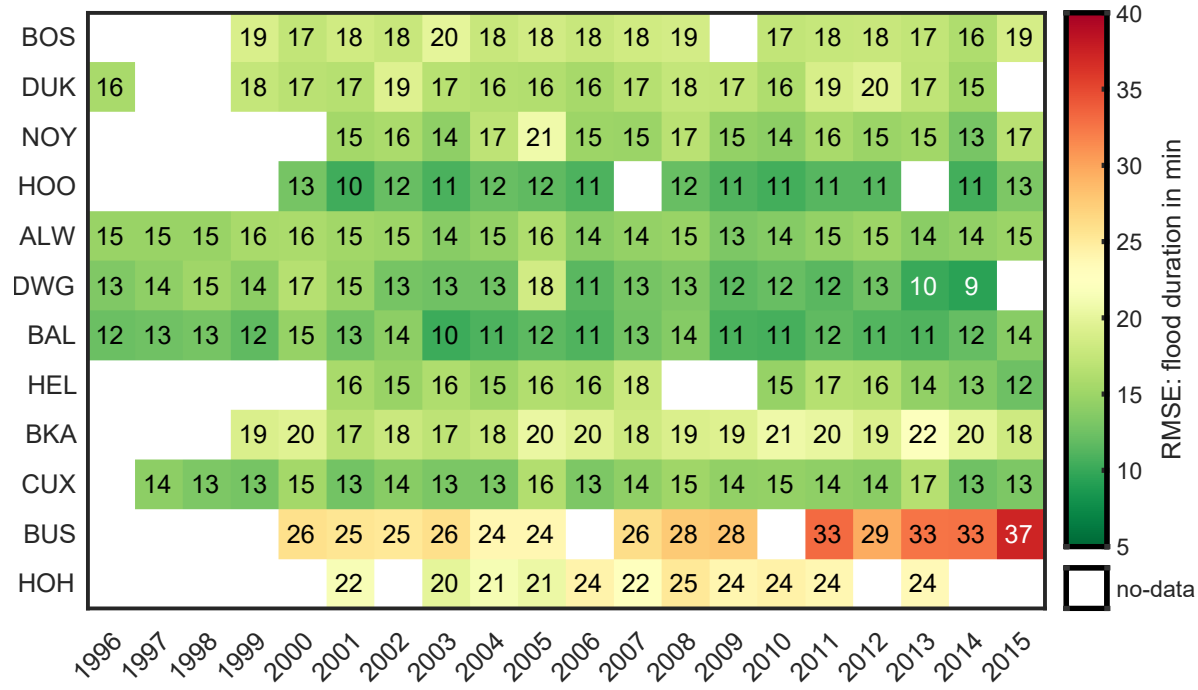

FIGURE 3.4: RMSE of the flood duration in the period of 1996 to 2015 at representative gauges (adapted from Hagen et al., 2021b).

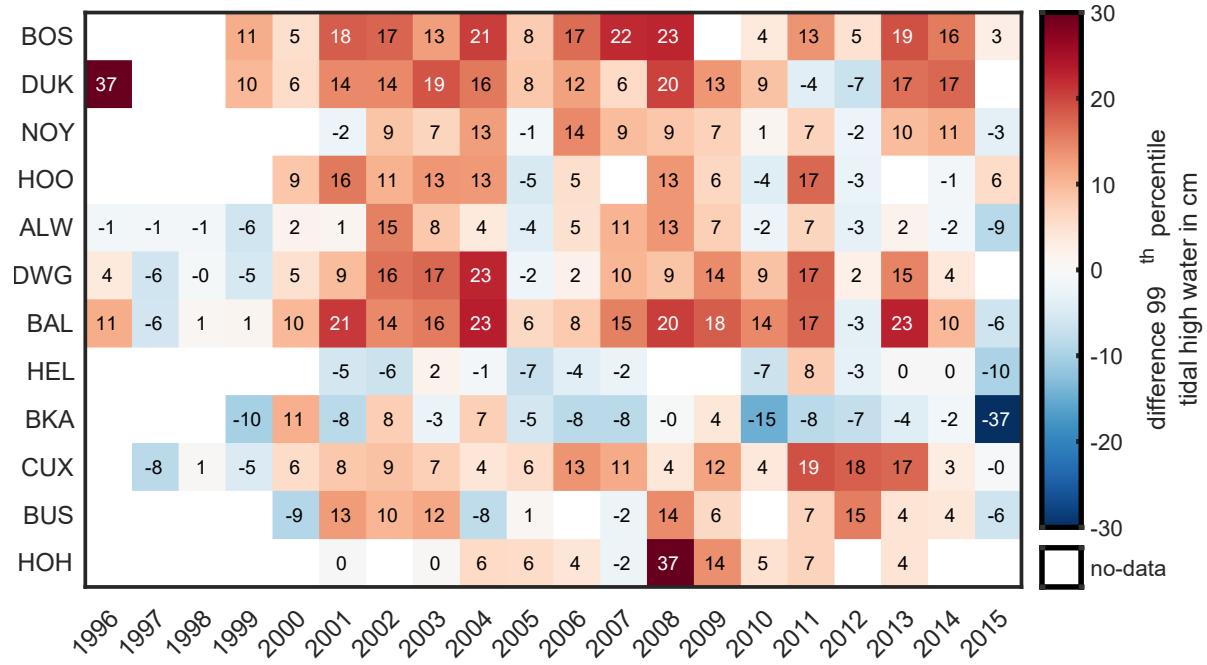

FIGURE 3.5: Error of the peak tidal high water in the period of 1996 to 2015 at representative gauges (adapted from Hagen et al., 2021b).

Current velocity magnitude

The validation of the current velocity magnitude was hampered by the low availability of observations and poor data quality. The uncertainty of current velocity measurements (van Rijn et al., 2000) and the sensitivity of computed current velocity to water depth and water depth gradients limit the comparability of observed and modeled current velocity. Nevertheless, I carried out a validation of current velocity magnitude for available data in the Ems, Elbe, and

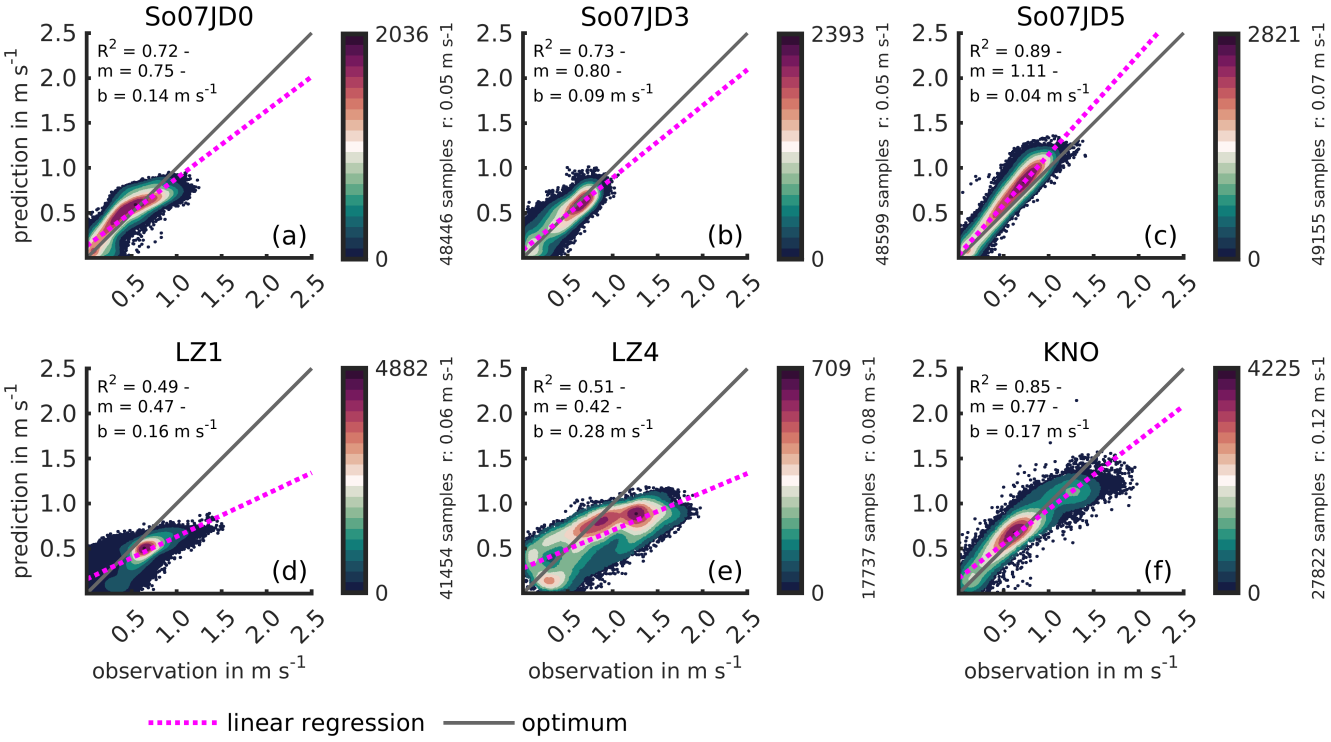

FIGURE 3.6: Scatter plots of current velocity magnitude at different gauges in the German Bight in the year 2012: So07JD0 (a), So07JD3 (b), and So07JD5 (c) in the Jade, LZ1 (d) and LZ4 (e) in the Elbe, and KNO (f) in the Ems estuary. Samples were colored according to sample density. The dotted line represents a linear regression with the regression slope m and y-intercept b. The solid gray line indicates an optimal correlation between observation and prediction. (adapted from Hagen et al., 2021b).

Jade estuary (Figure 3.6) with a statistical approach in the year 2012. For the purpose of validation, model data were extracted at the respective z-layer of the measurement devices and samples were colored in the plots according to sample density. The index of agreement R^2 and a linear regression with the slope m and the y-intercept b were used to obtain information about bias or time lag. The y-intercept b can be an indicator for bias and the slope m of potential phase lag (Winter, 2007).
R^2 indicated a mediocre to high correlation between the predicted and observed current velocity magnitude with values of 0.49 to 0.89. Comparisons at LZ1 and LZ4 in the mouth of the Elbe estuary exhibited lower R^2 values of less than 0.51. A wider spread was found in the observed velocity data at these locations which may be a reason why regression parameters indicate poor model skill. Comparisons in the Ems and Jade estuary contrasted the poor agreement with better skill although regression slopes below 0.77 were noted in So07JD0, LZ1, LZ4, and KNO indicating a slight offset between flood and ebb.

Waves

I compared the wave model results (significant wave height H_{m0}, mean wave period T_{m02}, peak period T_p, and mean wave direction θ_m) against wave measurements in the German Bight. It should be noted that only few wave observations were available that suffered from outliers and data gaps in contrast to, e.g., SSH gauges. Most wave observations were recorded in

TABLE 3.3: The RMSE of the significant wave height (H_{m0}), mean wave period (T_{m02}), peak wave period (T_p), and mean wave direction (θ_m) with water depth and completeness of the observed significant wave height at selected locations in the year 2007 (adapted from Hagen et al., 2021b).

location	completeness	depth	RMSE H_{m0}	RMSE T_{m02}	RMSE T_p	RMSE θ_m
	H_{m0} in %	in mNHN	in m	in s	in s	in degree
FINO1	70	29	0.61	1.4	2.7	47.7
Sylt	87	13	0.30	1.4	3.2	54.4
Elbe	89	25	0.40	1.3	1.8	50.2
NSB-II	25	44	0.74	1.2	2.3	42.5

short-term measuring campaigns covering years at best. Hence, I decided to assess model performance at a few locations only. The annual completeness of the measured significant wave height was given in Table 3.3 to indicate data gaps. Completeness hereby refers to the number of valid samples at model output times divided by the total number of model output times. Swell wave events from the Northern Atlantic could not be captured by the model because no open-boundary wave forcing along the ocean model boundary was prescribed. Therefore, an underestimation of peak wave periods during calm-weather conditions was observed in the study area.

Table 3.3 outlines wave validation results for a chosen year 2007 at the stations FINO1, Sylt, Elbe, and NSB-II. All stations suffered from limited completeness between 25 % and 89 %. Deep water measurements (FINO1, NSB-II) exhibited higher RMSEs while nearshore gauges

TABLE 3.4: RMSE of significant wave height (H_{m0}), mean wave period (T_{m02}), peak wave period (T_p), and mean wave direction (θ_m) in the period of 2003 to 2015 at FINO1. Note that FINO1 started operating in July 2003 which is why no earlier validation was conducted (adapted from Hagen et al., 2021b).

year	completeness	RMSE H_{m0}	RMSE T_{m02}	RMSE T_p	RMSE θ_m
	H_{m0} in %	in m	in s	in s	in degree
2003	23	0.66	1.6	2.2	42.2
2004	52	0.55	1.6	2.2	40.4
2005	89	0.56	1.6	2.1	42.7
2006	63	0.54	1.4	2.6	46.7
2007	70	0.61	1.4	2.7	47.7
2008	79	0.60	1.6	2.8	45.5
2009	42	0.47	1.4	2.7	46.5
2010	63	0.58	1.5	2.2	45.1
2011	91	0.59	1.5	2.7	45.6
2012	40	0.62	1.4	2.5	41.9
2013	97	0.57	1.5	2.6	39.2
2014	69	0.54	1.5	3.0	42.2
2015	90	0.61	1.4	2.7	41.1

(Sylt, Elbe) had lower errors. The model represented the significant wave height with a maximum RMSE of 0.74 m in NSB-II. The RMSE of T_{m02} and T_p remained lower than 3.2 s. The RMSE of the mean wave direction varied between 37.9 and 54.4 degree although it should be noted that mean wave directions from simulation results were compared with measured wave directions at the peak frequency. These two values differ episodically which is a likely explanation for poor model skill.
Table 3.4 shows an assessment of the simulated wave parameters against observations from FINO1 in the period of 2003 to 2015 (operational since July 2003). The annual RMSE of the significant wave height near FINO1 varied between 0.47 m and 0.66 m. RMSE values were in the same order for other locations in deeper water (included in supplement to Hagen et al., 2021b). The annual RMSE of the mean wave period at FINO1 varied between 1.4 s and 1.6 s and of the peak period at FINO1 between 2.1 s and 3.0 s. Peak wave period errors > 12 s could arise from neglecting open boundary wave conditions at the North Atlantic in the model set up or by differences between the observed and applied wind field. Moreover, the reliability of measurements for peak periods > 12 s with a directional wave rider buoy such as FINO1 remains questionable. For reasons explained above, the annual RMSE of the mean wave direction at peak wave period was estimated between 39.2 and 47.7 degree.

3.3.4 Data Overview

The 20-year numerical modeling hindcast in the period of 1996 to 2015 contains the subsequent data (Hagen et al., 2020a,b). I used these data for trend analysis of tidal and non-tidal forcing on the unstructured computational grid and as input parameters for the subtidal and intertidal zone classification:

- sea surface height (SSH) in 10-minute intervals
- depth-averaged current velocity in 10-minute intervals
- wave parameters in 10-minute intervals
- annual tidal characteristics
- annual SSH tidal constituents

3.4 Tidal Analyses

Tides are waves which are exerted by the periodic gravitational forces of the earth, sun, and moon. Their high predictability and periodicity enables the extraction of reoccurring parameters for e.g., SSH or current velocity. The synthesis of extensive periodical data from observations or numerical models to meaningful parameters is defined as tidal analyses. Common analyses methodologies are the harmonic (see Section 3.4.1) or tidal characteristic methods (see Section 3.4.2). Parts of this section were adapted from Hagen et al. (2021a).

3.4.1 Harmonic Analysis

The harmonic analysis (also referred to as satellite method) follows the development of tidal potential theory (Doodson, 1921, 1928) and is well documented with its modern formulations

(Foreman et al., 2009; Pugh, 1987). State-of-the-art harmonic tidal analysis software estimate the amplitude and phase of a harmonic function for tidal constituents from astronomically predefined frequencies. Tidal constituent designation follows the reoccurrence interval and gravitational origin. The semidiurnal moon tide, for example, is defined as M_2.
Tidal constituents underlie seasonal, annual, and perennial cycles and fluctuation. Seasonal variations were related to thermal stratification changes and sea ice melt (Gräwe et al., 2014; Müller, 2012; Müller et al., 2014) while annual variability was linked to meteorological fluctuations (Pugh, 1987) such as storminess. Longer tidal cycles (for overview see Haigh et al., 2011) are most prominently represented by the gravitational nodal tide (18.61 years), lunar perigee (8.85 years), or solar perigee (20,392 years).
A trend estimation of tidal constituents must consider the interannual and perennial variability of tidal constituents. I developed a nonlinear multiple regression approach for the long-term trend assessment and an estimation of the nodal modulation of annual tidal constituents (Hagen et al., 2021a, Equation 3.1) following the work of Peng et al. (2019).

$$H(t) = a_0 + a_1 t + a_2 (t - \varphi_1)^2 + a_3 \, sin(\omega t - \varphi_2) \tag{3.1}$$

$$\omega = \frac{2\pi}{18.61}$$

In Equation 3.1, a_0 represents the initial SSH, a_1 a linear, and a_2 an accelerated trend with a possible time lag φ_1. The nodal amplitude of each tidal constituent is given by a_3 and ω represents the nodal frequency of 18.61 years with a possible phase lag φ_2 and t represents the time in Julian years.

3.4.2 Tidal Characteristics

Tidal characteristic values describe physical coastal processes that have distinct flood and ebb properties. Figure 3.7 (a) gives an example of the basic tidal characteristic values based on a flood dominant M_2 and M_4 ($M_4/M_2 = 0.2$) SSH signal. A tidal cycle consists of two low water (LW) and one high water (HW) event. The flood duration (T_F) is limited by the first LW and the subsequent HW and the ebb duration (T_E) describes the duration from the HW to the second LW. Tidal range is estimated from the mean difference of the low water events and the corresponding high water in the tide duration (T_T).
A current velocity signal (e.g., Figure 3.7, b and c) is described by the peak flood $u_{f,peak}$ and peak ebb $u_{e,peak}$ current velocity magnitude as well as their slack durations s_f and s_e. The flood current duration (T_f) endures from ebb to flood and ebb current duration (T_e) from flood to ebb slack. A full tidal cycle is described by tide current duration (T_t). It should be noted that T_f and T_e occur after T_F and T_E in reality because of water body inertia. Whenever multiple tides are described, the mean, quantile, minimum, or maximum parameters may be estimated.

3.5 Eulerian Tidal Asymmetry Descriptors

The Eulerian tidal asymmetry framework (see Section 2.1.4) describes the flood and ebb characteristics of SSH and current velocity with the tidal duration asymmetry (TDA), flow velocity

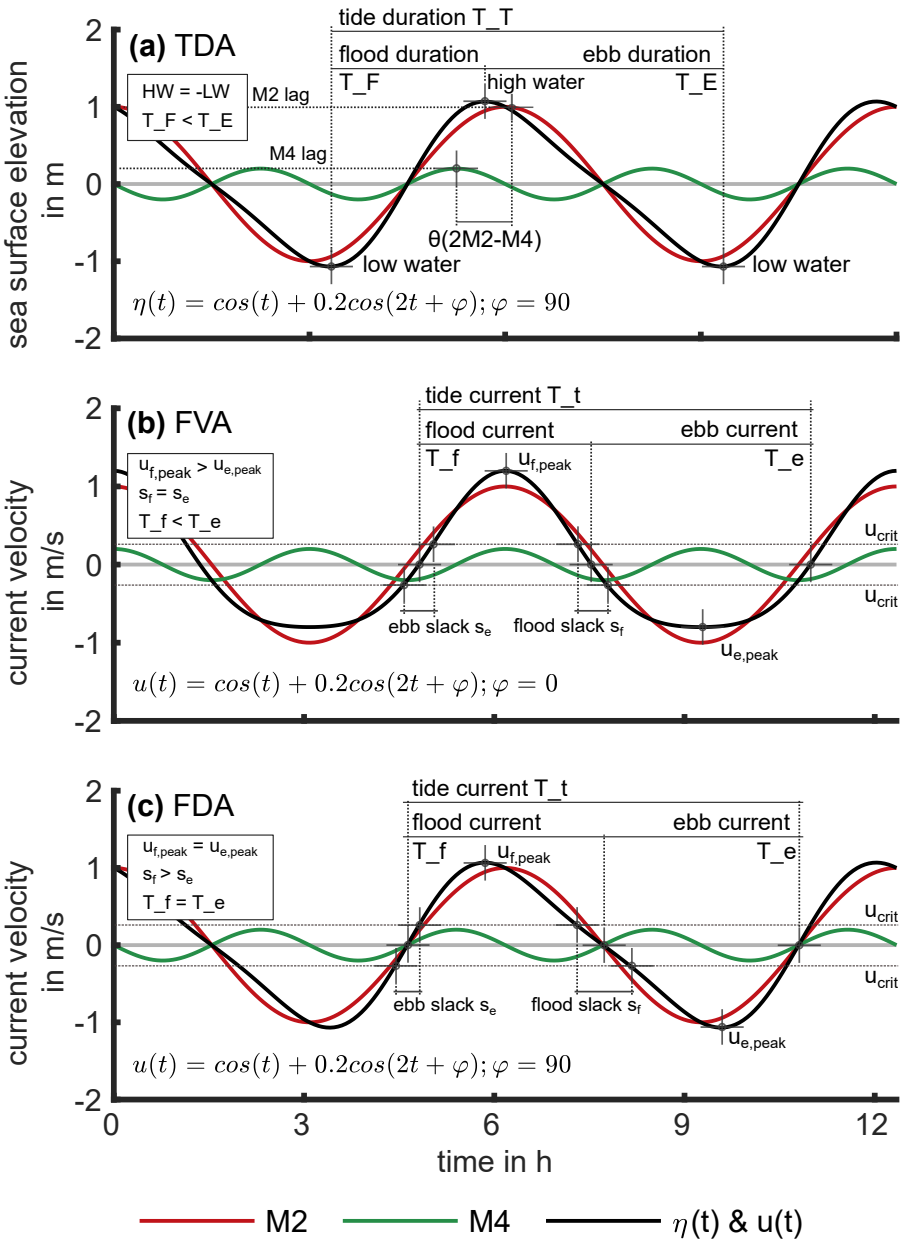

FIGURE 3.7: Reconstructed tidal signal from the M_2 and M_4 tidal constituents at maximum flood dominance including a definition of relevant harmonic and tidal characteristic values for tidal asymmetry. The tidal duration asymmetry (TDA) of a SSH signal is given in (a), the flow velocity asymmetry (FVA) in (b), and the flow duration asymmetry (FDA) in (c) of a current velocity magnitude signal are illustrated below. The critical velocity u_{crit} was chosen at 0.2 $m\ s^{-1}$ in this figure.

asymmetry (FVA), and flow duration asymmetry (FDA) following the definitions of Song et al. (2011) and Gong et al. (2016). A common TDA descriptor is the amplitude ratio between shallow water and main tidal constituents (e.g., the M_4 to M_2 amplitude ratio) for asymmetry strength in combination with a phase lag θ (e.g., the $\theta(2M_2\text{-}M_4)$ phase lag; Figure 3.7, a). Alternatively, tidal characteristic value ratios such as the flood to ebb duration ratio provide another insight into TDA by describing asymmetry strength and dominance of every tide.

If the phase offset φ of a current velocity signal is in quadrature to SSH (i.e., standing wave, Figure 3.7, b), the peak and mean flood current velocity magnitudes are larger than their ebb

TABLE 3.5: Overview of applied Eulerian tidal asymmetry descriptors (modified from Hagen et al., 2022).

tidal asymmetry parameter	category	flood dom.	symmetry	ebb dom.
$\theta(2M_2\text{-}M_4)$ phase lag (sea surface)	TDA	0 - 180 *deg*	180, 360 *deg*	180 - 360 *deg*
flood (T_F) to tide (T_T) duration	TDA	< 0.5	0.5	> 0.5
flood (T_f) to tide (T_t) current duration	TDA	< 0.5	0.5	> 0.5
mean flood ($v_{f,mean}$) to ebb ($v_{e,mean}$) ratio	FVA	> 1	1	< 1
peak flood ($v_{f,mean}$) to ebb ($v_{e,mean}$) ratio	FVA	> 1	1	< 1
flood slack duration s_f	FDA	–	–	–
ebb slack duration s_e	FDA	–	–	–

counterparts. Another tidal asymmetry perspective is expressed by the slack water asymmetry FDA (Figure 3.7, c) with u_{crit} defined at 0.2 $m\ s^{-1}$. I chose to regard the absolute flood and ebb slack durations in this thesis because the absolute duration is more relevant to coastal siltation than a ratio.

A variety of Eulerian duration and velocity asymmetry descriptors were selected in this thesis (Table 3.5) mainly following the ideas of Dronkers (1986) who stated that the residual transport of fine sediments is slack duration dominated while the movement of coarse sediment correlates with peak current asymmetry. Although this is a fairly simple definition, van Maren and Winterwerp (2013) demonstrated in a numerical model that sand and mud transport on tidal flats were in fact dominated by flow duration and peak current asymmetry.

I exchanged flood to ebb ratios for flood to tide durations to avoid a nonlinear amplification of flood dominance in flood to ebb ratios for practical reasons: If, for example, a flood duration decreases from 400 to 300 minutes along a tidal cycle of 700 minutes, the flood to ebb duration ratio changes nonlinearly from 1.33 to 0.75 while the flood to tide duration linearly from 0.57 to 0.43.

3.6 Stability Criteria

The evaluation of the bathymetry and tidal properties of estuaries or tidal basins may be used to predict its barotropic tidal asymmetry. The ratio of the mean tidal amplitude a to mean channel depth h (i.e., a/h), or the intertidal storage V_s to subtidal channel volume V_c ratio (Friedrichs and Aubrey, 1988) exist to estimate Eulerian tidal asymmetry of short shallow estuaries (Friedrichs, 2010, definition in Figure 3.8). It should be noted that observed tidal asymmetry may differ from stability criteria estimation notwithstanding inertia, runoff, reflection, or baroclinity.

For short and shallow estuaries (e.g., tidal channels), steep SSH gradients during a tidal cycle (large a/h) enhance flood dominance while width variations (large $\Delta b/b$) enhance ebb dominance (Pethick, 1980). Therefore, depth-change dominated systems (e.g., tidal channels without intertidal flats) tend to be flood dominant while the presence of intertidal flats facilitates ebb dominance. The intertidal storage volume V_s cannot overcome the depth-dependence if $2a/h \geq 0.5$ is present (Friedrichs, 2010). This balance of depth changes and width variations in a tidal system was summed up in the tidal asymmetry parameter $\gamma = a/h - 0.5\ \Delta b/b$ with $\gamma > 0$ indicating flood and $\gamma < 0$ ebb dominance (Friedrichs and Madsen, 1992).

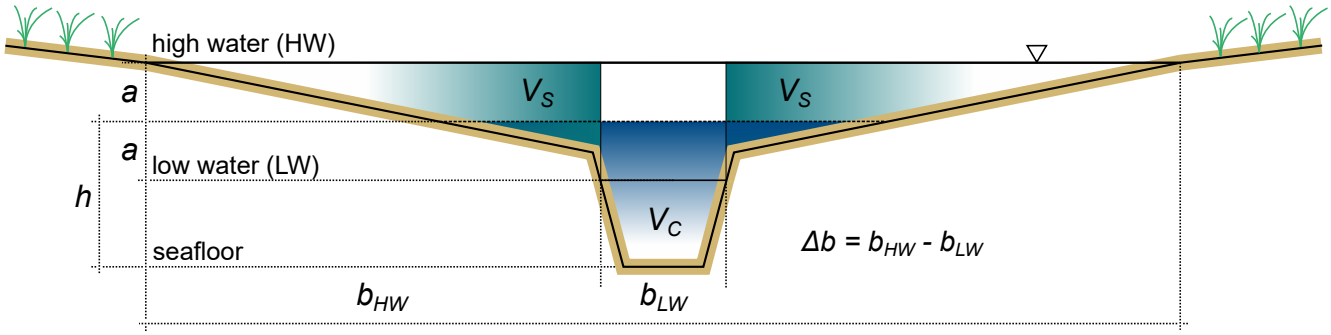

FIGURE 3.8: Schematic transverse trajectory of a channel-flat system. The intertidal storage volume V_s is marked by a cyan shade and the subtidal channel volume V_c by a dark blue shade. The intertidal width change during a tidal cycle Δb consists of the inundated width b_{hw} at tidal HW and b_{lw} at tidal LW.

The German Wadden Sea consists of complex branched channel systems (see Figure 1.5) which is why the important $\Delta b/b$ ratio could not be calculated consistently. Therefore, I deployed the V_s/V_c ratio instead (definition following Friedrichs and Aubrey, 1988) to estimate the influence of intertidal storage volume on tidal asymmetry. In any case, $a/h > 0.3$ indicate that the effect of intertidal storage volume V_s, and therefore intertidal width changes Δb, enhance flood dominance (Friedrichs, 2010). A numerical solution for in an idealized 1D channel showed that $V_s/V_c > 0.1$ with $a/h < 0.3$ always facilitated ebb dominance (Friedrichs and Aubrey, 1988).

3.7 Morphological Unit Averaging

Several tidal characteristics are a function of bathymetry gradients, channel convergence, tidal range, and intertidal width changes (Section 3.6). This section was reprinted and modified in wording and figure design from Hagen et al. (2022).
In coastal environments with complex bathymetry, shifts of flood vs. ebb dominance can happen within hundreds of meters. For this reason, I encountered the resulting high spatial variability of tidal characteristic values with a spatial averaging approach in small subsystems (i.e., morphological units from here on). Hereby, the spatial mean of a tidal characteristic value was taken as representative of a morphological unit instead of individual tide gauge locations. The validity of this approach for SSH was demonstrated in Hagen et al. (2022).
I defined morphological units for each tidal basin, via estuarine geometry, or near the location of a tide gauge. A morphological unit had to cover the tidal channels of interest within the entire analysis period. Therefore, some supratidal and intertidal areas close to the coastline were excluded as well as areas with artificial morphological changes, e.g., by port construction or by dredging. Shoreface polygons were limited seawards roughly by the -15 mNHN isobath, and inlet polygons include a small portion of the channel delta up to the -20 mNHN isobath. Additionally, the outer estuaries of the rivers Ems, Jade, Weser, and Elbe were divided into multiple units which mainly depended on the location of tide gauges.
Figure 3.9 (b) demonstrates the spatial variability for the annually averaged peak flood to peak ebb current velocity magnitude ratio in the Jade channel. First, data with invalid tidal events were discarded (c) and clipped to a chosen morphological unit (d) before averaging the parameter within the morphological unit (e). If underlying data were distributed on unstructured

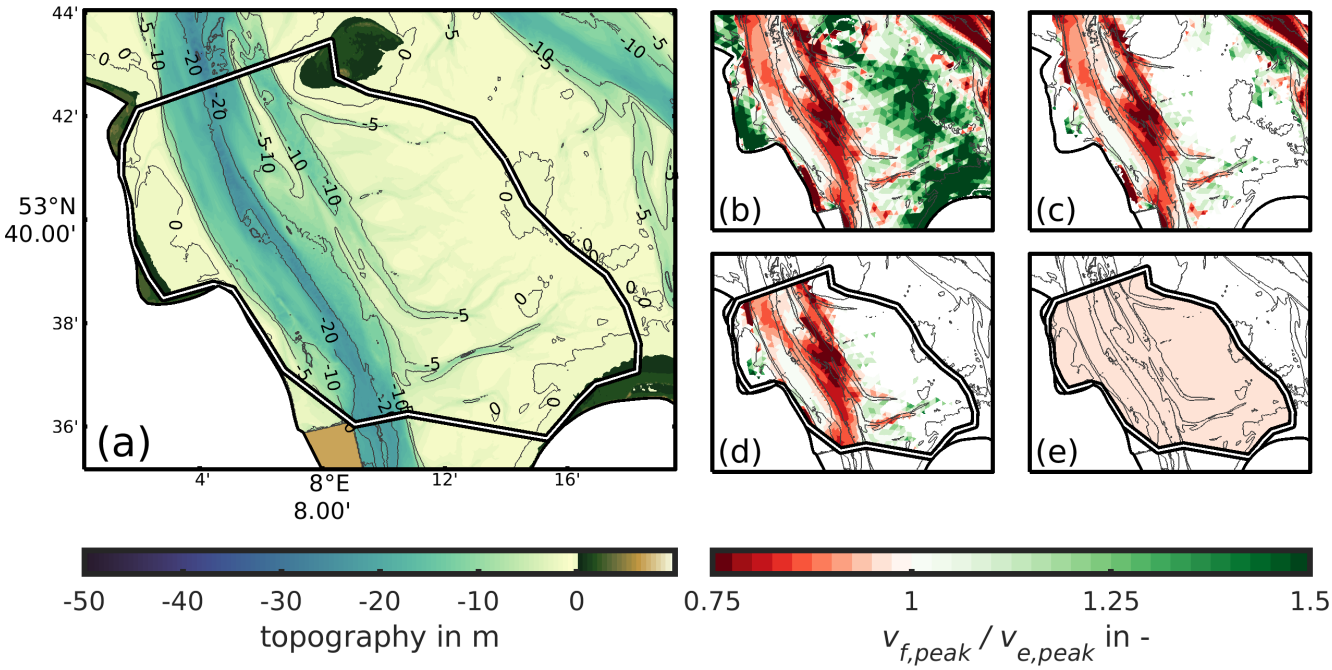

FIGURE 3.9: Calculation of the morphologically averaged mean peak flood to peak ebb current velocity ratio (b) in the Jade channel. Panel (a) shows the topography (black lines) with height isobaths (gray lines). First, data points with invalid tidal events were discarded from the analyzed data (c). Second, data outside of the morphological unit were clipped (d). Third, every data point in the morphological unit is averaged (e).

grids, the average was weighted by the respective elements area. I defined this procedure as the morphological unit averaging approach (MUA).
MUA considers intertidal wetting and drying by discarding parameters with invalid tidal events (see Section 3.4.2) before computing a morphological average. A current velocity tidal characteristic value furthermore requires one distinct flow direction to distinguish between flood and ebb current reliably. Hence, tidal events in a multidirectional flow situation, e.g., near amphidromes with a low tidal range or close to strong wave-current interaction, were excluded as well. All excluded tidal values are referred to as *invalid* in the following. MUA information can therefore only represent tidal characteristics in permanently inundated areas with bidirectional flow, i.e., tidal channels.

3.8 Bathymetry Analysis

Oceanography and marine biology distinguish coastal bathymetry into a sublittoral (also subtidal), eulittoral (also intertidal), and supralittoral (also supratidal) zone. The supratidal describes the rarely inundated area above the spring tide high water (SpHW), e.g., a salt marsh. The intertidal area extends in between the SpHW and the spring tide low water (SpLW), e.g., intertidal flats. The subtidal is situated below the SpLW and is almost permanently covered by water which would correspond to navigational channels or the coastal sea. I chose to limit the subtidal zone to the -15 mNHN seaward depth isobath because this considered most areas with a high bed elevation range in the period of 1996 to 2015.
The littoral classification methodology of Benninghoff and Winter (2018, 2019) was refined with annually varying tidal characteristic data from the numerical modeling hindcast (Section 3.3),

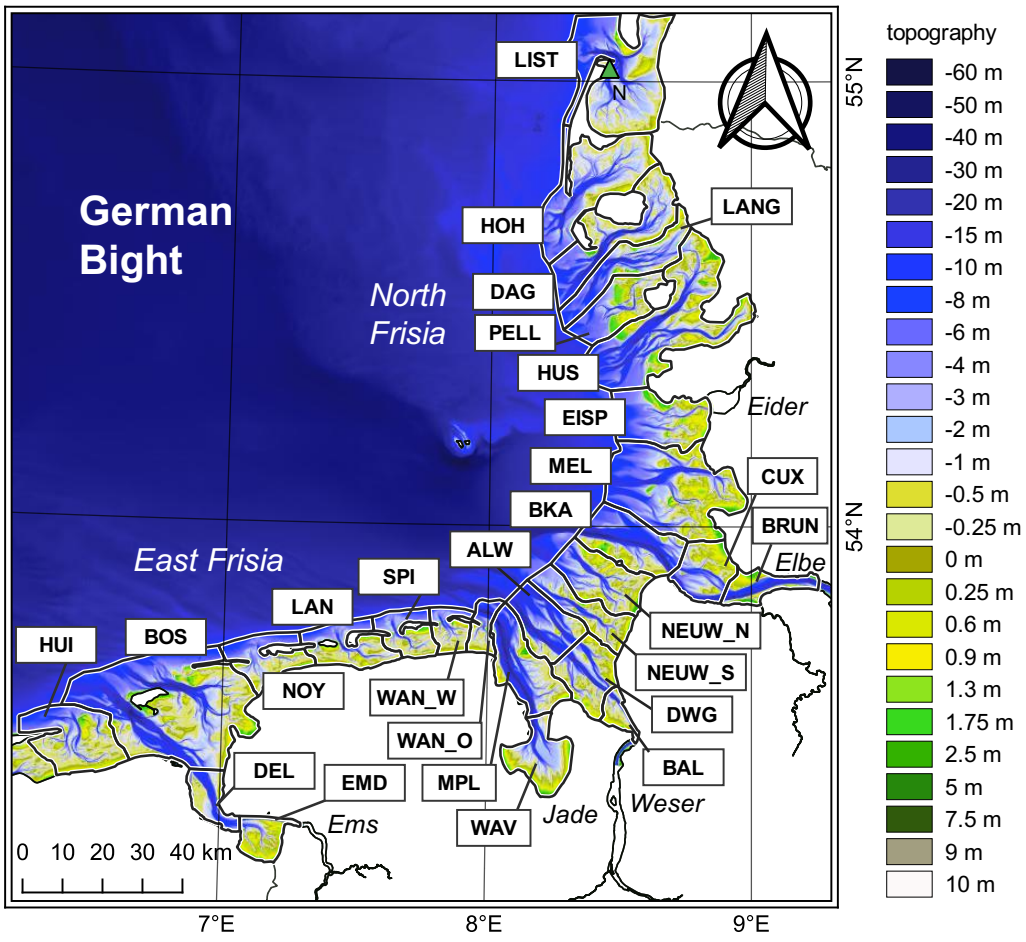

FIGURE 3.10: Morphological units for the bathymetry analysis (represented by black, solid lines and a letter-ID). The background shows the EasyGSH-DB topography in the German Bight in the year 2015.

a novel aggregation approach (Section 3.7), and with higher-resolution bathymetry data (i.e., 10 m instead of 50 m, Section 3.2).

The classification of bathymetry into a subtidal, intertidal, and supratidal zone required information on the SpHW and SpLW from the hindcast simulations (Section 3.3) at each bathymetric data point. The modeling data, however, was much coarser than the corresponding bathymetry (unstructured 200 m to 500 m cells vs. a regular 10 m grid) which is why I chose to average annual SpHW and SpLW in the morphological units from Figure 3.10 with the MUA method (Section 3.7). Morphological unit definition was modified for this purpose: I defined a morphological units extent by the approximate location of watersheds, by the tidal high and low water gradient in tidal channels, and the seaward -15 mNHN boundary to include the ebb-tidal delta in sediment volume calculations. This method makes a watershed separation or fixed channel-flat separation (Benninghoff and Winter, 2019; Elias et al., 2019) redundant as any bathymetric data point was classified dynamically based on the SpHW and SpLW of its unit within each year. However, this procedure is vulnerable against the annual variability of the SpHW and SpLW as marginal changes of SpHW, SpLW may overlay geomorphological adaptation. This uncertainty was quantified to ± 6 to ± 10 cm for the SpHW and to ± 6 to ± 12 cm for the SpLW using the average standard deviation of the SpHW and SpLW of each

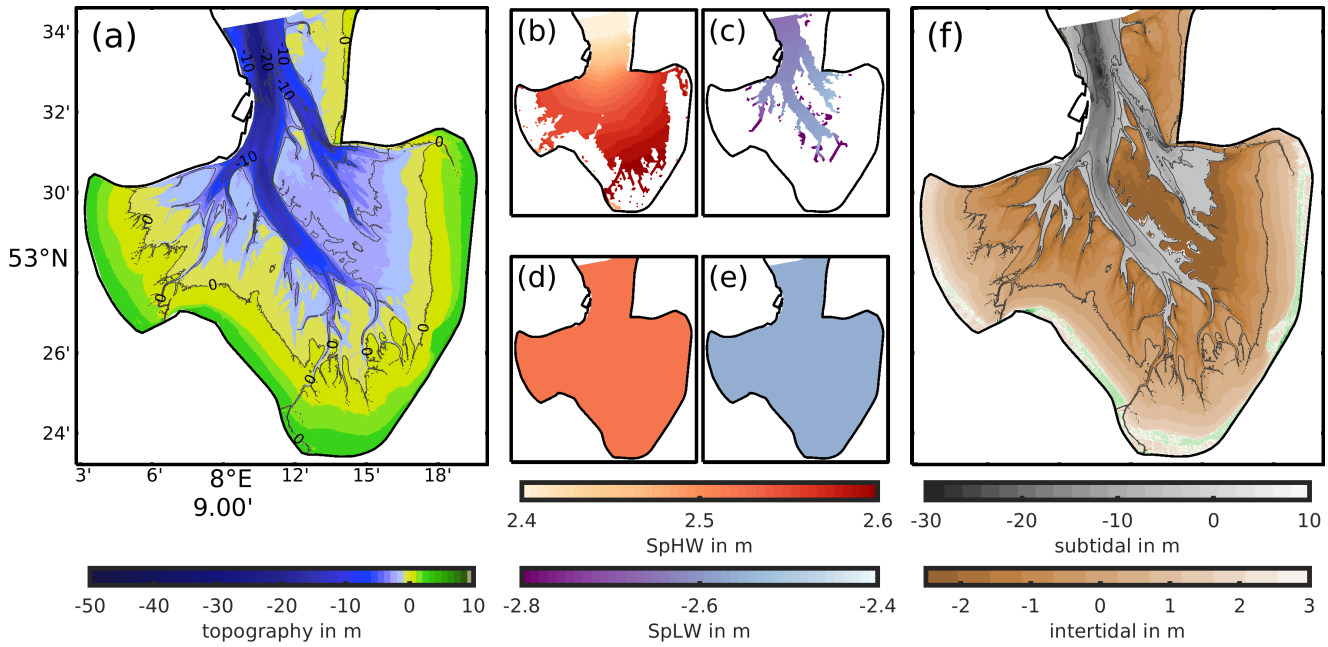

FIGURE 3.11: An exemplary tidal zone classification in the unit WAV in the year 2013 (see Figure 3.10) based on a 10 m grid of its bathymetry (a). The SpHW (b), and SpLW (c) were filtered for outliers and invalid tidal events and averaged in each unit (d, e). Averaged tidal SpHW and SpLW were then used for classification (f). Gray contours in (a) and (f) represent the -30, -20, -10, -5, 0, and 5 mNHN height isobaths.

year (Appendix C.1).
The SpHW was represented by the 95 % high water (HW) percentile and the SpLW by the 5 % low water (LW) percentile of the respective year. Outliers (with MATLABs `isoutlier()` function, last access 22.10.2022), invalid tidal events (see Section 3.4.2), and implausible data were removed before averaging the SpHW and SpLW in morphological units (Figure 3.11) with MUA. From here, bathymetry data points d_i were categorized as follows:

1. Subtidal zone: $d_i <$ SpLW
2. Intertidal zone: SpLW $\leq d_i \leq$ SpHW
3. Supratidal zone: SpHW $< d_i \leq +4$ mNHN

The ceiling of the supratidal was defined at $+4$ mNHN and the subtidal zone had no lower boundary.

3.9 Geological Tidal Flat Classification

Grain sizes in Germany are defined by the grain diameter in mm (DIN 18196, 2011) while international sources often apply the dimensionless Krumbein-φ scale ($\varphi = -log_2 \frac{d}{1\ mm}$). Both scales distinguish soil by their metric diameter d or by the dimensionless φ into sediment classes. A grain size distribution describes a soil sample by the cumulative percentage below or above predefined sieve. Cohesive sediments have a diameter $d \leq 0.063$ mm or $\varphi \geq 4$.
A Krumbein-φ distribution may be classified by distribution skewness (after Folk and Ward, 1957, Equation 3.2). Skewness indicates if a grain size distribution of a soil sample is skewed

towards fine ($Sk \leq -0,1$), or coarse ($Sk \geq -0,1$) sediment fractions. A grain size distribution may be considered symmetric if $-0,1 < Sk < 0,1$.

$$Sk = \frac{\varphi_{16} + \varphi_{84} - 2\varphi_{50}}{2(\varphi_{84} - \varphi_{16})} + \frac{\varphi_5 + \varphi_{95} - 2\varphi_{50}}{2(\varphi_{95} - \varphi_5)} \tag{3.2}$$

Tidal flat classifications in Germany differ either by the cohesive sediment content (Ragutzki, 1980; Sindowski, 1973) or by predominant median grain sizes (Reineck and Behre, 1978) in a tidal flat sediment sample. Other classifications divided tidal flats into sandy-, mixed-, or muddy which are further split into light, dark (Ragutzki, 1980) or rather muddy / sandy (Figge et al., 1980). I follow the simple definition of Ragutzki (1980) with sandy (fines $\leq$ 12 %), mixed (fines between 12 % and 50 %), and mudflats (fines $>$ 50 %) corresponding with Meyer and Ragutzki (1997).
Field data samples of sandy tidal flats had a median diameter d_{50} of 128 μm to 140 μm, mixed flats 100 μm, and mudflats 71 μm. Contrary to mixed or sandy flats, mudflats had an increased chalk and water content (6 % to 40 %) and more organics (approx. 5 %). Moreover, grain size distributions of sandy- and mixed flats were well-sorted whereas mudflats were skewed towards fines (Meyer and Ragutzki, 1997). Therefore, a non-cohesive median grain size diameter (i.e., $d_{50} \geq 0.063\ mm$) can still be part of a mudflat which means that the d_{50} alone does not describe the tidal flat type distinctively.
Based on these considerations, I defined classification criteria based on the d_{50} and the grain size distribution skewness Sk as an extrapolator for muddy and mixed tidal flats (data-driven approach in the following). The following parameter choices were based on the qualitative and quantitative agreement to validated remote sensing surveys in East Frisia and the Jade and Weser estuary in Section 4.3.1. The symbol $\wedge$ represents a logical «and» and $\vee$ stands for a logical «or» condition.

- sandy: $d_{50} > 0.08\ mm \wedge Sk \leq 0.15 \vee d_{50} \geq 0.10\ mm \wedge Sk > 0.15$
- mixed: $0.06\ mm < d_{50} < 0.08\ mm \wedge Sk \leq 0.15 \vee 0.07\ mm < d_{50} < 0.10\ mm \wedge Sk > 0.15$
- muddy: $d_{50} \leq 0.06\ mm \wedge Sk \leq 0.15 \vee d_{50} \leq 0.07\ mm \wedge Sk > 0.15$

CHAPTER 4
THE QUANTIFICATION OF RECENT COASTAL SILTATION

CONTENTS

4.1 Chapter Structure

I consider the term «coastal siltation» as the accommodation of fine sediments in the coastal zone (i.e., the subtidal and intertidal zone) in the following. Section 4.2 describes the observed bathymetry adaptation: First, the presence of significant bathymetry evolution is established (Section 4.2.1) before evaluating the development of subtidal and intertidal bulk bathymetric parameters and sediment volumina in the coastal zone (Sections 4.2.2 to 4.2.5). Section 4.3 starts by validating a data-driven tidal flat classification based on surface sediment data (Section 4.3.1) and presents the decadal development for multiple regions in the German Bight (Section 4.3.2).

4.2 Coastal Bathymetry in Transition

KEYPOINTS:

- Intertidal flats expanded laterally into the subtidal zone.
- The average subtidal depth decreased, while intertidal flats accreted by a multitude of current SLR.
- The subtidal channel water volume V_c decreased.
- Sediment budgets indicated sediment redistribution from the subtidal to the intertidal zone. Their sum, however, indicated only minor accretion.

This section assesses changes in bathymetry, water volume, and sediment volume in the period of 1996 to 2016 using EasyGSH-DB bathymetries (Section 3.2), hydrodynamic data from Section 3.3, morphological units from Figure 3.10, and the methodology from Section 3.8.
I distinguished the coastal bathymetry into the subtidal, intertidal, and supratidal zone and computed the sediment volume below a chosen reference depth $d_{ref} = -50\ m\text{NHN}$ that was

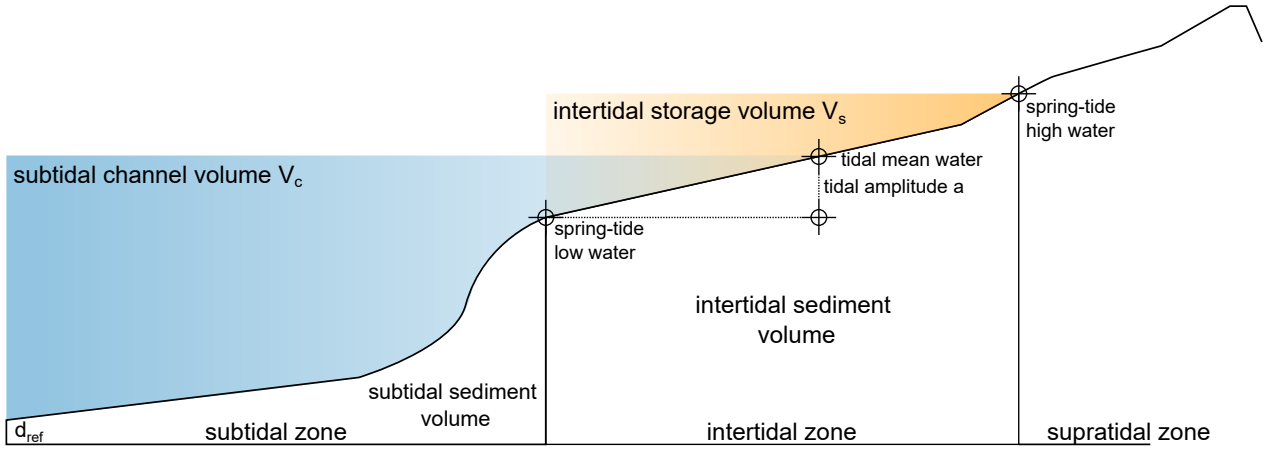

FIGURE 4.1: Schematic graphic representation of the intertidal and subtidal bathymetry parameters with a tidal zone definition (bottom), the respective sediment volume below a reference depth d_{ref}, the subtidal channel volume V_c, and the intertidal storage volume V_s.

lower than all bathymetric data points in my morphological units. The water volume was divided into the intertidal storage V_s and subtidal channel volume V_c (following Friedrichs, 2010, definition). I chose to exclude supratidal descriptors because their absolute area was negligible small, they were surveyed less frequently, and bathymetry accuracy on supratidal flats may be compromised by vegetation. All relevant parameters were summed up in Figure 4.1.

4.2.1 Can We Observe Trends in Bathymetry Parameters?

Let us look at the trend analysis of the normalized intertidal area (Figure 4.2, normalization by the maximum sum of subtidal and intertidal unit's area) and focus on sample distribution and goodness-of-fit. Ordinary linear regression was applied to estimate the development over time. Regression significance was expressed by an F-test of the linear regression slope ($\alpha = 0.05$) and the 95 % confidence intervals were considered (statistics described in Appendix B). An outlier

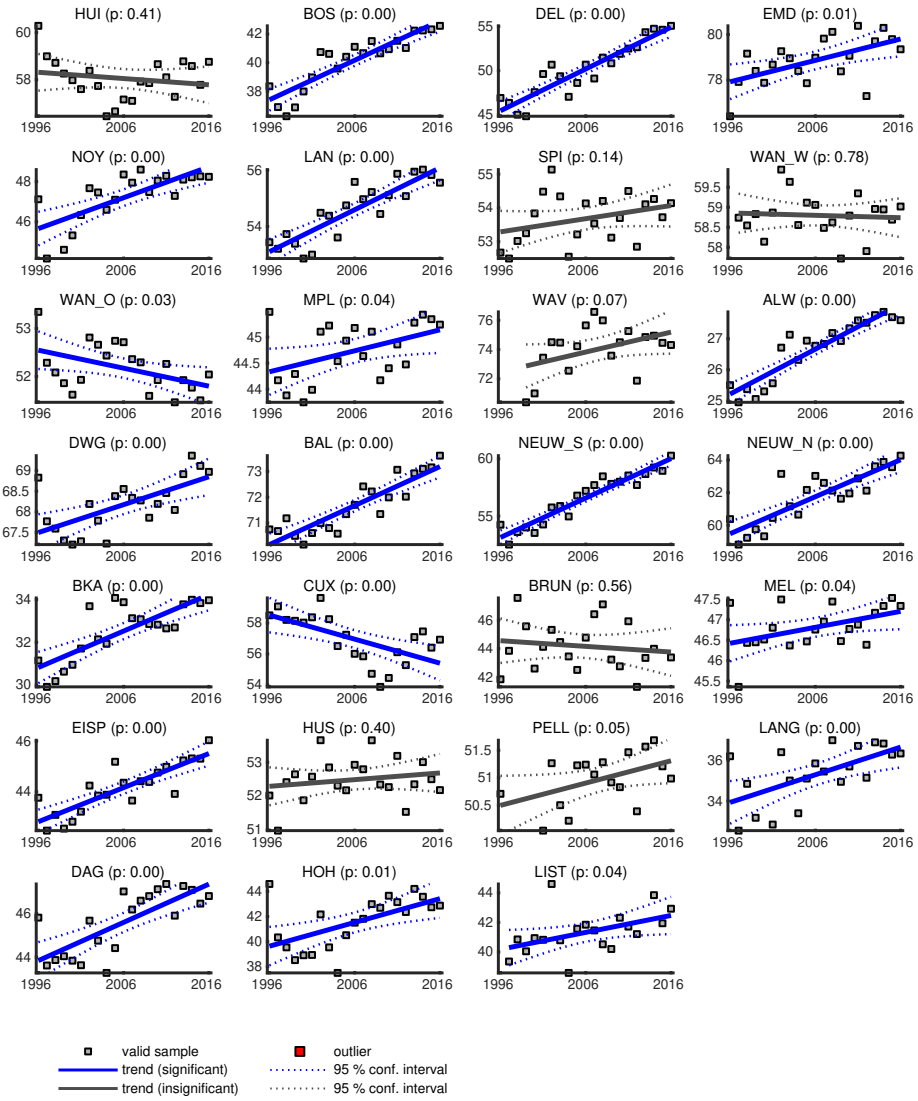

FIGURE 4.2: Exemplary trend evaluation of the normalized intertidal area in the period of 1996 to 2016. Gray squares indicate valid and red squares outlier samples. Significant trends and their 95 % confidence intervals are represented by solid and dashed blue lines and insignificant regression is indicated by gray lines. The p-value ($p < 0.05$ equals significance) of an $F-$test indicates statistical significance.

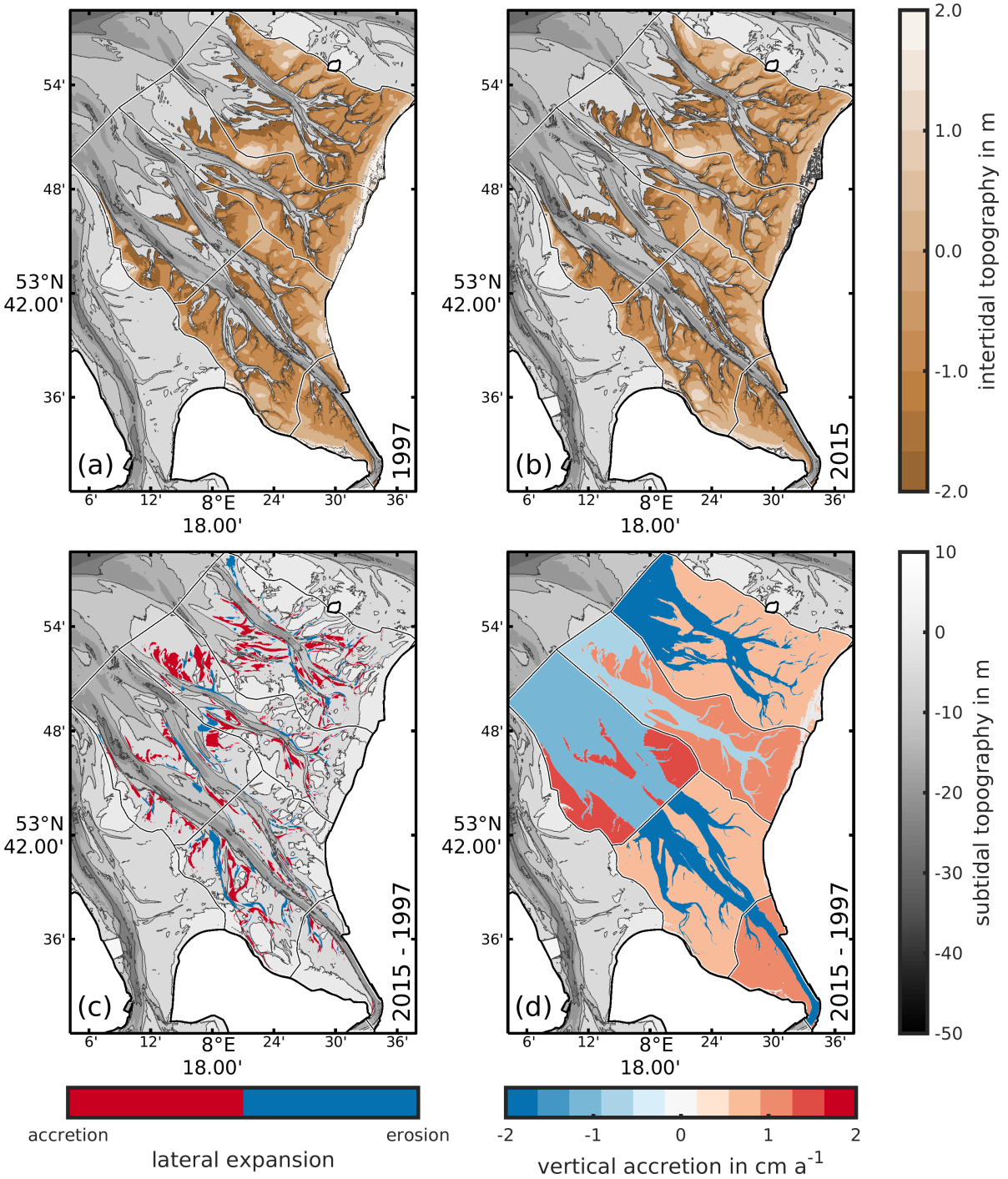

FIGURE 4.3: Representation of the intertidal zone in the years 1997 (a) and 2015 (b) in the eastern outer Weser with gray patches indicating subtidal and brown patches intertidal topography. Changes in lateral intertidal extent (c) and mean intertidal / subtidal height (d) between the two years are indicated by red and blue patches. Thin black lines indicate the respective morphological units.

filter was implemented to exclude implausible data such as height jumps on intertidal flats before airborne laser scanning (ALS) technology was available.

Most regression slopes in Figure 4.2 were statistically significant and obvious outliers were excluded reasonably. I noticed that most outliers were evident in the period of 1996 to 2000 which was expected because of the absence of ALS data. The annual spring tide high water (SpHW) and spring tide low water (SpLW) of the year 1996 were also responsible for local outliers as

an unusually long eastward wind period biased annual averages.
The evolution of the intertidal topography (Figure 4.3, a to b) confirmed expanding intertidal flats at the cost of a retreating subtidal visually which was in line with the observations of Benninghoff and Winter (2019, BW19 in the following). I noticed that small branched tidal channels narrowed or disappeared in the year 2015 and that the intertidal zone expanded seawards. The difference plot of the intertidal topographies (Figure 4.3, c) confirmed this impression (Figure 4.2, unit 12 to 16) as accretion was evident at tidal channel slopes and at the seaward border of the intertidal. In addition, all intertidal flat heights increased in height by more than 1 $cm\ yr^{-1}$ (Figure 4.3, d) while the subtidal zones deepened at even higher rates. The conformity of my trends with the work of BW19 and the reasonable visual agreement between trend and intertidal topography data led me to presume with a trend analysis of additional bathymetric parameters in the German Bight. All trend lines were documented in Appendices C.2 to C.5.

4.2.2 The Intertidal Zone Expands

Figure 4.4 displays changes in the normalized lateral expansion of the subtidal and intertidal zone in morphological units in the period of 1996 to 2016 from linear regression. Nearly all units revealed a statistically significant decline of their subtidal zone. The largest retreat was observed in the Ems (BOS & DEL), in the eastern outer Weser estuary (NEUW_S to BKA), and in North Frisia (LANG to LIST). The only significant subtidal expansion was noted in CUX which was overlain by the natural formation of a second major ebb channel in the period of 2006 to 2010.
The lateral expansion of the intertidal zone followed observed subtidal retreat. Most morphological units exhibited intertidal expansion of less than 5 % which still corresponds to multiple square kilometers. The smallest lateral expansion was found in EMD, SPI to MPL, MEL, HUS,

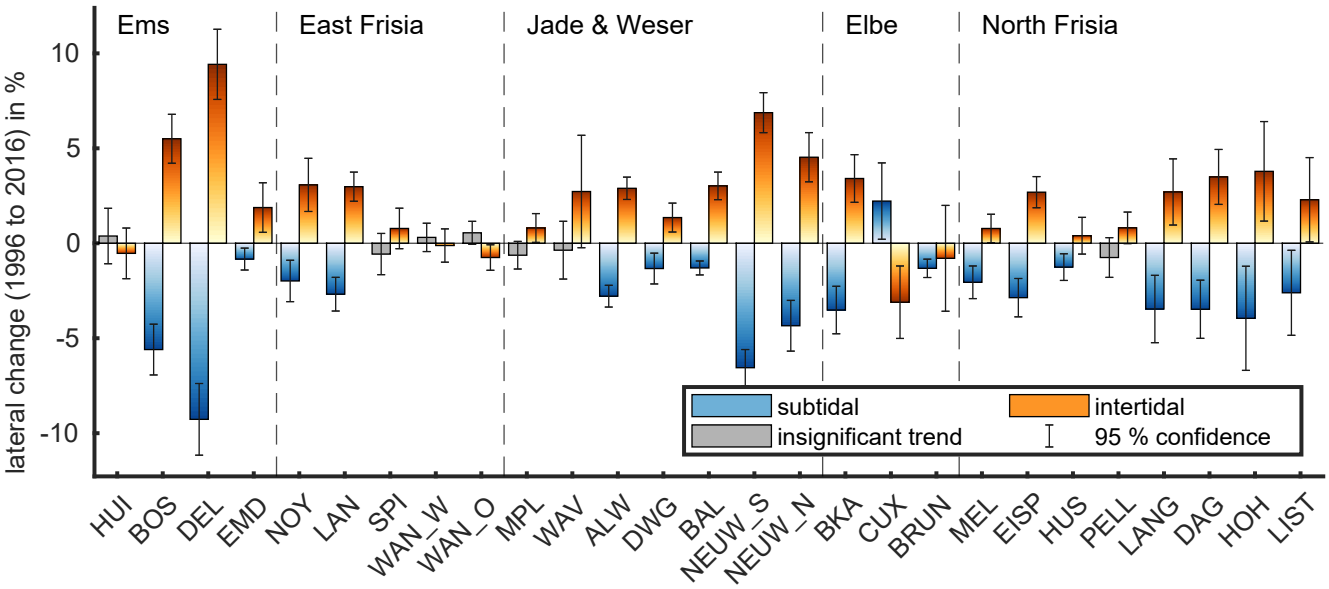

FIGURE 4.4: Normalized expansion (positive) or retreat (negative) of the subtidal (shaded blue bars) and intertidal (shaded brown bars) zones in the period of 1996 to 2016 from linear regression. Gray bars represent insignificant regression slopes.

and PELL. Again, retreating intertidal flats were found in CUX which I related to natural estuarine morphodynamics (see above). Intertidal expansion and subtidal retreat were linearly correlated ($R = -0.94$) which underlined that the intertidal expanded primarily into the subtidal rather than reclaiming supratidal areas. This was another indication that the development of the supratidal was negligible in comparison to subtidal and intertidal morphodynamics.

4.2.3 Subtidal Deepening and Intertidal Accretion

The mean subtidal height decreased by 28 *cm* on average with a peak at 132 *cm* (DEL) in the period of 1996 to 2016 (Figure 4.5). Most subtidal zones in the outer estuaries, East Frisia, and North Frisia deepened by 25 *cm* to 50 *cm*. Again, the unit CUX was an outlier as the subtidal mean height increased by approx. 60 *cm*.
Despite noteworthy lateral expansion, the mean intertidal height remained constant in the Ems and in north North Frisia and increased by tens of centimeters elsewhere. Peak accretion by 33 *cm* was noted in BKA and the average increase was 11.6 *cm*. Hence, the observed vertical accretion exceeded SLR in the same period twofold (SLR: 6.7 *cm*, see Section 2.2.2). Intertidal accretion was most prominent in morphological units in the southeastern German Bight (NOY to BRUN) as changes in North Frisia varied between growth of 14 *cm* in PELL to losses of 8 *cm* in LIST.
A comparison of my mean height changes vs. BW19's results was compromised because my morphological units covered a different spatial extent and included a larger portion of the subtidal channel deltas. Nonetheless, qualitative agreement of subtidal height changes was found

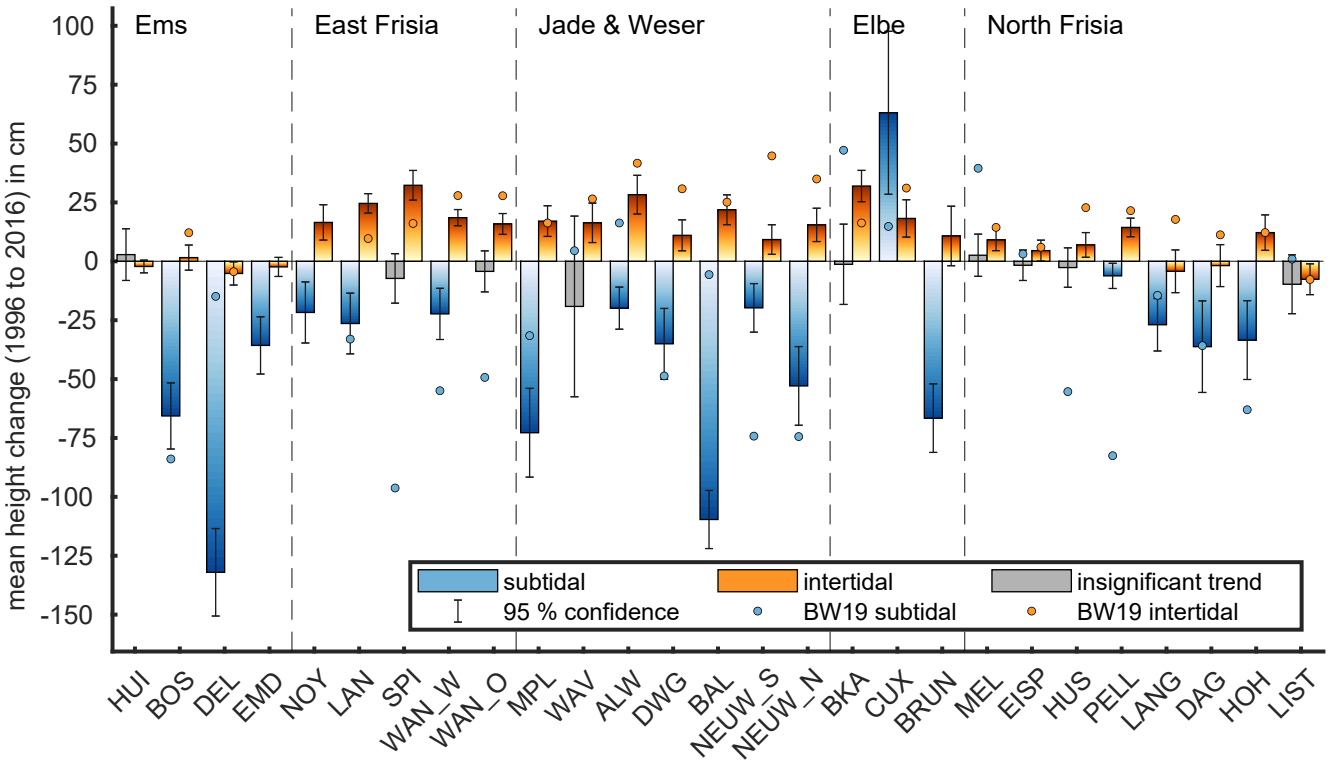

FIGURE 4.5: Mean subtidal (shaded blue bars) and intertidal (shaded brown bars) height changes in the period of 1996 to 2016 from linear regression. Gray bars represent insignificant regression slopes. Data of a similar morphological unit from Benninghoff and Winter (2019) is given by blue (subtidal) and brown (intertidal) dots.

in the outer Ems, in the outer Weser, and in North Frisia. The discrepancy was highest in East Frisia with higher mean subtidal depth decreases in BW19's approach. Estimated intertidal height changes also agreed qualitatively although the quantitative results differed locally. For example: Even though both trend assessments depicted no vertical accretion in the Ems estuary, my data indicated twice as much vertical accretion in east East Frisia and half as much in the Jade and Weser estuary. Further differences were found in North Frisia where BW19 extrapolated high accretion while my trends indicated rather stable conditions. This could be related to height jumps in BW19's topography data (i.e., the outdated AufMod data base).

4.2.4 Water Volume Changes

The lateral and vertical evolution of the subtidal and intertidal zone (Sections 4.2.2 to 4.2.3) implies consequences on the subtidal channel volume V_c and intertidal storage volume V_s (definition: Figure 4.1). I normalized each V_s and V_c by the maximum subtidal (V_c) and intertidal (V_s) area of the a morphological unit within the covered period to ensure comparability (in m^3/m^2, i.e., m).

Most morphological units lost subtidal channel volume despite increasing subtidal depths and SLR (Figure 4.6). Few units revealed locally isolated increasing (e.g., EMD, MPL, & BRUN) or stable V_c. Noteworthy V_c decreases were noted in East Frisia (LAN & SPI), in the eastern outer Weser (NEUW_S to BKA), and north of the Elbe estuary (MEL to PELL). Interestingly, increases or constant V_c clustered in the inner estuarine units (e.g., EMD, WAV, BAL, and BRUN) of the study area.

Changes in intertidal storage volume V_s followed a similar pattern. V_s increased most in the mouth of the Ems estuary which likely resulted from the considerable lateral intertidal expansion noted in Section 4.2.2. Several other small V_s increases of less than 0.25 m in North Frisia (LANG to LIST) coincided with lateral intertidal expansion as well. Areas with high lateral intertidal expansion and accretion (e.g., NEUW_S & BKA) demonstrated near constant V_s. In fact, the majority of units from NOY to PELL revealed constant or decreasing V_s. The water

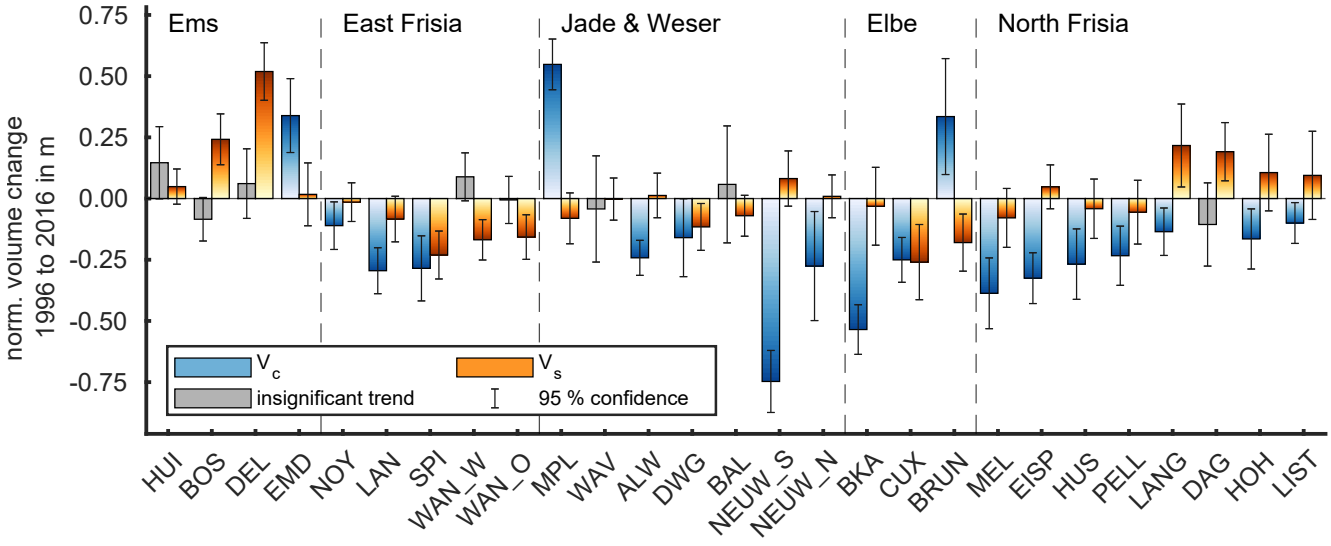

FIGURE 4.6: Normalized changes in subtidal channel volume V_c (shaded blue bars) and the intertidal storage volume V_s (shaded brown bars) in the period of 1996 to 2016 from linear regression. Gray bars represent insignificant regression slopes.

volume assessment showed an overall significant decrease of V_c at constant or also decreasing V_s in most units in the period of 1996 to 2016 despite SLR.

4.2.5 Implications on the Sediment Budget

Sediment volume changes were estimated by multiplying the difference between a depth sample and a chosen reference level which was lower than all depth samples ($d_{ref} = -50\ m$NHN) with the raster cell's area. The subtidal sediment volume was normalized by the maximum subtidal, the intertidal sediment volume by the maximum intertidal, and total sediment volume by the maximum sum of the inter- and subtidal area in the period of 1996 to 2016 in analogy to Section 4.2.4 (in m^3/m^2, i.e., m). The total sediment volume denotes the sum of the sub- and intertidal sediment volume.

Peak subtidal sediment volume losses of up to $-8.5\ m$ were noted in the Ems (DEL) and Weser estuary (NEUW_S & NEUW_N, Figure 4.7, a) with an average loss of $-2.2\ m$ across all units. In contrast, the intertidal sediment volume increased in most units with high accretion of 6.5 m (BOS), 8.4 m (DEL) in the Ems or 5.5 m (ALW) to 5.9 m (NEUW_S), or 5.3 m (BKA) in the outer Weser. The intertidal sediment volume increased on average by 2.4 m across all units in the observed period. Changes in subtidal sediment loss and intertidal volume gain were linearly correlated ($R = -0.84$) despite the resulting total sediment volume not being entirely closed (Figure 4.7, b).

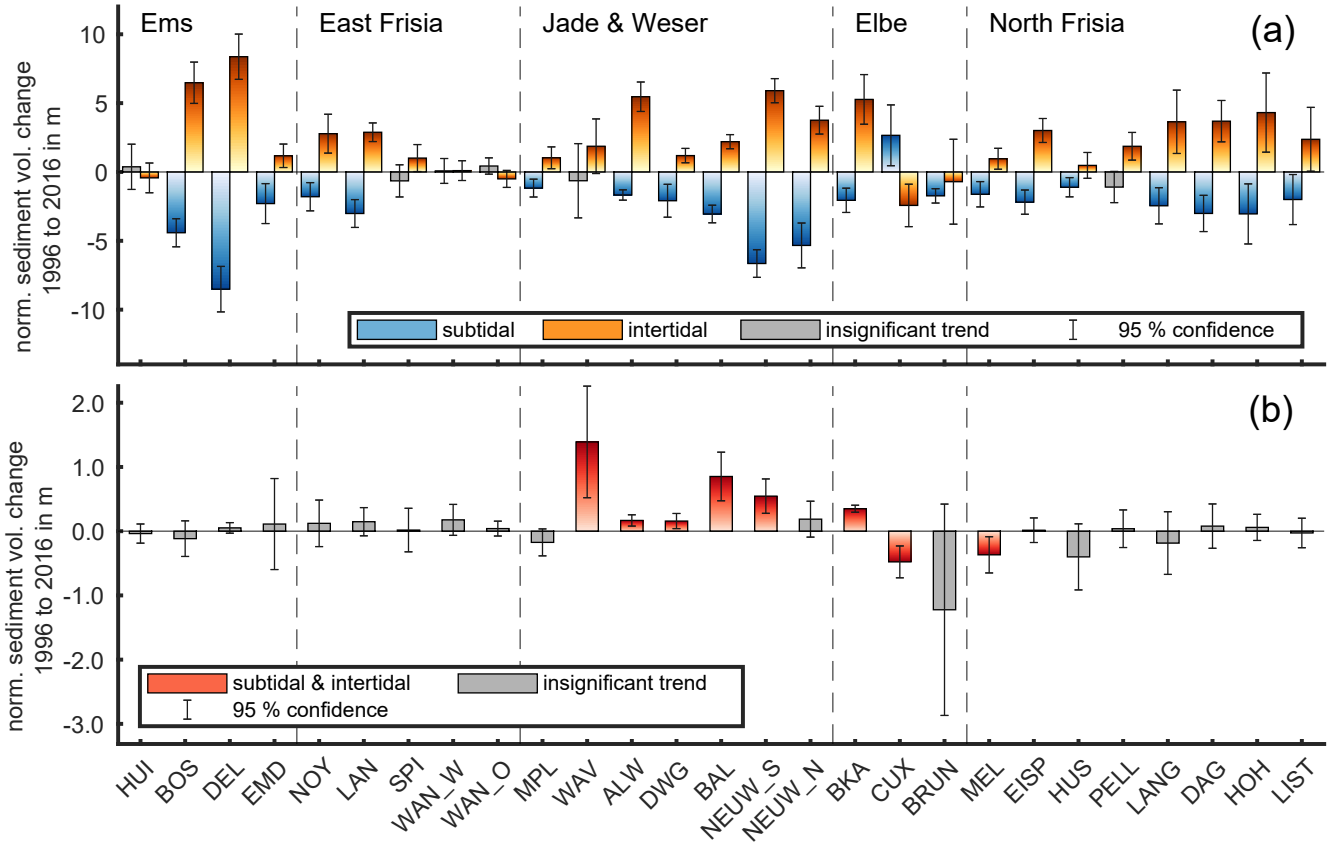

FIGURE 4.7: Normalized changes in subtidal (shaded blue bars in a), the intertidal (shaded brown bars in a), and total (shaded red bars in b) sediment volume in the period of 1996 to 2016 from linear regression. Gray bars represent insignificant regression slopes.

The total sediment volume was balanced across most units within the study area with peak significant gains of 1.4 m (WAV), 0.8 m (BAL), 0.5 m (NEUW_S), and 0.2 m (NEUW_N) in the Jade and Weser estuaries. Significant losses of sediment by -0.5 m (CUX) or -0.4 m (MEL) were observed within and north of the Elbe estuary. Many minor insignificant gains and losses in total sediment volume by less than 0.2 m were present in Ems estuary, in East Frisia, and in North Frisia which, again, indicated that the subtidal sediment loss was compensated by intertidal accretion. The overall average confirmed this impression with a gain of 0.05 m. Units in the Weser and Jade presented with an overall significant sediment gain which points towards enhanced sediment deposition. It should be noted that the increases in total sediment volume are small in comparison to the sediment volume shifts in the subtidal and intertidal zone (Figure 4.7, a).

4.3 Changes in Intertidal Surface Sediments

KEYPOINTS:

- Surface sediment data *indicated* more mixed and mudflats at the cost of sandy tidal flats in the southern German Bight.
- $^2/_3$ of the retreating sandy tidal flats transformed into mixed and $^1/_3$ into mudflats.

In this section, the mud content of intertidal flats and its development was extrapolated (for methodology see Section 3.9) using decadal surface sediment data (Section 3.2). Intertidal surface sediments were distinguished by their cohesive content into muddy, mixed, and sandy tidal flats (following the classification of Ragutzki, 1980). Mark that surface sediment observations underlay a vast amount of processing and interpolation steps to compensate a limited amount of observational samples. Additionally, the seasonal variability of the mud content cannot be captured by annual surface sediment data due to poor field data availability. Therefore, the results in this section can only be used as *indicators* as they possibly do not represent surface sediments at the respective time.

4.3.1 Review of the Data-Driven Tidal Flat Classification

First, the results of the calibrated data-driven tidal flat classification were compared to the verified remote sensing results of the year 1993 in the eastern outer Weser and East Frisia (Meyer

TABLE 4.1: Comparison of a remote-sensing vs. a data-driven tidal flat classification in the Jade and Weser estuary in the year 1996.

flat type	MR97 (abs.) in km^2	MR97 (rel.) in %	data-driven (abs.) in km^2	data-driven (rel.) in %
all	1,400	100	1,105	100
sandy	1,130	80.1	826	74.7
mixed	169	12.0	171	15.5
muddy	89	6.3 (+2.3)	107	9.7

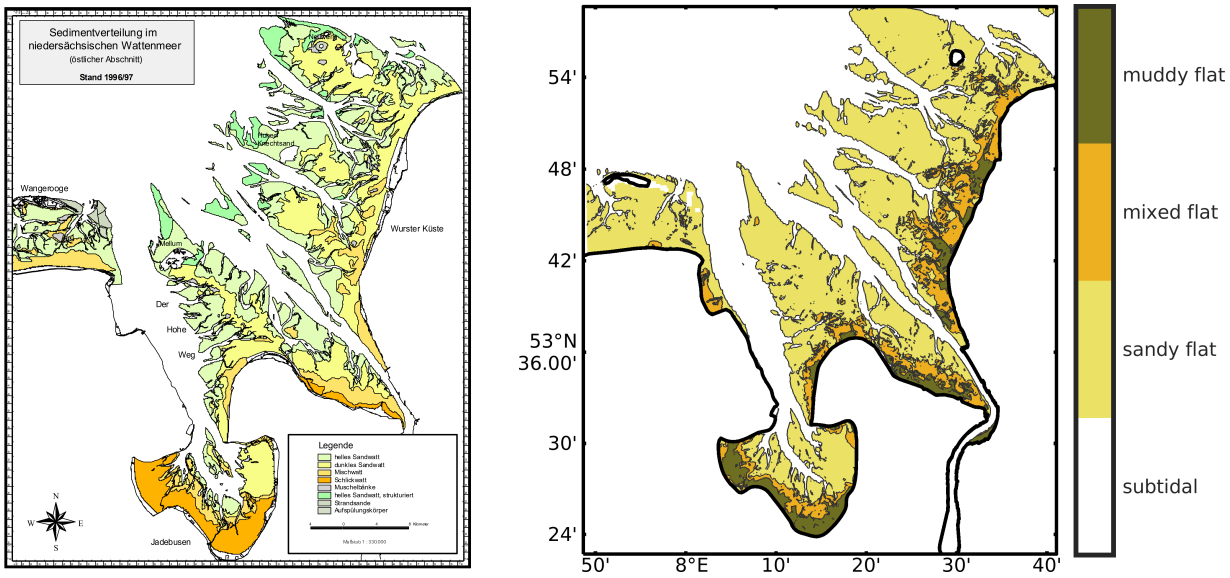

FIGURE 4.8: Visual comparison of remote-sensing tidal flat classification from MR97 (left) and a data-driven approach (right) with white patches representing the subtidal zone, yellow patches sandy, light-brown patches mixed, and dark-brown patches mudflats.

and Ragutzki, 1997, MR97 in the following).

The visual comparison (Figure 4.8) showed good qualitative agreement. Muddy and mixed patches were evident in the eastern outer Weser in the data-driven and in the remote-sensing approach alike and outer tidal flats were predominantly sandy. The visual agreement was poor at the sheltered flats behind the barrier island Wangerooge because remote sensing suggested mixed flats while the data-driven representation computed sandy flats. Furthermore, the lateral intertidal extent differed between both scenes which could be related to the time of the evaluated remote-sensing image or to inaccurate bathymetry data. In addition, MR97 included mussel banks (approx. 2.3 % of tidal flats in East Frisia in the year 1993) in their classification which cannot be captured by the median grain size and the grain size distribution skewness.

Another comparison of absolute and relative tidal flat type area in East Frisia (Table 4.1) solidified the good visual impression by showing reasonable relative agreement $\pm 6\%$. The total area disagreed by approx. 400 km^2 between both approaches which was likely related to the remote sensing scene of MR97: Even though MR97s scene was recorded at low water, the data-driven approach uses one of the lowest annual low waters (i.e., the SpLW, definition given in Section 3.8) of the year 1996.

4.3.2 Surface Sediment Data Suggest Intertidal Siltation

The data-driven classification method was subsequently applied in six subregions in the German Bight for closer examination: the entire German Bight, the Ems estuary, East Frisia, the Jade & Weser estuary, the Elbe & Eider estuary, and North Frisia. The classification revealed marginal changes for all tidal flat types in North Frisia which is why this region was not mentioned subsequently.

The data-driven surface sediment classification (Figure 4.9) showed an overall retreat of sandy flats by 4 % in the German Bight in the period of 1996 to 2016. Retreat rates were highest in the

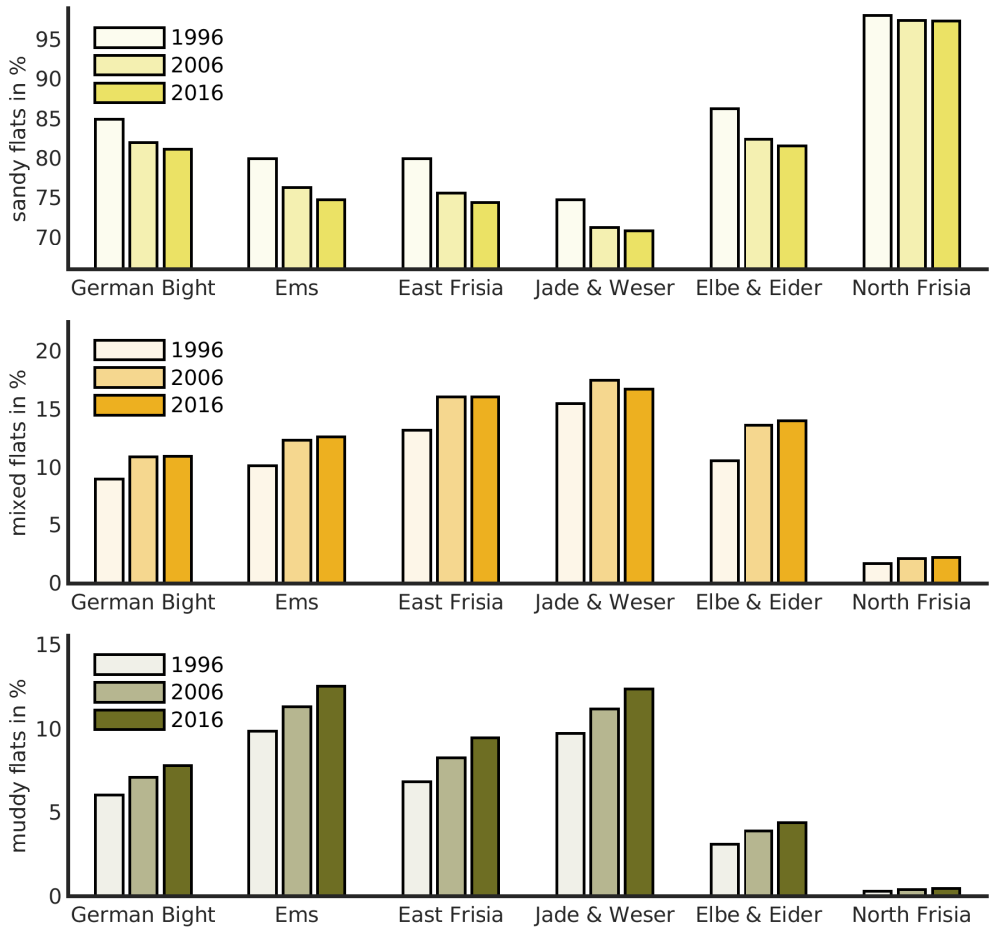

FIGURE 4.9: Changes of the geological intertidal flat type (after Ragutzki, 1980) in the years of 1996, 2006, and 2016.

Ems and East Frisia (approx. 10 %) and the difference between the years 1996 and 2006 was larger than 2006 to 2016 which was surprising given the linear lateral and vertical intertidal expansion noted in Sections 4.2.2 to 4.2.3. The data showed a similar decline of sandy flats in the Jade & Weser and in the Elbe & Eider area even though it should be noted that differences between 2006 vs. 2016 were marginal.

Retreating sandy flats coincided with expanding mixed and mudflats. Again, larger differences were seen in the period of 1996 to 2006 for mixed tidal flats as most mixed flat areas languished between the years 2006 and 2016. Conversely, muddy areas expanded linearly at lower rates (approx. 2.5 % per year). Slow siltation is reasonable considering the depositional properties and low sinking velocities of fines.

In summary, sandy flats declined while mixed and muddy areas expanded in the period of 1996 to 2016 despite lateral intertidal expansion. Since the newly expanded, often shoreface, parts of tidal flats are likely exposed to waves (i.e., high energy), I assume that they should be sandy. An increase of mixed and mudflats, despite new sandy shoals, therefore suggests enhanced coastal siltation − always considering the uncertainty of the input surface sediment data.

Chapter 5
Finding Changes in Tidal and Non-Tidal Forcing

Contents

5.1 Chapter Structure

This section evaluates recent changes in tidal and non-tidal forcing with a particular focus on changes in Lagrangian and Eulerian tidal asymmetry as indicators for an offset in the dynamical equilibrium in the German Wadden Sea. I chose to investigate the anomaly of the median SSH, peak SSH (Section 5.2), and waves (Section 5.3) with modeling data (Section 3.2) over the nodal cycle of 1997 to 2015 to estimate possible changes in Lagrangian asymmetry from external forcing. Then, I direct my attention to the development of tidal constituents (Section 5.4) and Eulerian tidal asymmetry descriptors (Section 5.5) as an estimate for changes in local sediment transport properties.

5.2 Sea Surface Variability

KEYPOINTS:

- Perennial mean sea level (MSL) fluctuation is higher than SLR in the nodal cycle of 1997 to 2015.
- No significant or noteworthy changes were found in peak SSH. A linear trend indicated a statistically insignificant increase of 10 $mm\ yr^{-1}$ to 15 $mm\ yr^{-1}$.

The following section is an assessment of the modeled SSH (see Section 3.2) with the quantile method (Woodworth and Blackman, 2004). The quantile method assumes the median SSH to be a good approximation for MSL and the 99.9^{th} SSH quantile to represent peak SSH. The 99.9^{th} quantile corresponds to annual 8.5 highest hourly samples of 10-minute equidistant data. Woodworth and Blackman (2004) furthermore suggested to subtract the median from the 99.9^{th} quantile to remove relative MSL fluctuation.
I used model data intentionally in this section as these data were continuous and did not underlie measurement error or data gaps. This section was aimed to translate *established* MSL trends into a local setting. It is recognized that the study period is too short for robust trend estimation; hence, the following data were intended primarily as a system description during the period of enhanced coastal siltation. The global MSL development is thoroughly documented in the most recent IPCC reports (currently: Oppenheimer et al., 2019) and summed up in Section 2.2.2. All data in this section were expressed by their anomaly, i.e., the study period's mean was subtracted from the respective annual data.

5.2.1 Mean Sea Level

The development of the modeled median SSH anomaly (median SSH $-$ average median SSH, Figure 5.1, top) varied in the low centimeter range in the nodal cycle of 1997 to 2015. The lowest median SSH anomalies were evident in the late 1990s to the mid 2000s. The data varied by few centimeters each year at the modeled tidal gauges. Peaks were observed in the years 2007, 2008, and 2015 and minima in the years 1997, 2010, and 2013.
An ordinary linear regression of the median SSH anomaly (slope in Figure 5.1, bottom) reflected current SLR rates with spatially varying increases between 0.5 $mm\ yr^{-1}$ to more than

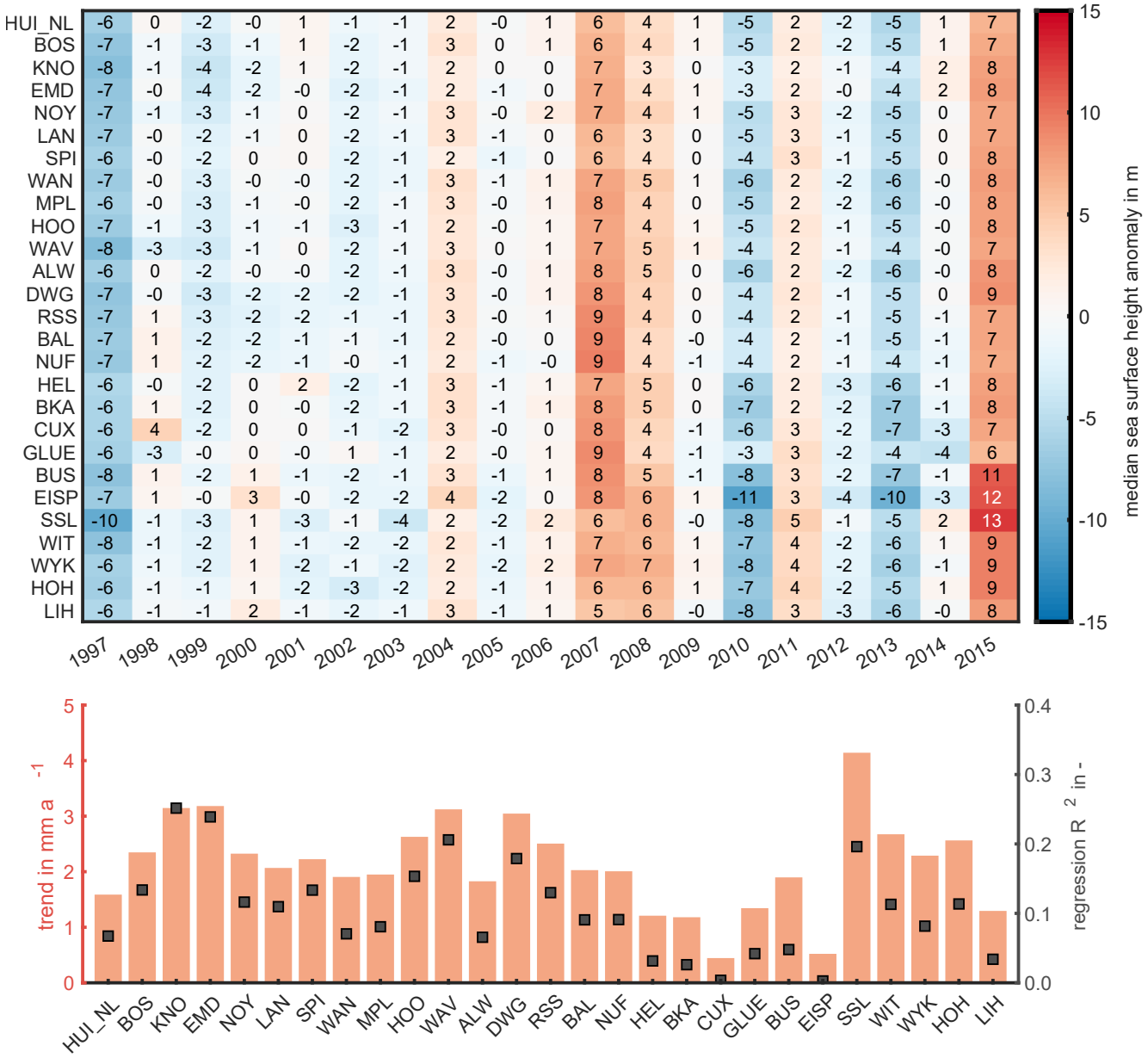

FIGURE 5.1: The development of the modeled median SSH anomaly at selected gauges in the nodal cycle of 1997 to 2015 (top) and a linear trend analysis (bottom) with red bars indicating the slope of the linear regression (left axis) and the gray dots the regressions index of agreement R^2 (right axis).

4 $mm\ yr^{-1}$. It must be noted that the indices of agreement R^2 indicated statistically insignificant linear regression notwithstanding which is why this information must be interpreted with care. The highest increase rates were observed in North Frisia (SSL), in the inner Ems (KNO, EMD), Jade (WAV), and Weser estuary (DWG). Contrary, the lowest rates were evident at the offshore gauges (HUI_NL, HEL, BKA), in the Elbe (CUX, GLUE), and Eider (EISP) estuaries. Although the linear regression slopes indicated similar annual increase rates as the IPCC report, perennial MSL fluctuation often outweighed the effect of SLR in the regarded time period. The median SSH anomaly in the period of 2010 to 2015 reflects this observation well with a span of more than 20 cm in relative MSL at several gauges.

5.2.2 Peak Sea Surface Heights

The previous MSL anomaly analysis was extended to peak SSH, as represented by the anomaly of the 99^{th} SSH quantile minus its median, in this section. I noticed SSH anomaly peaks in the years 1999 (storm Anatol), 2007 (storm Kyrill), and 2013 (storm Xaver). Within these peaks, only Xaver affected the entire German Bight while Anatol and Kyrill surpassed North Frisia. Minor peaks were evident in the years 2011 and 2015 and an ordinary linear regression of the peak SSH anomaly data revealed no statistically significant trends.
Insignificant regression results indicated an overall increase of peak SSH anomaly in the entire study area which is in line with literature (Dangendorf et al., 2013) and current climate projections (Ganske et al., 2016; Oppenheimer et al., 2019). All offshore stations (e.g., HUI_NL, HEL,

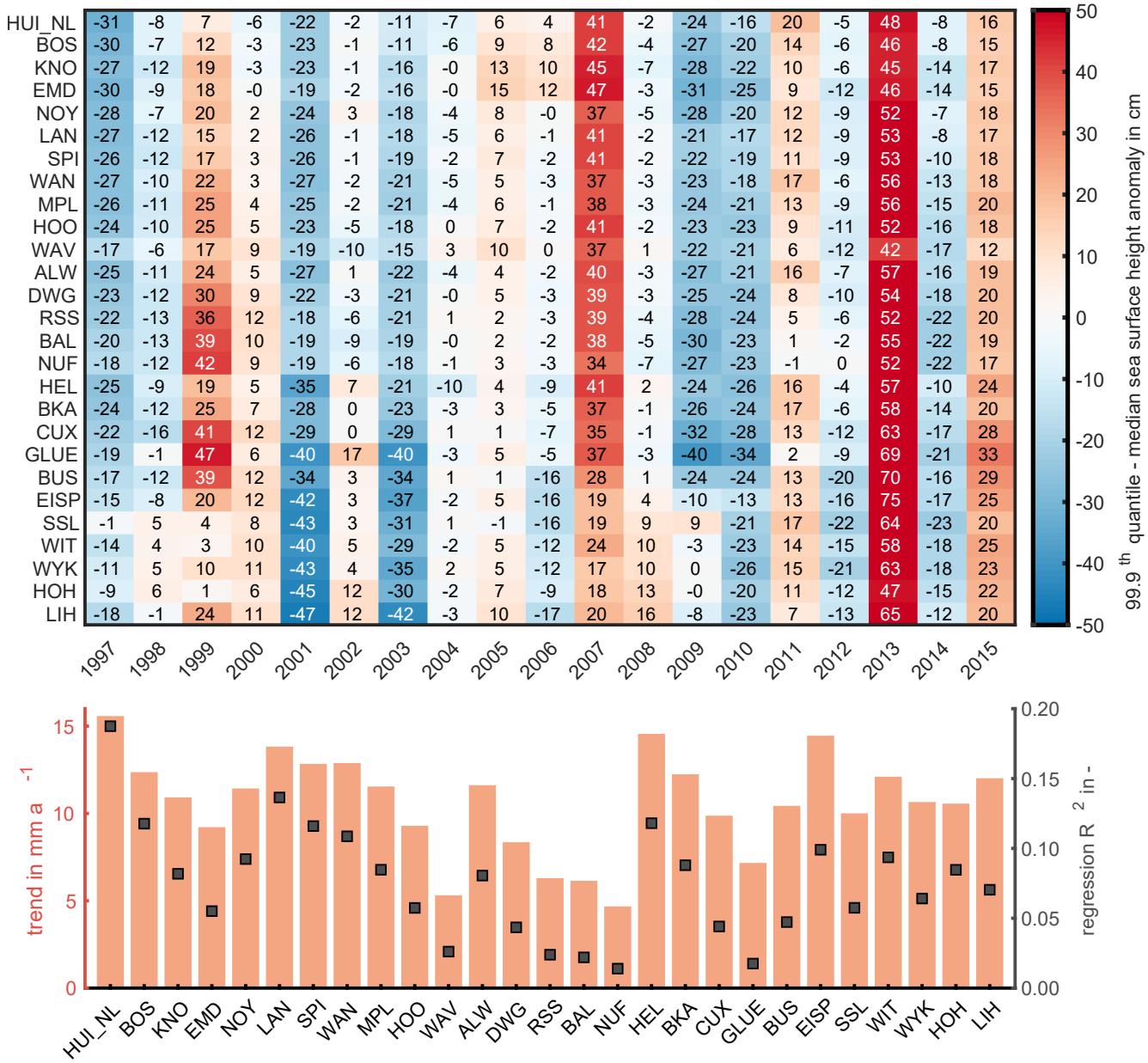

FIGURE 5.2: The development of the modeled peak SSH anomaly (expressed by the 99.9^{th} SSH quantile minus the median SSH) at selected gauges in the nodal cycle of 1997 to 2015 (top) and a linear trend analysis (bottom) with red bars indicating the slope of the linear regression (left axis) and the gray dots the regressions index of agreement R^2 (right axis).

ALW, BKA) exhibited a similar increase rate in peak SSH anomaly. Still, there was no evidence of noteworthy perennial fluctuation. More frequent or intense peak SSH were also not found in these data.

5.3 Wind-Waves

KEYPOINTS:

- No trends could be identified within the significant wave height's anomaly.
- The mean wave direction anomaly indicated more seaward-directed waves in the second half of the nodal cycle from 1997 to 2015.

This section presents the development of the modeled median and peak (i.e., the 99.9^{th} quantile) significant wave height anomalies at wave gauges in the German Bight over the nodal cycle of 1997 to 2015 (see Appendix D.1, Figures D.1 to D.2) and of the mean wave direction. Again, modeled wave data were chosen over observations because of poor gauge coverage and data quality.

5.3.1 Significant Wave Heights

The modeled median significant wave height anomaly remained nearly constant in the covered time with annual variation of less than 15 cm. A linear trend analysis (not included) indicated a statistically insignificant increase by less than 0.25 $cm\ yr^{-1}$ at all gauges. Only the gauge DB-WR demonstrated higher increase rates while the significant wave height at the sheltered Jade-I stations decreased marginally by 0.1 $cm\ yr^{-1}$. As most of these rates were below model accuracy (see Section 3.3), I assumed that the median significant wave heights at gauges remained unchanged in the study period.
Peak significant wave heights also did not reveal any noteworthy information. Peak significant wave height anomalies were noticed in the years 1999, 2007, and 2013 and minimum values in the years 2001, 2003, 2009, 2010, and 2014. A trend analysis (not included) confirmed that no significant trend was present.

5.3.2 Mean Wave Direction

The high RMSE of the modeled wave direction led me to split the wave direction at peak frequency into two categories: landwards (northwest to southwest), and seawards (southwest to northwest). Furthermore, I discarded all direction samples with small significant wave heights (i.e., $h_{m0} \leq 0.5\ m$) before estimating the landwards and seawards duration anomaly in days (Figure 5.3).
The duration anomaly of landward-oriented waves showed a high amount of annual and local variability. Offshore gauges (i.e., FINO-III, NSB-III, DB-WR) all exhibited a similar behavior with less landwards-oriented waves in the period of 2000 to 2003, followed by more landwards wave attack (2004 to 2006), and another less active period in the period of 2009 to 2014. Peaks of landwards-oriented wave duration anomaly were observed in the years 1998, 2004, 2007,

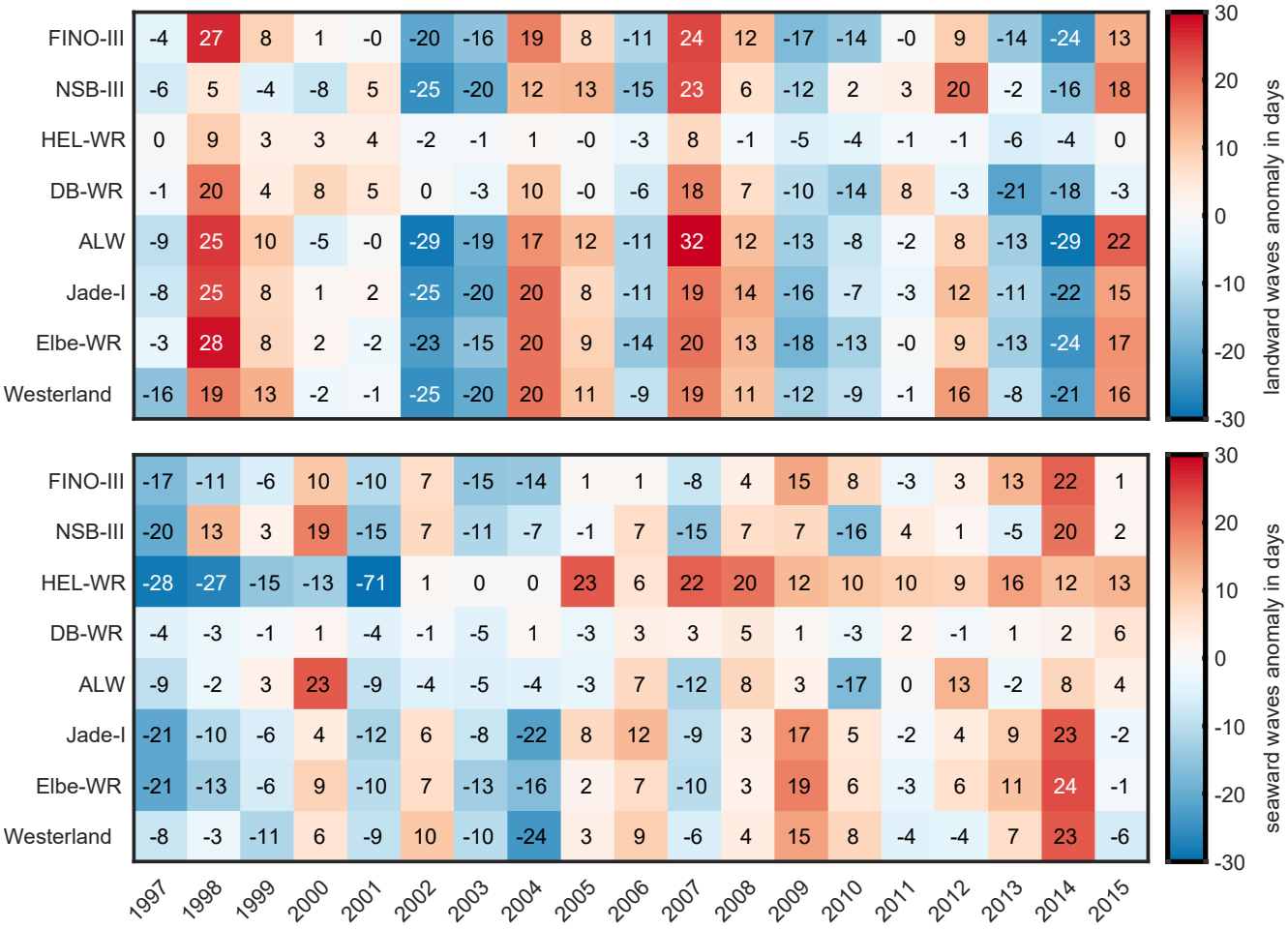

FIGURE 5.3: The development of the anomaly of the landward (top) and seaward (bottom) directed waves at selected gauges in the nodal cycle of 1997 to 2015.

2008, and 2015. Conversely, anomaly of the duration of seaward-oriented waves was lower in the first half of the evaluation period (1997 to 2004) and was slightly elevated by several days in the second half of the time period (2005 to 2014). Peaks of the seaward-oriented wave duration anomaly were observed in the years 2000, 2009, and 2014.

5.4 Recent Shifts of Tidal Constituents

KEYPOINTS:

- Diurnal and semidiurnal tidal constituent amplitudes adapted by ± 2 % while quarter and sixth-diurnal constituents changed by ± 30 % in the nodal cycle of 1997 to 2015.
- The phase of semidiurnal tidal constituents was delayed by approx. 4 degrees. Quarter- and sixth diurnal constituent phases delayed by 5 to 10 degree in the same period.

Eulerian asymmetry arises from the amount of frictional resistance a tide needs to overcome when entering and departing a tidal system. In other words, tidal distortion appears whenever tides enter shallow water. Harmonic analysis describes tidal asymmetry through the generation of higher frequency (i.e., quarter-, sixth-, to n-th diurnal) shallow water constituents

TABLE 5.1: Tidal constituent amplitudes in Cuxhaven Steubenhöft (CUX) from observations in the year 2015. The table shows all constituents with an amplitude ≥ 4 *cm*.

no.	tidal constituent	amplitude in m	no.	tidal constituent	amplitude in m
1	M_2	1.36	9	NU_2	0.07
2	S_2	0.33	10	O_1	0.07
3	N_2	0.22	11	MS_4	0.07
4	MU_2	0.13	12	K_1	0.07
5	L_2	0.13	13	$2MS_6$	0.07
6	M_4	0.11	14	K_2	0.07
7	SSA	0.11	15	λ_2	0.05
8	M_6	0.07	16	$2MN_6$	0.04

which drain energy from their parent constituents. The previously identified significant morphological changes in the German Wadden Sea (Chapter 4) make changes in Eulerian tidal asymmetry probable as indicated by the theoretical work of Friedrichs (2010, see Section 3.6). Spatial changes of the amplitude and phase of relevant tidal constituents were investigated with observations and model data to identify if, where, and to what extent changes in tidal constituents occurred.

However, tidal constituents underlie interannual, annual and perennial variability, and multidecadal trends (e.g., Müller, 2011). With respect to my research goals, interannual tidal constituent modulation was omitted by using annual time frames (following Hagen et al., 2021a). I recognize that seasonal tidal constituent modulation may be subject to change.

A review of tidal constituents at the estuarine gauge Cuxhaven Steubenhöft (CUX) in the Elbe estuary (Table 5.1) illustrates the dominance of semidiurnal tides ($F = A(\frac{O1+K1}{M2+S2}) = 0.08$) in the German Bight. Even though the shallow water constituent M_4 was among the largest amplitudes, the M_4/M_2 ratio was only at 8 %. The presence of multiple quarter and sixth-diurnal shallow water tides indicates tidal distortion.

5.4.1 Spatial Amplitude and Phase Changes

Let us review the spatial changes of the semidiurnal M_2 constituent and its first overtide M_4 (Figure 5.4). A harmonic analysis was conducted on modeled SSH at the nodal modulation maxima of the M_2 constituent in the years 1997 and 2015. Differences in tidal constituent properties can therefore only result from meteorological bias, thermohaline stratification changes, global or regional trends in tidal constituents, or bathymetry changes.

Figure 5.4 (a) shows changes of the M_2 amplitude in the order of centimeters in the reviewed period. The Ems and Elbe estuaries exhibited decreasing M_2 amplitude by 1 *cm* to 3 *cm* while slight increases were present in East Frisian inlets, in the Jade and Weser estuary, and in North Frisian inlets. The basins near Sylt indicated a noteworthy local increase in M_2 amplitude by more than 3 *cm* while the M_2 amplitude in the neighboring North Frisian basins increased by 1 *cm* to 2 *cm*. Changes in M_4 amplitude (Figure 5.4, c) remained local: Increases by several *cm* were observed in the Juist basin, in the Jade, Weser, and outer Elbe estuary as well as North Frisia. Contrary, East Frisian tidal inlets exhibited locally isolated decreases by 2 *cm* to 3 *cm*.

Despite locally varying amplitude changes, the phase of the M_2 constituent remained nearly

constant with a slight overall decrease of less than 5 degree (Figure 5.4, b). The M_4 phase (Figure 5.4, d) demonstrated more pronounced phase shifts with decreases of more than 10 degree in the Ems, Jade, and Weser estuary, and in East Frisian and North Frisian inlets. The M_4 amphidrome north of the Ems estuary moved northwestward which corresponds well with increased amplitudes in the German Bight. All tidal inlet systems exhibited M_4 phase changes of ± 10 degree except for the Sylt basins which remained constant. The observed amplitude

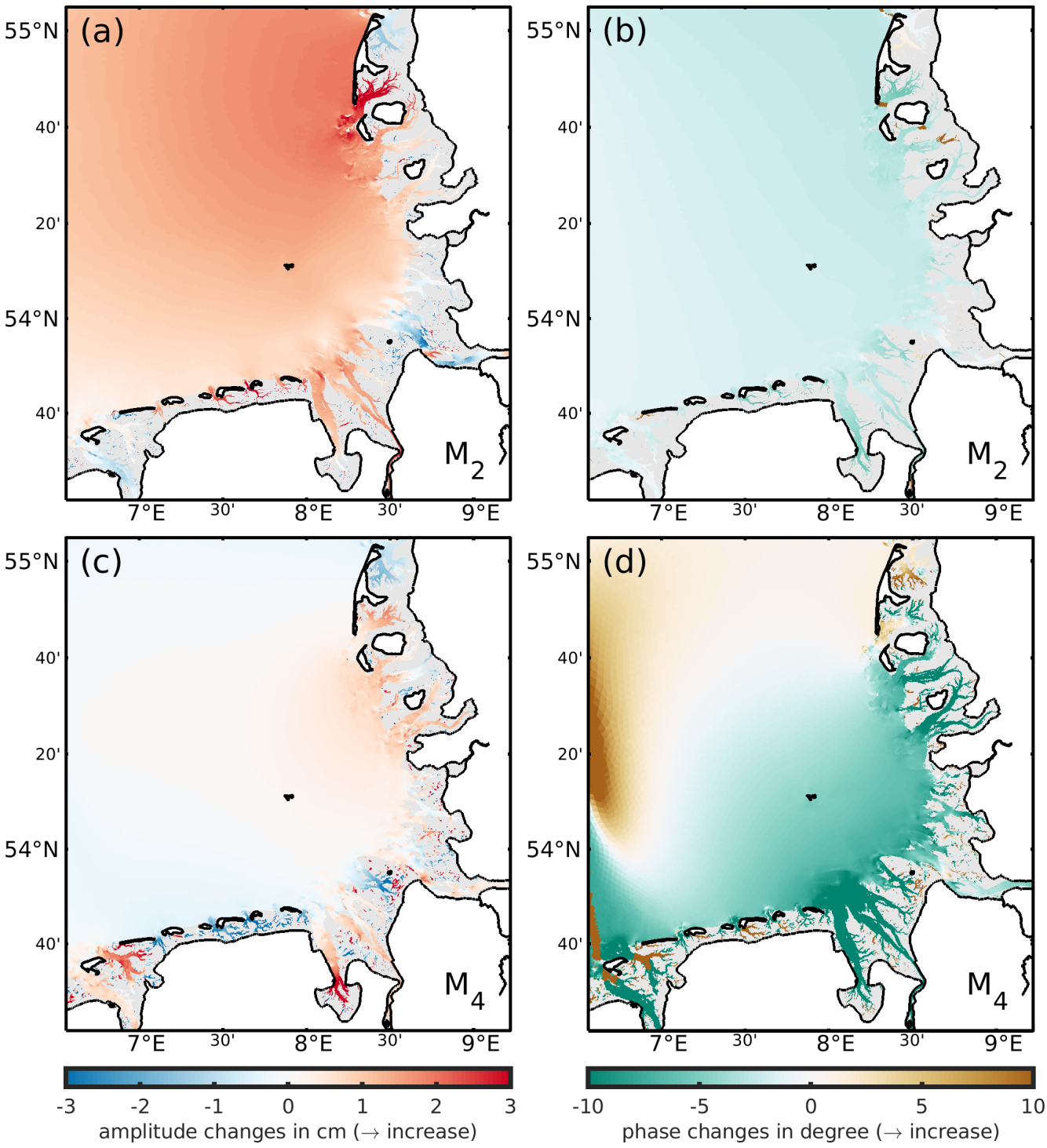

FIGURE 5.4: Spatial differences of the modeled M_2 (a, b) and M_4 (c, d) amplitude (a, c) and phase (b, d) at the diurnal nodal minimum in the years 1997 and 2015 ($\Delta = 2015 - 1997$). White patches indicate land and gray patches intertidal flats.

and phase development were remarkable considering the short time frame of one nodal cycle.

5.4.2 Observational Data Trend Assessment

The changes in amplitude and phase of M_2 and its first overtide M_4 (Figure 5.4) indicated changes in tidal properties. Moving forward, relevant constituents (i.e., Table 5.1) were examined with multiple nonlinear regression (see Section 3.4.1) to extract information on their long-term development. This method requires long SSH time series ($\Delta t > 18.6\ a$) which is why I switched from modeled to observational gauge data in this section only. I used the same data mentioned in Hagen et al. (2021a) at their maximum survey length (data availability: Section 3.2). An exemplary trend analysis of the M_2 amplitude in CUX in the period of 1918 to 2018 illustrates a near-linear amplitude increase with a slight acceleration in the 1990s and the nodal amplitude modulation (Figure 5.5). Numerous observed M_2 samples deviated from the nonlinear regression line which I related to estuarine engineering in combination with natural morphodynamics in the mouth of the Elbe estuary over the course of the 20^{th} and 21^{st} century. The nonlinear multiple regression (including nodal modulation) failed to meet the criterion for statistical significance (i.e., $R^2 > 0.5$ after Hagen et al., 2021a; Peng et al., 2019) for the amplitude of the SSA, μ_2, NU_2, λ_2, and L_2 tidal constituents. The nonlinear dependence of tidal constituents on the development of related constituents, MSL variability, and local bathymetry evolution are likely explanations that also reflect in the locally varying statistical significance of the shallow water constituents. Remaining significant data were evaluated for the nonlinear regression parameters a_0, a_1, and a_2 (from Equation 3.1) at the diurnal nodal modulation minimum in the years 1997 and 2015. I calculated amplitude changes by $\Delta A = 1 - \frac{A_{1997}}{A_{2015}}$, and phase shifts by $\Delta g = g_{2015} - g_{1997}$ (Figure 5.6).
Most diurnal and semidiurnal amplitudes varied by $\pm 2\%$ with few examples. Despite the small relative deviation of M_2, absolute changes resulted in the largest absolute variations (maximum: $5\ cm$). Other diurnal and semidiurnal constituent amplitudes decreased in the Dutch

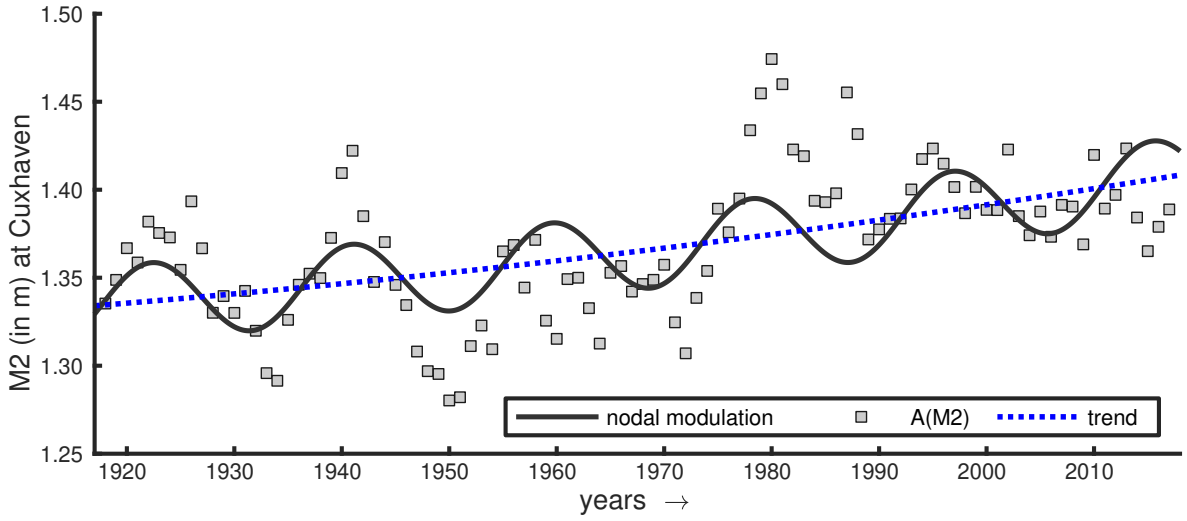

FIGURE 5.5: Exemplary multiple nonlinear regression analysis with the blue dashed line representing the multi-decadal development and the gray solid line the nodal modulation for the amplitude of the semidiurnal M_2 tidal constituent (gray squares) in Cuxhaven Steubenhöft (CUX) in the period of 1918 to 2015.

Wadden Sea (IJB NL to SMG NL) and increased in the German Bight (BOS to WYK) by few percent. The quarter- and sixth-diurnal shallow water tides amplitudes in the Dutch Wadden Sea (HAR NL to SMG NL) and in the Ems estuary (EEM NL to DEL NL) increased from 2 % to more than 20 %. The gauges HEL and ALW exhibited only marginal changes in the shallow water domain which was expected because of their deep water setting. Shallow water tide shifts in BUS could be related to ongoing morphodynamic adaptation after a land reclamation campaign in the 1970s. Summarizing, an overall increase of the diurnal and semidiurnal tidal amplitudes by few percent in combination with locally varying significant changes of the quarterdiurnal and sixthdiurnal shallow water amplitudes in the German Bight was noticed.

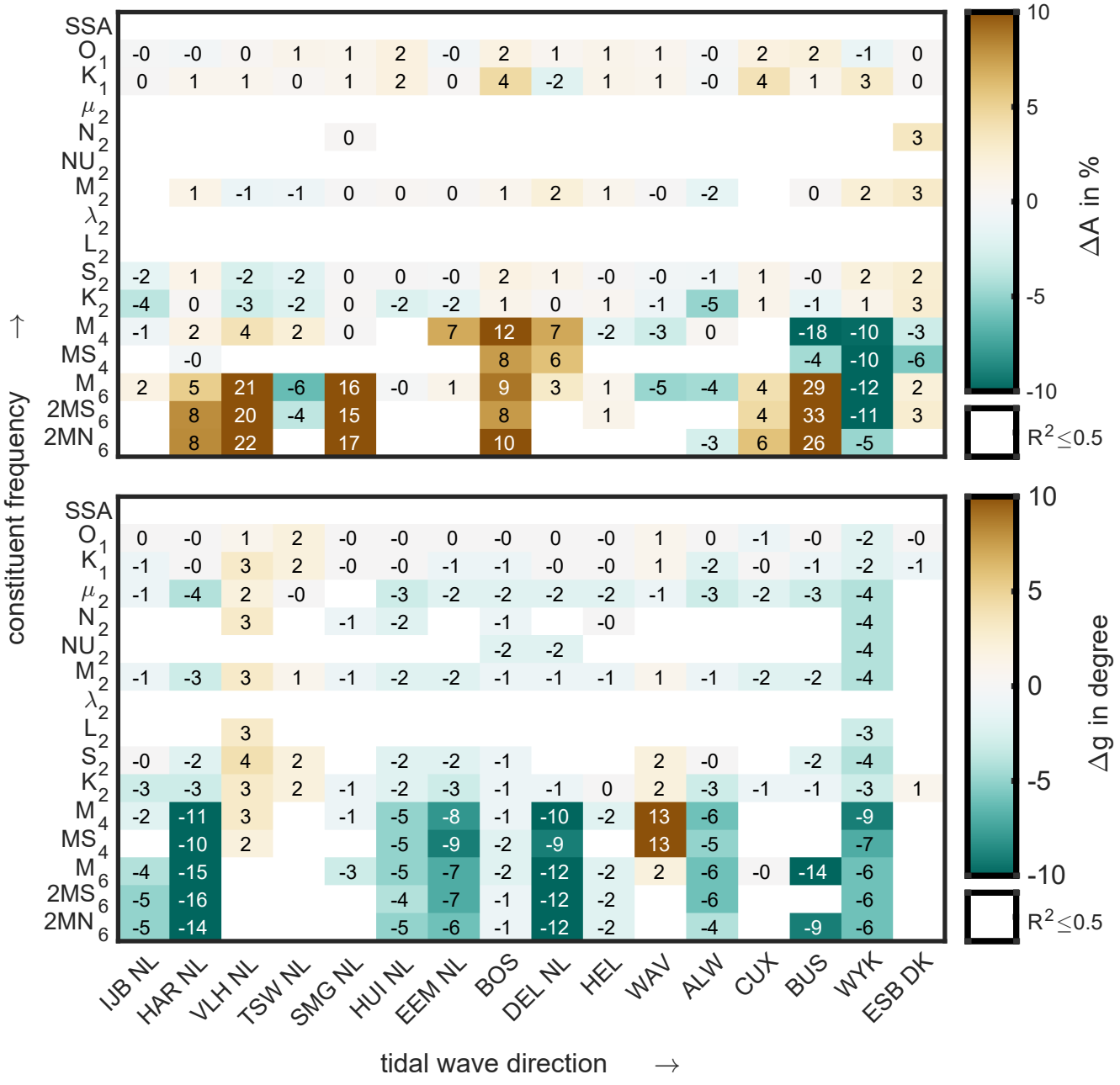

FIGURE 5.6: Observed tidal constituent amplitude (top) and phase (bottom) changes in the period of 1997 to 2015 from nonlinear multiple regression (excluding nodal modulation). Brown patches indicate increases and cyan patches decreases in amplitude and phase over time. All values with $R^2 \leq 0.5$ were considered statistically insignificant (white patches).

Phase differences revealed that nearly all gauges and constituents were delayed by several degree in the year 2015 with few local exceptions (e.g., VLH NL, TSW NL, and WAV). Diurnal constituents remained mostly unchanged while semidiurnals delayed between 2 to 4 degree (5 degree correspond to approx. 10 minutes for the M_2). As most phase shifts were regionally consistent, a tidal constituent phase shift or amphidrome movement in the entire Wadden Sea could be possible (as also indicated in Figure 5.4). Again, changes in the quarterdiurnal and sixthdiurnal constituents were more pronounced with most gauges being delayed by up to 16 degree (5 degree are $\approx$ 20 minutes for the M_4). It was a reoccurring pattern that nearshore gauges demonstrated strong shifts in the shallow water domain.

5.5 Changes in Eulerian Tidal Asymmetry

KEYPOINTS:

- Tidal basins and estuaries in the German Bight became less flood dominant or more ebb dominant (TDA, FVA) in the period of 1996 to 2016.
- Competing local and regional phenomena were found: North Frisia, e.g., was affected by a large-scale increase and by a local decrease in flood duration.
- The mean flood velocity decreased more than its ebb counterpart.
- Increasing flood and ebb slack duration was found. Flood slack usually increased more than ebb slack (i.e., increasing FDA).

Bathymetry evolution (Section 4.2) and shifts in tidal constituent amplitude and phase (Section 5.4) suggest changes in tidal dynamics and asymmetry. As distinct flood and ebb properties are also established estimators for the residual sediment transport in coastal waters (Section 2.1), this section focuses on the development of Eulerian tidal asymmetry (i.e., TDA, FDA, and FVA, see Table 3.5) at the study site with the morphological averaging method (see Section 3.7) in the period of 1996 to 2016. The results, methodology, tables, and figures in this section were visually modified and reworded from Hagen et al. (2022). It should be noted that all analyses from this section focus on tidal channels as the main pathways of sediments on long time scales.

5.5.1 Morphological Unit Definition

Morphological units were defined in each tidal basin, via estuarine geometry, or near the location of a tide gauge (Figure 5.7). A morphological unit must cover the tidal channels of interest within the entire analysis period. Therefore, some supratidal and intertidal areas close to the coastline were excluded as well as areas with artificial morphological changes e.g., by port construction or dredging. Shoreface polygons (e.g., 11, 15, 20) were limited seawards roughly by the -15 mNHN isobath, and inlet polygons (e.g., 5 to 9) included a small portion of the channel delta up to the -20 mNHN isobath. The outer estuaries of the rivers Ems (1 to 4), Jade (11 to 14), Weser (15 to 19) and Elbe (20 to 25) were divided into multiple units which mainly depend on the location of tide gauges (e.g., green triangles in Figure 5.7).

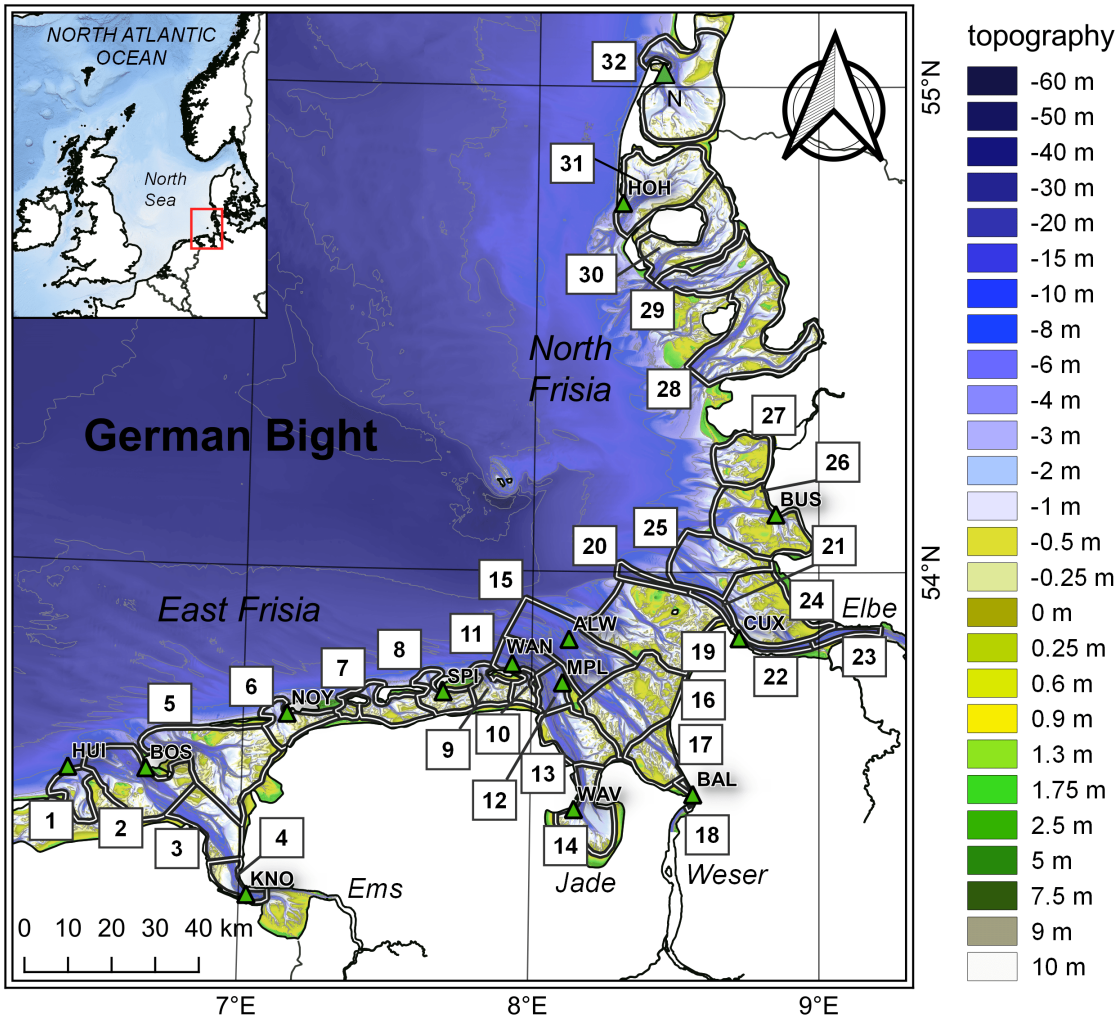

FIGURE 5.7: Morphological units (represented by black and white, solid lines with a number-ID) for subsequent analyses. The background shows the EasyGSH-DB topography (2015) in the German Bight (adapted from Hagen et al., 2022).

5.5.2 Local and Regional Changes in Flood Duration

To obtain an overall impression of changes in tidal asymmetry, the difference between the annually averaged flood duration in the years 1997 and 2015 was calculated (Figure 5.8). Both years represent the diurnal minimum of the nodal tide to minimize astronomical bias. It should be noted that baroclinic bias may be present. However, these processes are unlikely to offset annual averages as, e.g., storm surges are highly episodic and occur only a few times each year. In the following, the term *regional* was used for large-scale (e.g., the German Bight) and *local* for processes in the morphological units (e.g., a tidal basin).

A first observation was that flood duration increased by few minutes in the southwestern and decreased by up to 20 minutes in the northeastern German Bight. Regional changes were either enhanced (southwest) or counteracted (northeast) within local tidal channels. A second observation was that regional changes did not carry over to all tidal systems. In fact, several northeastern tidal channels showed increasing flood duration despite a different regional tendency. Similar phenomena were evident in the southeastern German Bight with flood duration increases of more than 10 minutes in local tidal channels and slight decreases seawards. For

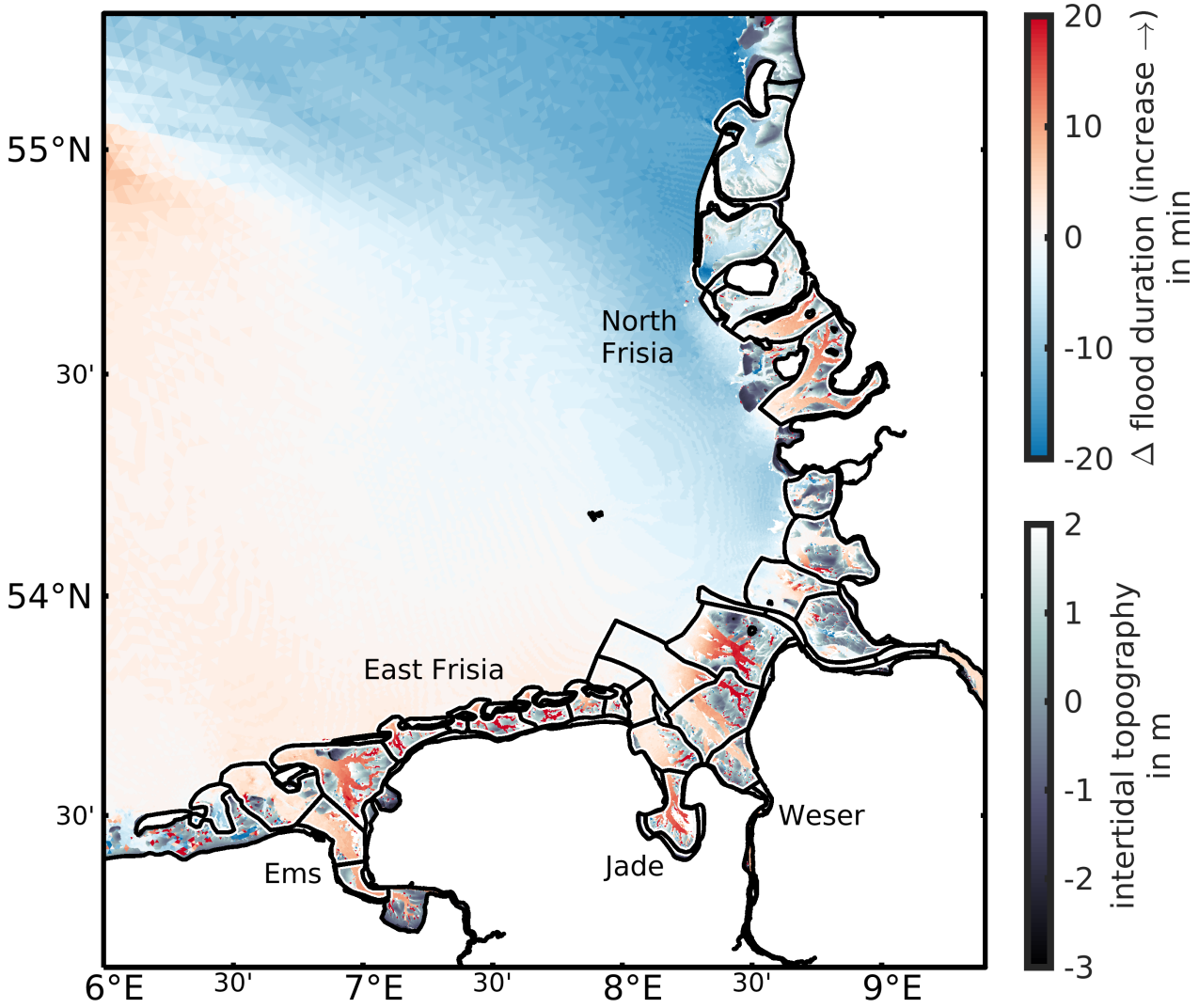

FIGURE 5.8: Difference of the mean flood duration between the years 1997 and 2015 with the red patches indicating increasing and blue patches indicating decreasing flood duration. Only permanently inundated samples of both years are displayed. Land is represented with white patches, the intertidal zone by gray shades, and the morphological units are indicated by black and white solid contours (visually modified from Hagen et al., 2022).

this reason, I presumed that regional tidal dynamics may compete with local processes for flood duration changes.

Inspired by this observation, morphologically averaged trends for the flood to tide duration ratio were estimated in the period of 1996 to 2016 (Figure 5.9). Note that morphological units with insignificant linear trends were also displayed as the consistent temporal evolution of adjacent morphological units may also be of interest (e.g., units 23 to 26). Statistically significant trends were achieved in 24 of 32 morphological units and the local increase in flood duration (i.e., increasing flood to tide duration) from units 1 to 18 confirmed the findings from Figure 5.8. The signal in North Frisia (units 26 to 32) became locally both more and less flood dominant; hence it was likely influenced locally and regionally. Trends in units 27, 31, and 32 exhibited increasing flood dominance that matched with the evident decrease in flood duration. Conversely, adjacent units 28 and 30 indicated decreasing flood dominance in accordance with increasing flood duration in Figure 5.8.

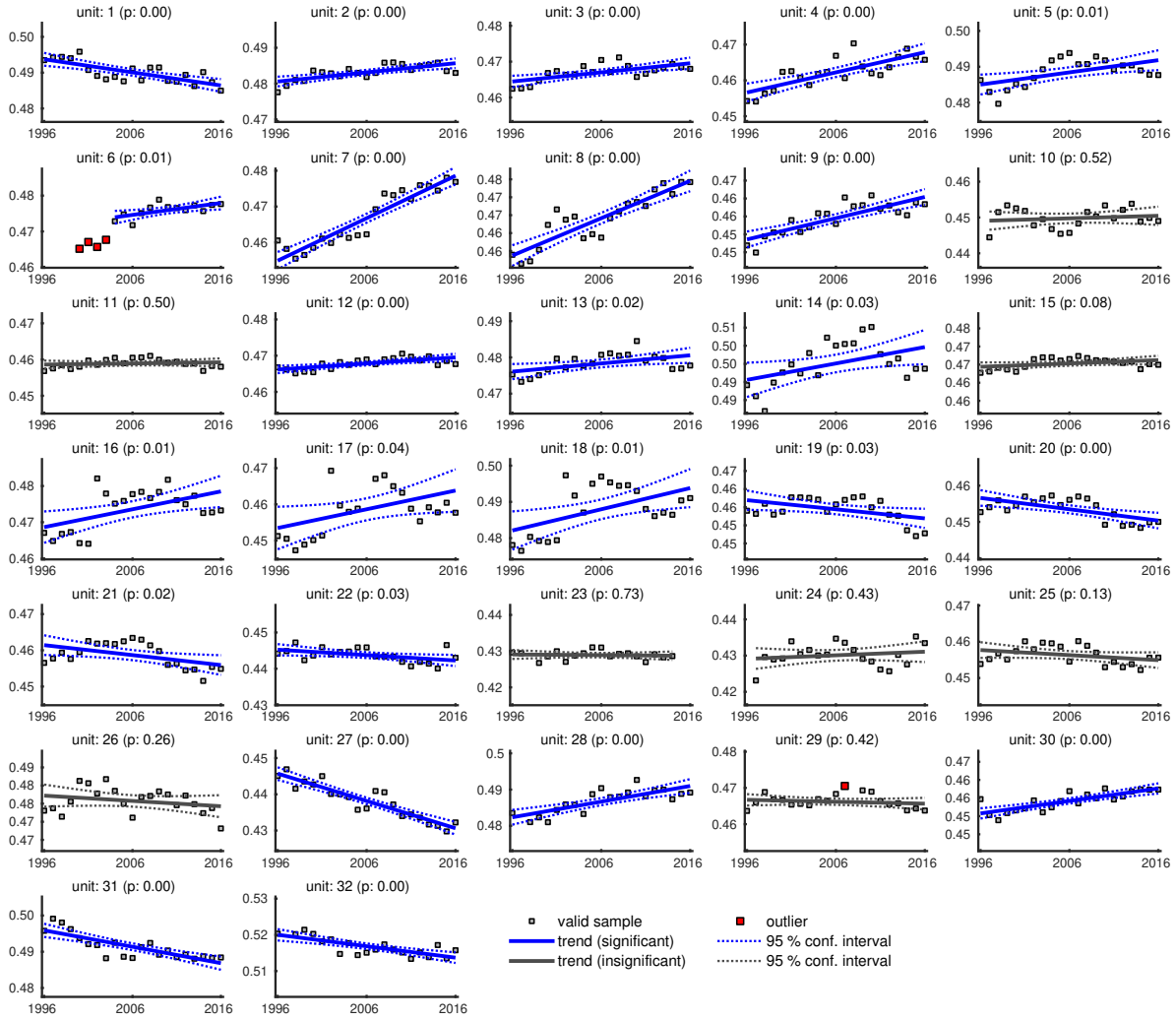

FIGURE 5.9: Linear regression of flood to tide duration ratio for morphological units from Figure 5.7 with ratios < 0.5 representing flood dominance. Solid blue lines indicate significant ($p < 0.05$) trends with their 95 % confidence intervals (dashed). Solid gray lines represent insignificant fitting with their 95 % confidence intervals (dashed). Valid samples within the 95 % confidence intervals are represented by gray and outliers by red squares. Outliers were not considered in trend estimation (adapted from Hagen et al., 2022).

5.5.3 Driving Processes

In idealized systems, tidal asymmetry can be explained based on morphological constraints such as the relative tidal amplitude (i.e., tidal amplitude to mean channel depth ratio a/h) or the intertidal storage volume V_s to subtidal channel storage V_c ratio V_s/V_c (see Section 3.6). In the following section, the development of the (1) tidal range, (2) a/h, and (3) V_s/V_c was investigated using the EasyGSH-DB bathymetries (Section 3.2) and the numerical hindcast (Section 3.3).

Annual changes in mean tidal range exhibited regionally varying increases between 3 $mm\ yr^{-1}$ to 5 $mm\ yr^{-1}$ in North Frisia to less than 2 $mm\ yr^{-1}$ in the Ems estuary and in East Frisia (Figure 5.10). My increase rates were lower than the recently reported 3.3 $mm\ yr^{-1}$ (Jänicke et al., 2020) with a mean increase rate of 1.1 $mm\ yr^{-1}$ which was attributed to slowing increases of tidal range in the past 20 years (Leon Jänicke, personal communication) compared to the period of 1958 to 2014. Local decreases in unit 26 and 27 (near the tidal gauge BUS) were previously

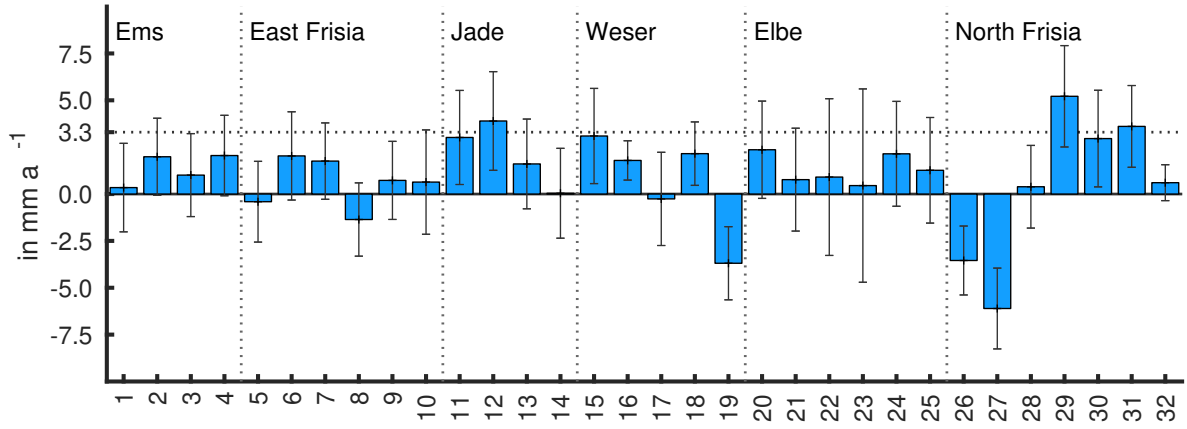

FIGURE 5.10: Morphologically averaged trends of the tidal range in the period of 1996 to 2016 with 3.3 $mm\ yr^{-1}$ indicating averaged annual tidal range increase at tide gauges from Jänicke et al. (2020). Error bars represent the 95 % confidence of the linear regression and blue bars represent the annual trend of the mean tidal range across the morphological units on the x-axis (adapted from Hagen et al., 2022).

related to land reclamation and dredging in the Meldorfer Bight (Jänicke et al., 2020). Therefore, locally varying increases in tidal range across the study site can be confirmed with few local exceptions.

Despite the overall increasing tidal range, a/h ratios decreased across the entire study area except for units 1 and 24 to 27 which implied that local subtidal deepening exceeded tidal amplitude increase (Figure 5.11, a). The largest decreases in a/h were found in the river Ems (3, 4) and in the adjacent East Frisian units (5 to 8) as well as the inner Jade (13, 14). The predominant increase in flood duration, e.g., in morphological units 2 to 18 (Figure 5.10), was in line with theoretical expectation that lower a/h ratios enable decreasing flood dominance (Friedrichs and Aubrey, 1988).

As most a/h values from Figure 5.11 (a) were small, the storage to channel volume ratio V_s/V_c could determine flood or ebb dominance. V_s/V_c in Figure 5.11 (b) varied between 0 in purely subtidal units in the mouth of the Elbe estuary and 1.8 in East and North Frisia. V_s/V_c increased in most units (3 to 7, 19, and 25 to 32) with unit 27 showing the largest increase. Units 8 to 10 in East Frisia exhibited noteworthy V_s/V_c decreases which may account for lower increases in flood duration compared to the Ems estuary despite high a/h. Figure 5.11 (c) illustrates the relationship between both parameters. For reference, the numerical solution for friction-dominated short shallow estuaries (Friedrichs, 2010; Friedrichs and Aubrey, 1988) was added to estimate flood or ebb dominance depending on the stability parameters a/h and V_s/V_c. I observed that most points advanced further towards the ebb dominant side of the numerical solution which was facilitated by the predominant increase in V_s/V_c at decreasing a/h.

In contrast to theoretical expectation, Figure 5.8 demonstrated decreasing flood duration in units 31 and 32 (i.e., increasing flood dominance) despite marginally increasing V_s/V_c at constant a/h. Here, local changes in tidal amplitude, inter- or subtidal volume were likely counteracted by the regional changes in flood duration. Units 28 to 30, however, exhibited increasing flood duration which corresponded well to increasing V_s/V_c.

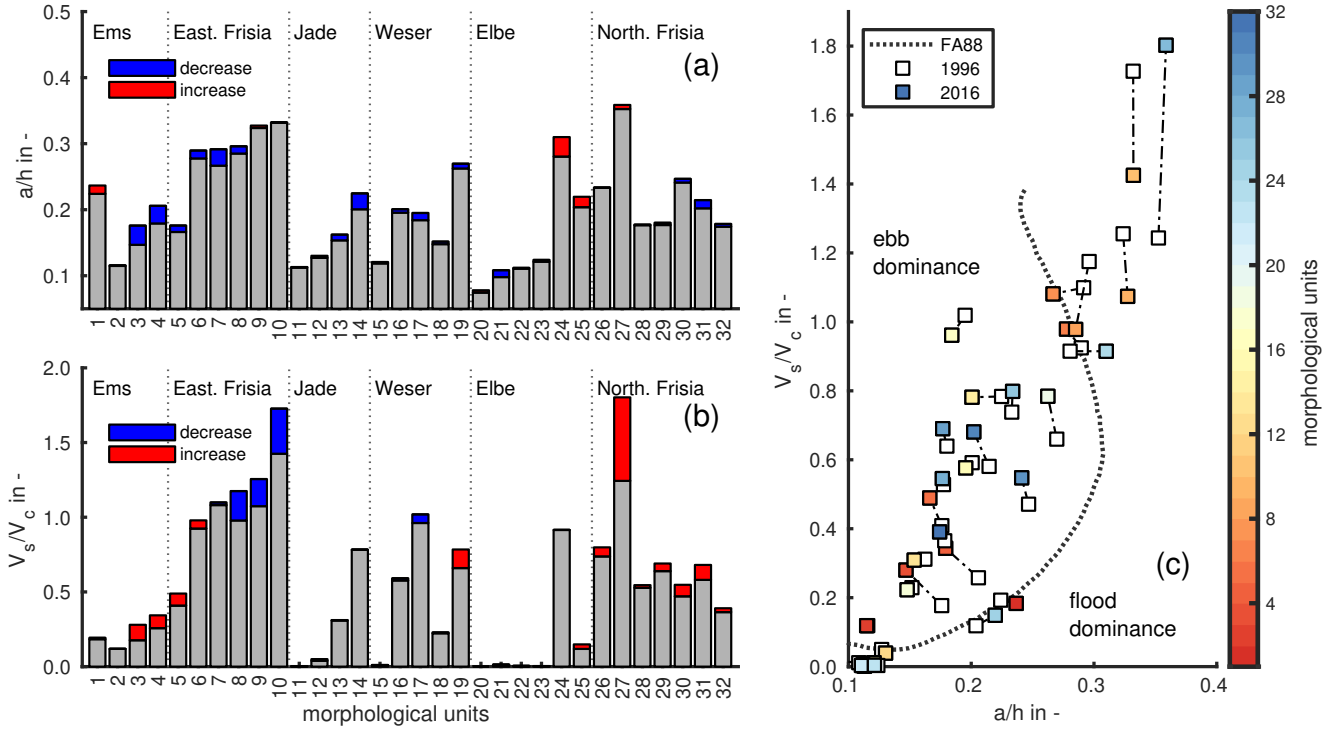

FIGURE 5.11: Changes in the geometrical asymmetry parameters a/h (a), V_s/V_c (b), and a combined view of a/h and V_s/V_c (c) with the numerical solution for flood and ebb dominance (dotted gray line) of Friedrichs and Aubrey (1988). White squares in (c) represent the year 1996 and the respective connected to colored squares indicates the year 2016. Colored markers determine the morphological unit index. No-data or small V_s/V_c values (e.g., unit 20 in b) can occur in (nearly) purely subtidal units. All values are based on linear regression estimates (adapted from Hagen et al., 2022).

5.5.4 Tidal Duration Asymmetry

The morphological unit averaging approach (MUA) was subsequently applied in the period of 1996 and 2016 for tidal duration asymmetry (TDA) descriptors (see Table 3.5). The full trend analyses (analogous to Figure 5.9) was published in the supplemental material to Hagen et al. (2022).

Statistically significant trends were derived for the SSH $\theta(2M_2 - M_4)$ phase lag, the flood to tide duration ratio, and the flood to tide current duration ratio (see Figure 5.12). Results exhibited different regional characteristics with decreasing flood dominance or increasing ebb dominance. The $\theta(2M_2 - M_4)$ phase lag and the flood to tide ratio in Figure 5.12 (a, b) showed decreasing flood dominance in most units in East Frisia and the rivers Ems, Weser, and Jade Bay as well as increasing flood dominance in the river Elbe in unit 27. The $\theta(2M_2 - M_4)$ phase lag, however, indicated increasing flood dominance in East Frisia while the flood to tide duration ratio decreased strongly. Trends of adjacent morphological units generally demonstrated a consistent signal within broader regional units, i.e., for East Frisia and the rivers Ems, Weser, and Elbe. North Frisia imposed an exception as both increasing and decreasing flood dominance were present. This observation was consistent with the spatial differences of flood duration in Figure 5.8 which showed a similar regional distribution of trends. In addition, I observed local signals such as increasing flood dominance in the mouth of the Elbe estuary (20 to 25). This local signal was likely related to the development of a second tidal channel in the outer Elbe

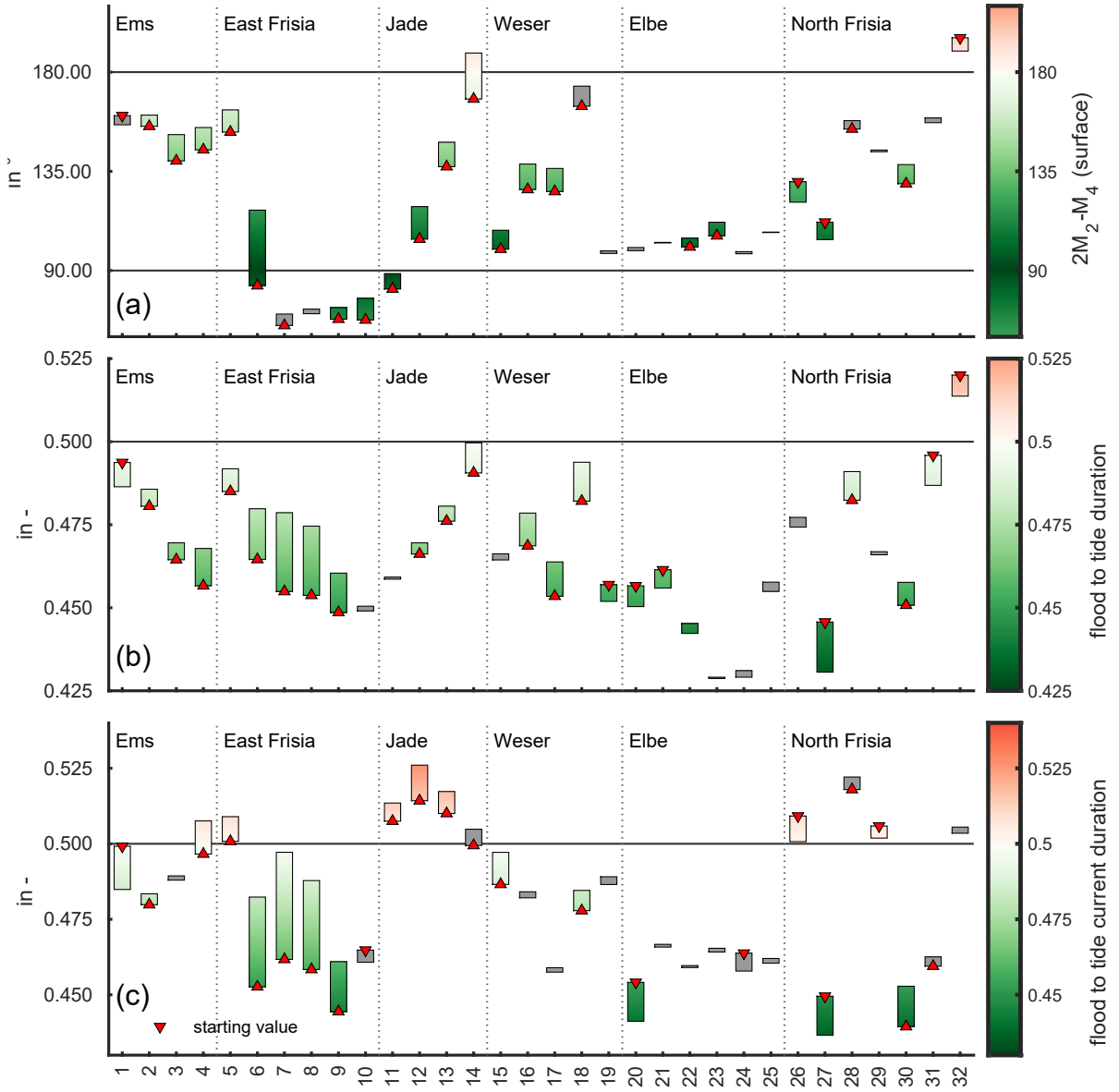

FIGURE 5.12: Development of the tidal duration asymmetry (TDA) parameters: $\theta(2M_2 - M_4)$ phase lag (a), the flood to tide duration ratio (b), and the flood to tide current duration ratio (c) in the period in the period of 1996 to 2016 from linear regression. Gray bars indicate insignificant and colored bars significant trends. The green color represents flood dominance, white symmetry, and red ebb dominance. Triangles mark the starting point in the year 1996 and the end of the bar represents the year 2016. The x-axis enumerates the morphological units defined in Figure 5.7 (modified visually from Hagen et al., 2022).

estuary in the year 2008. The comparison between the $\theta(2M_2 - M_4)$ phase lag and the flood to tide duration was coherent apart from East Frisia where the $\theta(2M_2 - M_4)$ phase lag falsely indicated increasing flood dominance in some parts. A possible explanation could be the very small M_4 amplitudes in East Frisia.

Flood to tide current duration ratios (Figure 5.12, c) strengthened previous findings about the flood to tide duration ratio (Figure 5.12, b) with more pronounced changes. Increasing ebb dominance (4, 5, 11 to 13) or decreasing flood dominance (6 to 10) was observed in East Frisia. Units in the Weser and Elbe estuary (15 to 25) demonstrated less variability with few local exceptions. In some cases, trends in TDA descriptors indicated opposing dominance (e.g., unit 3,

11, or 31).
Unexpectedly, changes in North Frisia were less pronounced than East Frisia with slight decreases in ebb dominance (26, 27, 29) and decreasing flood dominance (30, 31) considering comparable changes in tidal amplitude, a/h, or V_s/V_c. A comparison of the regional changes (Figure 5.8) in TDA in the context of the morphological development of individual units (Chapter 4) confirmed competing local and regional adaptation. The development of the geometrical tidal asymmetry indicators (Section 5.5.3) therefore suggested that regionally increasing flood duration (i.e., decreasing flood dominance) in North Frisian tidal channels was counteracted by the morphological development as the tidal amplitude was also dominated by depth changes. Hence, local tidal asymmetry changes mismatched the morphological asymmetry descriptors because they were superimposed by regional changes in tidal dynamics. As these trends were absent in the southern German Bight (units 1-18), the morphological development reflected decreasing flood duration well.

5.5.5 Flow Velocity Asymmetry

A linear regression of the morphologically averaged mean flood flow velocity indicated a statistically significant decrease between units 5 and 19 although the increasing tidal range may suggest otherwise (see Figure 5.10). The mean flood flow velocity also decreased more strongly (up to 20 %) than the mean ebb flow velocity (less than 10 %) in East Frisia (Figure 5.13). This

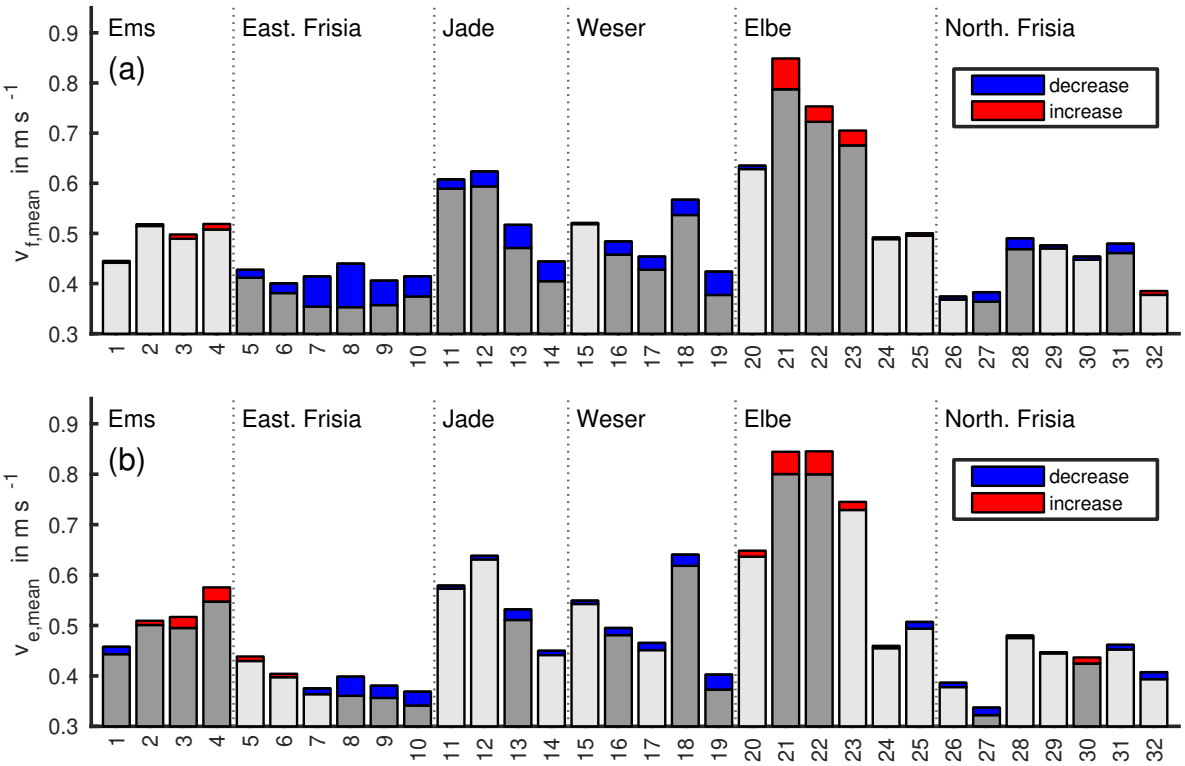

FIGURE 5.13: Changes in annually averaged mean flood (a) and mean ebb (b) flow velocity magnitude in the period from 1996 to 2016 from linear regression with blue increments indicating decreasing and red increments indicating increasing flow velocity magnitude. Light gray bars represent insignificant and dark gray bars represent significant regression (adapted from Hagen et al., 2022).

reflects previously noted decreasing TDA flood dominance either by enhanced mean ebb velocity (e.g., units 3, 4) or by declining flood velocity (e.g., units 5 to 19). Contrary to predominantly decreasing velocities, higher flood and ebb flow velocity were noted in the Elbe and slightly increased ebb velocity in the Ems estuary which may be related to local morphodynamics such as the loss of intertidal storage or the formation of new tidal channels.
Uneven changes in mean flood and ebb current velocity magnitude must provoke a response in FVA (Figure 5.14). Note that flood to ebb ratios < 1 were scaled visually to consider nonlinearity. Several morphological units in Figure 5.14 (a) switched from flood to ebb dominance (e.g., 5, 6) or from strong flood dominance to near-symmetry (e.g., 7, 8). Ebb dominance increased in Jade Bay and the outer Weser estuary (12 to 19). The Elbe estuary and North Frisia exhibited both decreasing and increasing flood dominance. Although many units decreased in flood or increased in ebb dominance, most mean flood to mean ebb flow velocity ratios remained flood dominant.
Peak flood to peak ebb flow velocity ratios followed the trend of the mean flood to mean ebb flow velocity ratio. Small differences between the ratios of mean and peak flood current velocity occurred with different dominance (e.g., units 3 and 17) or differing decreases in flood dominance (e.g., units 3, 10). Similar to the mean flood to mean ebb current velocity ratio, decreasing flood dominance in East Frisia and increasing ebb dominance in Jade Bay and the Weser estuary was evident. Almost no changes were observed for the mouth of the Elbe with

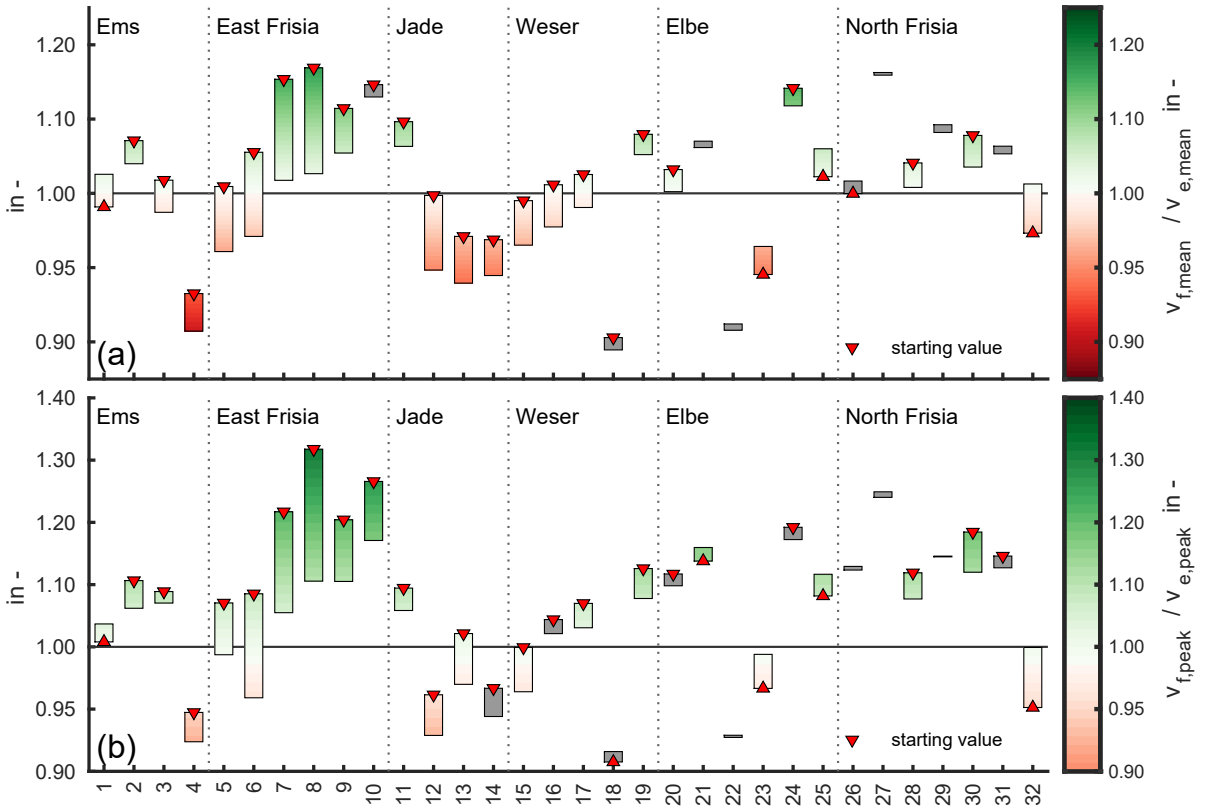

FIGURE 5.14: Trend of the annually averaged mean flood to mean ebb flow velocity magnitude ratio (a) and the annually averaged mean peak flood to peak ebb flow velocity magnitude ratio (b) in the period from 1996 to 2016 from linear regression. Green bars represent flood dominance, white bars represent symmetry, red bars represent ebb dominance. Triangles mark the starting point in 1996 and the end of the bar represents 2016. The x-axis represents the morphological unit index defined in Figure 5.7 (adapted from Hagen et al., 2022).

slightly increasing flood dominance in the inner units. North Frisian units mostly showed declining flood dominance except for unit 32 which may be attributed to increasing mean ebb velocity at decreasing flood current velocity (see Figure 5.13).

5.5.6 Slack Duration and Flow Duration Asymmetry

Several studies emphasized the importance of FDA for the accretion of fines in coastal environments through settling and scour lag mechanisms (see overview in Winterwerp et al., 2021, and Section 2.1.3). Decreasing flood and ebb flow velocity magnitudes and less flood dominant TDA and FVA likely also affected the absolute slack water duration and its asymmetry (i.e., FDA). The slack water duration (i.e., flow duration below 0.2 $m\ s^{-1}$) after flood current s_f and ebb current s_e was estimated from modeled data for each tide and averaged over the respective year. Similar to previous sections, I conducted MUA to estimate morphologically averaged trends. All trend lines were displayed in Appendix D.2.
The flood slack duration s_f increased by 10 to 20 minutes. Peak increases in s_f were observed in East Frisia (units 7 to 10), followed by local increases in the outer Ems (units 1 & 2), and eastern outer Weser (units 17 & 18). Another locally isolated insignificant increase in flood slack was observed in North Frisia (unit 29). Significant decreases of s_f of less than 10 minutes were

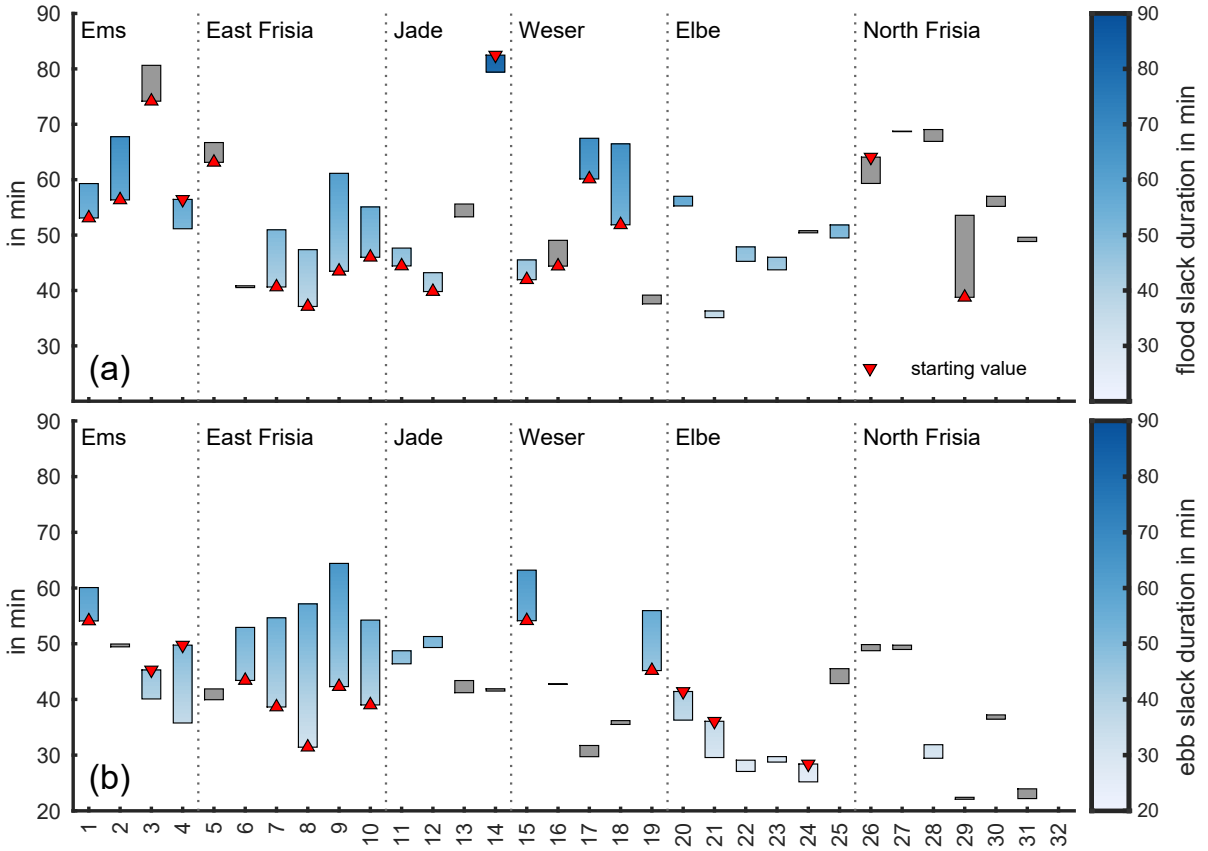

FIGURE 5.15: Development of the flood (a) and ebb slack duration (i.e., estimators for FDA) in the period of 1996 and 2016 from linear regression. Gray bars indicate insignificant and blue bars significant regression. Dark blue patches indicate high and white patches low slack duration with triangles marking the starting point in 1996 and the end of the bar representing 2016. The x-axis enumerates morphological units defined in Figure 5.7. Unit 32 was omitted due to insignificance and negligible low slack duration.

only present in the inner Ems (unit 4), and in Jade Bay (unit 14). Other units exhibited either small increases, insignificant trends, or marginal changes in flood slack.
The mean ebb slack duration s_e increased remarkably by more than 20 minutes in East Frisia (units 6 to 10) and by less than ten minutes in outer Weser estuary (units 15 & 19). Ebb slack duration s_e remained constant in the Jade (units 11 to 14) and Weser estuary (units 16 to 18) as well as North Frisia (units 26 to 32). Decreases of up to 15 minutes were found in the inner Ems (units 3 & 4) and in the entire Elbe (units 20 to 24) estuaries.

CHAPTER 6
DISCUSSION AND OUTLOOK

CONTENTS

6.1 Revisiting the Thesis Objectives

This section discusses the presented research results (Chapters 4 to 5) in context to my thesis' objectives (Section 1.2).

6.1.1 Research Question 1: Coastal Siltation

Is there evidence of enhanced coastal siltation in the period of 1996 to 2016?

Enhanced coastal siltation seems probable for the following reasons: (1) My bathymetry data analysis found increasing sediment volumes in the intertidal zone of the German Bight in the period of 1996 to 2016 which resulted from lateral expansion and vertical accretion. (2) Decadal surface sediment data also indicated siltation in the intertidal zone as sandy flats retreated while mixed and mudflats prevailed. These statements are subject to considerable data uncertainty (see Section 6.3).

Discussion

Benninghoff and Winter (2019, in the following referred to as BW19) analyzed the digital elevation models from the AufMod and EasyGSH-DB data collections in the period of 1996 to 2016 and discovered lateral expansion and vertical accretion of intertidal flats combined with subtidal deepening in the German Wadden Sea. Their results therefore already suggested that recent sediment deposition has been unusually high. However, there was no information about the accreting sediment types; they used constant tidal high and low water boundaries for subtidal and intertidal classification; and their bathymetry data base suffered from height jumps and outliers that could not be mitigated completely. I decided to refine their methodology by using more recent, higher resolution bathymetry data and estimated annually varying tidal high and low water boundaries using a numerical model to consider MSL variability and tidal amplification.

My bathymetry analysis confirmed the lateral expansion and vertical accretion of the intertidal zone in the German Bight at a declining and deepening subtidal in the period of 1996 to 2016. Linear regression was statistically significant and the development was well within the 95 % confidence interval. Height jumps or other outlier data, e.g., resulting from the availability of airborne laser scanning (ALS) bathymetry in the 2000s, were successfully mitigated with an outlier filter although this in turn further diminished the already small sample pool. It must be emphasized that the applied bathymetry data are subject to uncertainty of approximately ± 20 *cm* at best (as discussed in Section 6.3). The annually varying tidal high and low water data from the numerical model also had a RMSE in the low decimeter range. I therefore agree with BW19 that trends from bathymetry analysis can be and will remain *indicators* as long as bathymetry cannot be captured more accurately. Nonetheless, I would argue that a similar conclusion reached in mine and BW19's bathymetry data analyses in a comparable period enhances the credibility of the presented trends. A limitation of my method was that annually variable tidal high and low water impose bias on the estimated size and mean height of the subtidal and intertidal zones. The observed lateral expansion may partially result from changes in MSL, tidal high, and low water which are probable given increasing tidal range (Figure 5.10).

Despite all limitations, similar lateral expansion was noticed in several (predominantly eastern) tidal basins in the Dutch Wadden Sea (Nederhoff et al., 2017), although morphodynamics in the Dutch Wadden Sea are still overlain by the closure dams of the Zuidersee and Lauwersoog in the mid 20^{th} century (Alonso et al., 2021; Elias et al., 2012; Wang et al., 2018). Intertidal accretion without lateral expansion by approximately 1 $cm\ yr^{-1}$ has also been observed in the Dutch Western Scheldt estuary since 2001 (de Vet et al., 2017). This is in agreement with the findings of BW19 and my own results. An opposing trend in mean intertidal height was documented in the diked Dutch Eastern Scheldt estuary with annual decreases of 0.7 $cm\ yr^{-1}$ (de Vet et al., 2017) which emphasizes the importance of morphological unit definition and local features especially at managed coastlines.
A difference between BW19 and my analysis, which may be a matter of discussion, relates to the sediment volume: BW19 found a net sediment import into the coastal zone while my findings suggested a redistribution from the subtidal into the intertidal zone. Still, some basins also demonstrated considerable local net import, e.g., in Jade Bay or in the outer Weser estuary. A high correlation between subtidal and intertidal sediment volume changes ($R = -0.84$), on the one hand, and nearly balanced overall subtidal and intertidal sediment volumes, on the other hand, supported the redistribution argument. I relate this discrepancy to the different spatial extent of morphological units in both analyses. BW19 excluded large portions of the ebb tidal deltas which is why their analysis cannot show redistribution from the shoreface subtidal delta as was also suggested in the Dutch Wadden Sea. There, intertidal accretion was related to noteworthy delta erosion (Elias et al., 2012). Besides, I found decreasing subtidal channel volume at near constant and slightly decreasing intertidal storage. This also implies a sediment transfer considering lateral intertidal expansion and SLR. Morphodynamic SLR impact modeling also suggested an increased transfer of channel and ebb delta sediments onto intertidal flats (Becherer et al., 2018; Hofstede et al., 2018) although these studies also indicated gradual drowning of the intertidal zone on multi-decadal time scales. Another conceptual morphodynamic modeling study confirmed that tidal flats accrete under SLR especially near the predominant sediment source (i.e., the seaward boundary, Elmilady et al., 2022) which corresponds well with my observations. It must be noted that sediment supply is limited in nature and that the considerable sand volume required for sustainable intertidal accretion and lateral expansion in the German Wadden Sea will diminish soon at this rate. This is a worrying thought because the eventual drowning of tidal flats under SLR is then probable. Future research is therefore recommended to gain more knowledge about pathways and quantities of mud and sand in the entire Wadden Sea as a part of an efficient trilateral sediment management strategy.
In view of coastal siltation, decadal surface sediment data in the German Bight were analyzed to corroborate reports of enhanced siltation with scientific evidence. The surface sediment data indicated a near-linear increase of mudflats. This corresponds to a study conducted in the Dutch Wadden Sea which found that tidal basins had primarily imported mud in the past 20 years (Alonso et al., 2021). Hence, it could be argued that the lateral expansion and vertical accretion of the intertidal resulted from the subtidal supply of sandy material while enhanced siltation results from the import of marine fines. Nevertheless, more frequent surface sediment surveys are needed to confirm this hypothesis as the underlying sediment data quality remains questionable.

6.1.2 Research Question 2: Recent Changes

What are the forcing change(s) that facilitated enhanced coastal siltation?

No noteworthy changes in non-tidal forcing were detected aside from slightly longer seaward-facing wave spells and minor SLR. Forcing-induced changes thus appeared improbable at first glance. However, the observed intertidal expansion and increasing tidal flat elevation should cause energy levels on the flat to cease which would promote coastal siltation. Observed local changes in Eulerian tidal asymmetry, as indicators for residual sediment import, seemed to contradict this hypothesis with decreasing tidal duration (TDA) and flow velocity (FVA) flood dominance in tidal channels. Diminishing flood dominance should decrease the net import of sediments into the coastal zone per tidal cycle. Longer flood and ebb slack durations along with decreased flood flow velocity were also found which increases the accommodation of fines. All changes combined, a less flood dominant tide with lower flood flow velocity, a longer slack duration, and less energy on the intertidal flat could have enhanced siltation in the German Wadden Sea despite decreasing net sediment import.

Discussion

The recently enhanced coastal sediment accretion in the period of 1996 to 2016 (see Chapter 4) indicates a morphological disequilibrium in the German coastal zone. I focused on identifying changes in the barotropic drivers within the dynamical equilibrium (i.e., tides, mean sea level, and waves) using the Lagrangian and Eulerian tidal asymmetry framework (following the review of Friedrichs, 2011). Changes in forcing were regarded with modeled mean and peak sea surface height (SSH) and wind-wave height as well as wind-wave direction. Tidal dynamics were assessed using the flood and ebb slack duration and Eulerian tidal asymmetry descriptors with the tidal duration asymmetry (TDA), flow velocity asymmetry (FVA), and flow duration asymmetry (FDA) frames of reference (following Gong et al., 2016; Song et al., 2011). Some drivers of Lagrangian asymmetry were already investigated in other studies. Several studies found evidence of below-average storminess since the 1990s (Section 2.2.2), of mean sea level rise (SLR) by multiple $mm\ yr^{-1}$, and of increasing tidal range (Section 2.2.3). Therefore, I focused my work on transferring their findings to a local context in the recent past. A novel data aggregation approach was used to conduct in-depth trend evaluations of recent changes in SSH, wind-wave conditions, tidal constituents, and tidal asymmetry.
This discussion is structures as follows: First, changes in Lagrangian tidal asymmetry are discussed from a non-tidal forcing and a basin-wide perspective. The focus lies on changes in slack duration (i.e., FDA) and in energy. Second, the development of Eulerian asymmetry descriptors is described by examining the changes in TDA and FVA in the light of recent bathymetry evolution and SLR.

Hindcast modeling data at tidal gauges initially suggested constant Lagrangian asymmetry drivers: I found annually varying mean and peak SSH and waves with weak insignificant positive trends. Steady wind-wave conditions and peak SSH elevations were to be expected in view of the near-constant geostrophic wind magnitude and storminess in the past 30 years over the North Sea (Feser et al., 2015; Krieger et al., 2021; Quante and Colijn, 2016). It seemed unlikely that regional changes in wind-waves were a dominant mechanism. A noteworthy observation was that modeling data indicated shorter spells of landward directed waves with

significant wave heights $> 0.5\ m$ which could have decreased the erosion of fines (see Section 2.1.5).
Although wind-wave forcing and peak SSH remained near-constant at coastal tide gauges, I argue that Lagrangian asymmetry changes in the coastal zone are still probable. Tidal energy on the intertidal flats must have decreased given the previously established lateral expansion and vertical accretion of intertidal flats in the study area. Lower water depths during inundation (considering both vertical accretion and SLR) diminish tidal and wave-related shear stress. If energy levels in the channels are assumed to be constant, the energy gradient between channel and flat must grow which in turn increases the net landward sediment transport (Friedrichs, 2011). Another observation was the significant increase in flood and in ebb slack duration in the tidal channels and a more flood dominant or less ebb dominant FDA. Flood dominant FDA strengthens net landwards transport. It should be noted that longer slack durations always enhance sediment deposition as settling and scour lag are dependent on the duration of low energy rather than flood and ebb water level (Gatto et al., 2017; Postma, 1961). In other words, increased FDA flood dominance, longer slack durations, and a higher energy gradient between channel and shoal should enhance coastal siltation under conditions of infinite sediment availability without river runoff (Dronkers, 1986; Friedrichs, 2011).
More coastal siltation seemingly contradicts the fact that longer flood duration in the coastal zone led to diminishing TDA and FVA flood dominance in tidal channels. Less flood dominance should reduce the net sediment import to the coast. I relate the changes in TDA and FVA to competing local and regional phenomena: On the one hand, a regional change in tidal composition (Section 5.4.2) occurred and, on the other hand, significant intertidal expansion and vertical accretion along with subtidal deepening altered local tides. The increasing relative intertidal storage V_s/V_c and the decreasing relative tidal amplitude a/h resulted in locally diminishing flood dominance (following the numerical solution of Friedrichs and Aubrey, 1988). Coastal morphology changes increased the resistance for incoming floods which slowed local flood rise (Friedrichs, 2010; Friedrichs and Madsen, 1992). Surprisingly, a/h subsided despite increasing tidal range; hence, recent subtidal deepening overcompensated rising tidal amplitude. The development of the geometrical stability criteria is reflected in the decreasing mean flood flow velocity at near constant mean ebb flow velocity in the channels.
Let us use Dronkers (1986) ideas to distinguish the implications of changes in tidal asymmetry on the sand and mud import. The weakening TDA and FVA flood dominance suggests that the sand import into the coastal zone is declining. The dependency of the residual sand transport on FVA was also demonstrated by van Maren and Winterwerp (2013). A lower mean flood flow velocity magnitude furthermore reduces the erosive energy which in turn enhances the deposition of sediments through settling and scour lags (Gatto et al., 2017). Moreover, a longer slack duration and a more flood dominant FDA amplify the import of fines. Following this line of thoughts, enhanced coastal siltation could result from the hampered import of sand and from the improved settling conditions for fines. An increasing mud import along with a diminishing sand import was already observed in the Dutch Wadden Sea (Alonso et al., 2021). Future research should quantify these phenomena: The evolution of energy levels and tidal asymmetry, as indicators for the residual sediment transport of sand and fines, should be investigated in conceptual modeling of a channel-shoal environment using different V_s/V_c to understand and identify feedback mechanisms between morphodynamics and SLR.
Another future research question relates to the separation of drivers and effects concerning

the observed bathymetry evolution. This would aid in resolving a chicken-and-egg dilemma: One could either argue that bathymetry evolution triggered local and remote hydrodynamic changes (as shown by Jacob and Stanev, 2021; Jacob et al., 2016; Jordan et al., 2021) or one could show that the evolution of the coastal morphology was dependent on shifts in tidal amplitude (Jänicke et al., 2020), tidal characteristics (Jänicke, 2021), tidal asymmetry (Hagen et al., 2022), or SLR (e.g., Becherer et al., 2018; Hofstede et al., 2018, among others). In other words, it remains unclear if changes in forcing provoked the observed bathymetry evolution or vice versa. The role of SLR in this matter also remains uncertain.
I follow the hypothesis that observed coastal morphodynamics were driven by SLR which led to nonlinear local and regional feedback because of the dynamical equilibrium concept. If the mean height of intertidal flats does follow MSL, intertidal accretion is a consequence of SLR (Elmilady et al., 2022; Guo et al., 2021). For now, the bathymetry data confirmed the latter as natural unrestricted tidal flats with available accommodation space (e.g., in the eastern outer Weser estuary) accreted by roughly 1 $cm\ yr^{-1}$ and expanded seaward. A puzzling observation was that vertical accretion overcompensated current SLR which also contradicts morphodynamic predictions. Becherer et al. (2018), for instance, predicted an increase in mean intertidal flat height by only 6 *cm* for the Lister Tief basin (North Frisia) until the year 2100. Furthermore, the intertidal flat area should decline under SLR which contrasts the observed development. Hence, it appears probable that nonlinear feedback, e.g., locally increasing tidal amplitude or changes in tidal asymmetry, amplifies sediment accretion in the intertidal zone.

6.2 Relevance

Unusually high sediment deposition was found in the intertidal zone in the German Bight in the period of 1996 to 2016. Therefore, I assumed that the German Wadden Sea is currently in a morphological disequilibrium. Intertidal sediment accretion correlated with a sediment loss in the local or adjacent subtidal zone, i.e., tidal channels or ebb tidal deltas. External barotropic forcing (storms, waves, regional tides) remained constant at coastal tidal gauges in the evaluation period which indicated to me that the morphological equilibrium was disturbed by mean sea level rise (SLR), by local feedback mechanisms, or both. In any case, the observed coastal bathymetry evolution likely enhanced coastal siltation because larger, higher-lying flats are less exposed to erosive energy. Longer flood and ebb slack add to this effect.
The implications on coastal sediment transport are ambiguous: On the one hand, I found local and regional changes in tides and flow velocity (i.e., asymmetry and amplitude) which should decrease the import of sediments into the coastal zone. On the other hand, slack duration increased and tidal energy likely ceased which should increase the net landwards transport of fines. If we assume that the changes in tidal asymmetry hamper the import of sands and that increases in slack duration and lower energy in the coastal zone facilitate the deposition of fines, more siltation becomes the logical consequence.
As the driver behind the observed bathymetry evolution remains uncertain, no recommendation can be made to revert the demonstrated changes in the sediment transport regime. If we want to reduce coastal siltation, methods are well-known: Conventional efforts such as increasing accommodation space, intentional sediment trapping, decreasing navigational channel depths, sediment removal on land, or offshore dumping must be utilized. MSL will rise

faster in the future which is why it remains questionable how long conventional strategies remain viable. New strategies must be explored and the valuable resource sand must be retained at the coast to maintain sediment availability for tidal flat adaptation.

6.3 Limitations and Uncertainty

6.3.1 Bathymetry and Surface Sediment Data

The annual bathymetric and decadal surface sediment data from the EasyGSH-DB data collection (Sievers et al., 2020a,b) are subject to the same uncertainty as all merged bathymetry data sets. The data were collected in a number of different measuring campaigns with varying accuracy before being merged to annual bathymetry data via interpolation in time and space (Milbradt et al., 2015). Bathymetric data quality depended on the accuracy of the measuring instruments with a range of 5 cm to 1 m at higher water depths and on the interpolation error that has not yet been quantified as different surveying frequency (i.e., high frequency in navigational channels, low frequency on intertidal flats) and surveying technique (ALS, multibeam, single-beam, etc.) complicate a confidence assessment significantly. Benninghoff and Winter (2019) and the AufMod documentation suggested a mean bathymetry data accuracy of ± 20 cm which I considered reasonable for the bathymetry data used in this thesis as well.
The observational surface sediment sampling frequency and sample density were considerably lower and had unsatisfying time coverage. Roughly 90 % of all sediment samples within the EasyGSH-DB sediment data were older than the year 2000. Poor data availability was compensated with an anisotropic interpolation method (Sievers et al., 2021) in which the valid area of a sediment sample was estimated with modeled bed shear stress. Although bed shear stress is a fair metric to assess the valid area of a sandy sediment sample, it is dependent on model implementation, model validity, horizontal, and vertical grid resolution. The dependence of the estimated surface sediments on modeled data will lead to different results for different shear stress magnitude and direction even if the underlying in-situ sediment samples remained identical.
Sediment samples themselves also impose uncertainty. The interpolation of an outdated sample on a newer bathymetry leads to implausible results as changes in water depth alter the grain size distribution. From a practical standpoint, most of the available sediment samples were sieved so that diameters below 0.063 mm were only captured as sieve remainder (DIN 18196, 2011). Therefore, cohesive fractions may be underrepresented in the EasyGSH-DB surface sediment data and different cohesive fractions can rarely be distinguished.

6.3.2 Numerical Modeling Data

The solution of all numerical models is only an approximation of physical processes described by principle differential equations on computational grids. The inaccuracy and uncertainty of the initial and boundary data transfers to a numerical simulation which is why modelers rely on numerous tuning parameters to fit their models against observational data. It must also be noted that all 3D hydrodynamic, numerical models (HN-models) are sophisticated software frameworks which require elegant and efficient implementation. To this day, numerous HN-models are still under development and are steadily improved (see overview in Fringer et al.,

2019); hence, implementation errors can never be ruled out, more efficient numerical solutions will be found, or novel equations may improve the approximation of natural physical processes.
A thorough model calibration and validation were therefore imperative to my research as most identified trends and changes would otherwise lie within model confidence (BAW Technische Berichte et al., 2020; Hagen et al., 2021b). Physical processes that are nonlinearly dependent (e.g., salinity and temperature) were included in the model because they were considered relevant for describing the study site in a model. This could either be interpreted as a thorough interpretation or as too complex for practical use. The multitude of physical processes was also computationally expensive which is why a more detailed horizontal and vertical grid resolution was infeasible at the time. I mitigated parts of this issue by using the well-established subgrid approach (Casulli, 2009) in UnTRIM^2 (Sehili et al., 2014) to refine the computational grid at reasonable computational cost. The resulting net simulation time of one year was between 8 and 12 days.

6.3.3 Tidal Analyses

The harmonic, quantile, and tidal characteristic analysis of semidiurnal tidal data are well-established methods with low uncertainty. An estimation of tidal constituents using harmonic analysis, for example, yielded confidence intervals of less than 1 *cm* or 1 degree for the dominant tidal constituents. Tidal characteristic data in the entire computational domain were related to each other in a Lagrange-like approach to track tidal waves along the path of tidal propagation. The tidal characteristic approach is invalid in the following scenarios:

- Mixed diurnal-semidiurnal tides hamper the separation of flood and ebb properties,
- small tidal range is overlain by short and long period waves,
- data points are dry during a tidal cycle, or
- non-bidirectional flow (e.g., at low tidal range or at wave-tide interaction) impedes the analysis of flood and ebb current velocity parameters.

All analysis data on tidal flats had to be omitted as wetting and drying reduced the number of valid samples within each tidal cycle. Observed changes, e.g., in Eulerian tidal asymmetry, can therefore only apply to permanently inundated samples with bidirectional flow.

6.3.4 Trend Estimation and Sample Pool

I used nonlinear and linear regression approaches frequently to quantify changes in morphology and forcing. The short evaluation period of 1996 to 2016 limited the sample pool to a maximum of only 21 years which is why each derived trend must be interpreted carefully. Further expansion of the numerical model and bathymetry data was impractical because of poor bathymetry accuracy before 1996. This can be seen in the bathymetry analysis with a number of outliers before the availability of ALS in the 2000s.
I chose to estimate statistical significance with an F-test over a double t-test because the regression model was used to predict sample variance over sample mean. However, the F-test procedure has its shortcomings: The p-value of an F-test may indicate insignificance if a trend

is absent as an equal distribution of test samples prohibits variance. Moreover, the *F*-test (and double *t*-test) were developed for large data sets which contrasts my sample pool. To mitigate this limitation, I always included a full visual representation of all valid and excluded samples, the trend line, and the 95 % confidence intervals for all linear regressions.
The significance of the multiple nonlinear regression had a larger sample pool with observational time series of several decades at tidal gauges. Applicability and validity of the approach its statistical significance were discussed in Hagen et al. (2021a, section 2.3).

6.4 Outlook and Future Research

The Wadden Sea has always been a sediment sink. Despite this well-established fact, I observed an unusual sediment redistribution from the subtidal to the intertidal zone in the period of 1996 to 2016 in recent bathymetry data. This sediment transfer led to intertidal lateral expansion and vertical accretion by a multitude of current mean sea level rise (SLR) which in turn weakened local flood dominance in tidal channels at near constant external forcing. Although there were several indications, drivers and effects underlying the bathymetry evolution could not be distinguished because the observed developments are a chicken-and-egg dilemma: Was bathymetry evolution and siltation triggered by SLR, did the intertidal morphology changes facilitate changes in local tidal asymmetry to enhance siltation, or both? I hypothesized that bathymetry evolution is likely driven by changes in large-scale forcing and MSL which is why I suggested future research to systematically investigate the sensitivity of coastal bathymetry changes to SLR and to tidal dynamics.
I furthermore recommend to investigate the extraordinary intertidal accretion. It was a puzzling observation that height growth exceeded increases in tidal amplitude (i.e., 1.1 $mm\ yr^{-1}$) and SLR (i.e., more than 3 $mm\ yr^{-1}$). This contradicted predictions about the correlation of intertidal accretion in the order, or lower than increases in tidal amplitude or MSL. Recreating the recent development in a detailed morphodynamic model would be a first step in understanding the underlying mechanisms at play. Conceptual modeling of tidal basins and estuaries with a particular focus on sediment fluxes and energy levels with varying V_s/V_c could also be a way forward.
In conclusion, I consider the recently enhanced coastal siltation as a consequence of the observed bathymetric development under SLR. However, the observed intertidal accretion and lateral expansion does not indicate a future in which the Wadden Sea is resistant against drowning under SLR. We cannot interpret my results as a sign of relief. Once the limited availability of sand in tidal channels and ebb tidal deltas eventually diminishes, sediment accretion in the intertidal will cease because suspended fines from the North Sea can only deposit in low-energy areas such as high-lying flats or wave sheltered areas such as harbors. Maintaining our intertidal flats in the Wadden Sea is imperative, as it is an important carbon sink, provides irreplaceable coastal protection, and inherits numerous unique biological habitats. For this reason, I emphasize that future sediment management should direct significantly more attention towards increasing the sediment availability of sandy material in the coastal zone to enable a favorable morphodynamic development under SLR. My results suggested that sediment is redistributed well from the subtidal channels and ebb deltas to their adjacent intertidal flats. It is important to remember that maintaining the extent and functionality of

today's Wadden Sea requires tremendous amounts of sediment: Raising the intertidal zone of the German Wadden Sea in the year 2016 by just 1 cm without intertidal expansion would require $3,800\ km^2 \times 1\ cm = 3.8\ 10^7\ m^3$ of sediment which corresponds to roughly $6.1\ 10^7\ t$ of sand or $1.9\ 10^7\ t$ of mud given a bulk density of $1,600\ kg\ m^{-3}$ or $500\ kg\ m^{-3}$.

References

Albers, T. and von Lieberman, N. "Morphodynamics of Wadden Sea Areas – Field Measurements and Modeling". In: *The International Journal of Ocean and Climate Systems* 1.3-4 (2010), pp. 123–132. ISSN: 1759-3131. DOI: 10.1260/1759-3131.1.3-4.123.

Alonso, A. C., van Maren, D. S., Elias, E., Holthuijsen, S. J., and Wang, Z. B. "The contribution of sand and mud to infilling of tidal basins in response to a closure dam". In: *Marine Geology* (2021), p. 106544. ISSN: 00253227. DOI: 10.1016/j.margeo.2021.106544.

Aubrey, D. G. and Speer, P. E. "A study of non-linear tidal propagation in shallow inlet/estuarine systems Part I: Observations". In: *Estuarine, Coastal and Shelf Science* 21.2 (1985), pp. 185–205. ISSN: 02727714. DOI: 10.1016/0272-7714(85)90096-4.

BAW Technische Berichte, Hagen, R., Freund, J., Plüß, A., and Ihde, R. *Validierungsdokument EasyGSH-DB Nordseemodell. Teil UnTRIM2 - SediMorph - UnK*. Ed. by Bundesanstalt für Wasserbau. 2020. DOI: 10.18451/k2_easygsh_1.

Becherer, J. et al. "The Wadden Sea in transition - consequences of sea level rise". In: *Ocean Dynamics* 68.1 (2018), pp. 131–151. DOI: 10.1007/s10236-017-1117-5.

Benninghoff, M. and Winter, C. "Decadal evolution of tidal flats and channels in the Outer Weser estuary, Germany". In: *Ocean Dynamics* 68.9 (2018), pp. 1181–1190. DOI: 10.1007/s10236-018-1184-2.

Benninghoff, M. and Winter, C. "Recent morphologic evolution of the German Wadden Sea". In: *Scientific reports* 9.1 (2019), p. 9293. DOI: 10.1038/s41598-019-45683-1.

Bollmeyer, C. et al. "Towards a high-resolution regional reanalysis for the European CORDEX domain". In: *Quarterly Journal of the Royal Meteorological Society* 141.686 (2015), pp. 1–15. ISSN: 00359009. DOI: 10.1002/qj.2486.

Burchard, H., Schuttelaars, H. M., and Ralston, D. K. "Sediment Trapping in Estuaries". In: *Annual review of marine science* 10 (2018), pp. 371–395. DOI: 10.1146/annurev-marine-010816-060535.

Casulli, V. and Cattani, E. "Stability, accuracy and efficiency of a semi-implicit method for three-dimensional shallow water flow". In: *Computers & Mathematics with Applications* 27.4 (1994), pp. 99–112. ISSN: 08981221. DOI: 10.1016/0898-1221(94)90059-0.

Casulli, V. "Semi-implicit finite difference methods for the two-dimensional shallow water equations". In: *Journal of Computational Physics* 86.1 (1990), pp. 56–74. ISSN: 00219991. DOI: 10.1016/0021-9991(90)90091-E.

Casulli, V. "A high-resolution wetting and drying algorithm for free-surface hydrodynamics". In: *International Journal for Numerical Methods in Fluids* 60.4 (2009), pp. 391–408. ISSN: 0271-2091. DOI: 10.1002/fld.1896.

Casulli, V. and Stelling, G. S. "Semi-implicit subgrid modelling of three-dimensional free-surface flows". In: *International Journal for Numerical Methods in Fluids* 67.4 (2011), pp. 441–449. ISSN: 0271-2091. DOI: 10.1002/fld.2361.

Casulli, V. and Walters, R. A. "An unstructured grid, three-dimensional model based on the shallow water equations". In: *International Journal for Numerical Methods in Fluids* 32.3 (2000), pp. 331–348. ISSN: 0271-2091. DOI: 10.1002/(SICI)1097-0363(20000215)32:3<331::AID-FLD941>3.0.CO;2-C.

Chang, T. S., Bartholomä, A., and Flemming, B. W. "Seasonal Dynamics of Fine-Grained Sediments in a Back-Barrier Tidal Basin of the German Wadden Sea (Southern North Sea)". In: *Journal of Coastal Research* 222 (2006), pp. 328–338. ISSN: 0749-0208. DOI: 10.2112/03-0085.1.

Chang, T. S., Joerdel, O., Flemming, B. W., and Bartholomä, A. "The role of particle aggregation/disaggregation in muddy sediment dynamics and seasonal sediment turnover in a back-barrier tidal basin, East Frisian Wadden Sea, southern North Sea". In: *Marine Geology* 235.1-4 (2006), pp. 49–61. ISSN: 00253227. DOI: 10.1016/j.margeo.2006.10.004.

Colosimo, I. et al. "The Impact of Wind on Flow and Sediment Transport over Intertidal Flats". In: *Journal of Marine Science and Engineering* 8.11 (2020), p. 910. ISSN: 2077-1312. DOI: 10.3390/jmse8110910.

Dangendorf, S., Mudersbach, C., Jensen, J., Anette, G., and Heinrich, H. "Seasonal to decadal forcing of high water level percentiles in the German Bight throughout the last century". In: *Ocean Dynamics* 46.2 (2013), p. 277. DOI: 10.1007/s10236-013-0614-4.

De Swart, H. E. and Zimmerman, J. "Morphodynamics of Tidal Inlet Systems". In: *Annual Review of Fluid Mechanics* 41.1 (2009), pp. 203–229. ISSN: 0066-4189. DOI: 10.1146/annurev.fluid.010908.165159.

De Vet, P. L. M. et al. "Variations in storm-induced bed level dynamics across intertidal flats". In: *Scientific reports* 10.1 (2020), p. 12877. DOI: 10.1038/s41598-020-69444-7.

De Vet, P., van Prooijen, B. C., and Wang, Z. B. "The differences in morphological development between the intertidal flats of the Eastern and Western Scheldt". In: *Geomorphology* 281 (2017), pp. 31–42. DOI: 10.1016/j.geomorph.2016.12.031.

DIN 18196. *Erd- und Grundbau, Bodenklassifikation für bautechnische Zwecke*. Mai 2011. Vol. DIN 18196. Deutsche Normen. Berlin: Beuth, 2011.

Doodson, A. T. "The harmonic development of the tide-generating potential". In: *Philosophic Transaction of Royal Society* 100 (1921), pp. 305–329. URL: https://doi.org/10.1098/rspa.1921.0088.

Doodson, A. T. "The Analysis of Tidal Observations". In: *Philosophical Transactions of the Royal Society A: Mathematical, Physical and Engineering Sciences* 227.647-658 (1928), pp. 223–279. DOI: 10.1098/rsta.1928.0006.

Dreier, N., Männikus, R., and Fröhle, P. "Long-term Changes of Waves at the German Baltic Sea Coast: Are There Trends from the Past?" In: *Journal of Coastal Research* 95.sp1 (2020), p. 1416. ISSN: 0749-0208. DOI: 10.2112/SI95-274.1.

Dronkers, J. "Tidal asymmetry and estuarine morphology". In: *Netherlands Journal of Sea Research* 20.2-3 (1986), pp. 117–131. ISSN: 00777579. DOI: 10.1016/0077-7579(86)90036-0.

Dyer, K. R. and Moffat, T. J. "Fluxes of suspended matter in the East Anglian plume Southern North Sea". In: *Continental Shelf Research* 18.11 (1998), pp. 1311–1331. ISSN: 02784343. DOI: 10.1016/S0278-4343(98)00045-4.

Elias, E. P., van der Spek, A. J., Pearson, S. G., and Cleveringa, J. "Understanding sediment bypassing processes through analysis of high-frequency observations of Ameland Inlet, the Netherlands". In: *Marine Geology* 415 (2019), p. 105956. ISSN: 00253227. DOI: 10.1016/j.margeo.2019.06.001.

Elias, E., van der Spek, A., Wang, Z. B., and de Ronde, J. "Morphodynamic development and sediment budget of the Dutch Wadden Sea over the last century". In: *Netherlands Journal of Geosciences - Geologie en Mijnbouw* 91.3 (2012), pp. 293–310. ISSN: 0016-7746. DOI: 10.1017/S0016774600000457.

Elmilady, H., Wegen, M., Roelvink, D., and Spek, A. "Modeling the Morphodynamic Response of Estuarine Intertidal Shoals to Sea-Level Rise". In: *Journal of Geophysical Research: Earth Surface* 127.1 (2022). ISSN: 2169-9003. DOI: 10.1029/2021JF006152.

EMODnet Bathymetry Consortium. "EMODnet Digital Bathymetry (DTM 2018)". 2018. DOI: 10.12770/18ff0d48-b203-4a65-94a9-5fd8b0ec35f6.

Feser, F. et al. "Storminess over the North Atlantic and northwestern Europe—A review". In: *Quarterly Journal of the Royal Meteorological Society* 141.687 (2015), pp. 350–382. ISSN: 0035-9009. DOI: 10.1002/qj.2364.

Fettweis, M. and van den Eynde, D. "The mud deposits and the high turbidity in the Belgian–Dutch coastal zone, southern bight of the North Sea". In: *Continental Shelf Research* 23.7 (2003), pp. 669–691. ISSN: 02784343. DOI: 10.1016/S0278-4343(03)00027-X.

Figge, K., Köster, R., Thiel, H., and Wieland, P. *Schlickuntersuchungen im Wattenmeer der Deutschen Bucht - Zwischenbericht über ein Forschungsprojekt des KFKI*. Heide: Boyens & Co, 1980.

Flemming, B. W. and Nyandwi, N. "Land reclamation as a cause of fine-grained sediment depletion in backbarrier tidal flats (Southern North Sea)". In: *Netherlands Journal of Aquatic Ecology* 28.3-4 (1994), pp. 299–307. ISSN: 1380-8427. DOI: 10.1007/BF02334198.

Folk, R. L. and Ward, W. C. “Brazos River bar [Texas]; a study in the significance of grain size parameters”. In: *SEPM Journal of Sedimentary Research* 27.1 (1957), pp. 3–26. ISSN: 1527-1404. DOI: 10.1306/74D70646-2B21-11D7-8648000102C1865D.

Foreman, M. G. G., Cherniawsky, J. Y., and Ballantyne, V. A. “Versatile Harmonic Tidal Analysis: Improvements and Applications”. In: *Journal of Atmospheric and Oceanic Technology* 26.4 (2009), pp. 806–817. ISSN: 0739-0572. DOI: 10.1175/2008JTECHO615.1.

Friedrichs, C. T. “Tidal Flat Morphodynamics”. In: *Treatise on Estuarine and Coastal Science*. Elsevier, 2011, pp. 137–170. ISBN: 9780080878850. DOI: 10.1016/B978-0-12-374711-2.00307-7.

Friedrichs, C. T. “Barotropic tides in channelized estuaries”. In: *Contemporary Issues in Estuarine Physics*. Ed. by A. Valle-Levinson. Cambridge: Cambridge University Press, 2010, pp. 27–61. ISBN: 9780511676567. DOI: 10.1017/CBO9780511676567.004.

Friedrichs, C. T. and Aubrey, D. G. “Non-linear tidal distortion in shallow well-mixed estuaries: A synthesis”. In: *Estuarine, Coastal and Shelf Science* 27.5 (1988), pp. 521–545. ISSN: 02727714. DOI: 10.1016/0272-7714(88)90082-0.

Friedrichs, C. T. and Madsen, O. S. “Nonlinear diffusion of the tidal signal in frictionally dominated embayments”. In: *Journal of Geophysical Research* 97.C4 (1992), p. 5637. ISSN: 0148-0227. DOI: 10.1029/92JC00354.

Fringer, O., Dawson, C. N., He, R., Ralston, D. K., and Zhang, Y. J. “The future of coastal and estuarine modeling: Findings from a workshop”. In: *Ocean Modelling* 143 (2019), p. 101458. ISSN: 1463-5003. DOI: 10.1016/j.ocemod.2019.101458.

Ganske, A., Tinz, B., Rosenhagen, G., and Heinrich, H. “Interannual and Multidecadal Changes of Wind Speed and Directions over the North Sea from Climate Model Results”. In: *Meteorologische Zeitschrift* 25.4 (2016), pp. 463–478. ISSN: 0941-2948. DOI: 10.1127/metz/2016/0673.

Gatto, V. M., van Prooijen, B. C., and Wang, Z. B. “Net sediment transport in tidal basins: Quantifying the tidal barotropic mechanisms in a unified framework”. In: *Ocean Dynamics* 67.11 (2017), pp. 1385–1406. DOI: 10.1007/s10236-017-1099-3.

Gayer, G., Dick, S., Pleskachevsky, A., and Rosenthal, W. “Numerical modeling of suspended matter transport in the North Sea”. In: *Ocean Dynamics* 56.1 (2006), pp. 62–77. DOI: 10.1007/s10236-006-0070-5.

Geyer, B. “High-resolution atmospheric reconstruction for Europe 1948–2012: CoastDat2”. In: *Earth System Science Data* 6.1 (2014), pp. 147–164. ISSN: 1866-3516. DOI: 10.5194/essd-6-147-2014.

Gong, W., Schuttelaars, H., and Zhang, H. “Tidal asymmetry in a funnel-shaped estuary with mixed semidiurnal tides”. In: *Ocean Dynamics* 66.5 (2016), pp. 637–658. DOI: 10.1007/s10236-016-0943-1.

Groll, N. and Weisse, R. "A multi-decadal wind-wave hindcast for the North Sea 1949–2014: CoastDat2". In: *Earth System Science Data* 9.2 (2017), pp. 955–968. ISSN: 1866-3516. DOI: 10.5194/essd-9-955-2017.

Gräwe, U., Burchard, H., Müller, M., and Schuttelaars, H. M. "Seasonal variability in M 2 and M 4 tidal constituents and its implications for the coastal residual sediment transport". In: *Geophysical Research Letters* 41.15 (2014), pp. 5563–5570. ISSN: 00948276. DOI: 10.1002/2014GL060517.

Gräwe, U. et al. "A numerical model for the entire Wadden Sea: Skill assessment and analysis of hydrodynamics". In: *Journal of Geophysical Research: Oceans* 121.7 (2016), pp. 5231–5251. ISSN: 21699275. DOI: 10.1002/2016JC011655.

Gulev, S. K. and Grigorieva, V. "Variability of the Winter Wind Waves and Swell in the North Atlantic and North Pacific as Revealed by the Voluntary Observing Ship Data". In: *Journal of Climate* 19.21 (2006), pp. 5667–5685. ISSN: 0894-8755. DOI: 10.1175/JCLI3936.1.

Guo, L., Wang, Z. B., Townend, I., and He, Q. "Quantification of Tidal Asymmetry and Its Nonstationary Variations". In: *Journal of Geophysical Research: Oceans* 124.1 (2019), pp. 773–787. ISSN: 21699275. DOI: 10.1029/2018JC014372.

Guo, L. et al. "Morphodynamic adaptation of a tidal basin to centennial sea-level rise: The importance of lateral expansion". In: *Continental Shelf Research* 226.1–2 (2021), p. 104494. ISSN: 02784343. DOI: 10.1016/j.csr.2021.104494.

Gönnert, G. "Sturmfluten und Windstau in der Deutschen Bucht Charakter, Veränderungen und Maximalwerte im 20. Jahrhundert". In: *Die Küste* 67 (2003).

Hagen, R., Plüß, A., Schrage, N., and Dreier, N. *EasyGSH-DB: Themengebiet - synoptische Hydrodynamik*. Ed. by Bundesanstalt für Wasserbau. 2020. DOI: 10.48437/02.2020.K2.7000.0004.

Hagen, R., Winter, C., and Kösters, F. "Changes in tidal asymmetry in the German Wadden Sea". In: *Ocean Dynamics* 5 (2022), pp. 325–340. DOI: 10.1007/s10236-022-01509-9.

Hagen, R. et al. *EasyGSH-DB: Themengebiet - Hydrodynamik*. Ed. by Bundesanstalt für Wasserbau. 2020. DOI: 10.48437/02.2020.K2.7000.0003.

Hagen, R. et al. "A Combined Modeling and Measurement Approach to Assess the Nodal Tide Modulation in the North Sea". In: *Journal of Geophysical Research: Oceans* (2021). ISSN: 21699275. DOI: 10.1029/2020JC016364.

Hagen, R. et al. "An integrated marine data collection for the German Bight – Part 2: Tides, salinity, and waves (1996–2015)". In: *Earth System Science Data* 13.6 (2021), pp. 2573–2594. ISSN: 1866-3516. DOI: 10.5194/essd-13-2573-2021.

Haigh, I. D., Eliot, M., and Pattiaratchi, C. "Global influences of the 18.61 year nodal cycle and 8.85 year cycle of lunar perigee on high tidal levels". In: *Journal of Geophysical Research: Atmospheres* 116.C6 (2011), p. 25249. ISSN: 01480227. DOI: 10.1029/2010JC006645.

Haigh, I. D. et al. “The Tides They Are A-Changin’: A Comprehensive Review of Past and Future Nonastronomical Changes in Tides, Their Driving Mechanisms, and Future Implications”. In: *Reviews of Geophysics* 58.1 (2020). ISSN: 8755-1209. DOI: 10.1029/2018RG000636.

Herrling, G., Benninghoff, M., Zorndt, A., and Winter, C. “Drivers of channel-shoal morphodynamics at the outer Weser estuary”. In: *Coastal Dynamics* 261 (2017).

Herrling, G. and Winter, C. “Tidal inlet sediment bypassing at mixed-energy barrier islands”. In: *Coastal Engineering* 140 (2018), pp. 342–354. ISSN: 03783839. DOI: 10.1016/j.coastaleng.2018.08.008.

Heyer, H., Schrottke, K., and Zeiler, M. *Synthese der interdisziplinären Forschung in AufMod*. Karlsruhe: Bundesanstalt für Wasserbau, 2015.

Hofstede, J. L., Becherer, J., and Burchard, H. “Are Wadden Sea tidal systems with a higher tidal range more resilient against sea level rise?” In: *Journal of Coastal Conservation* 22.1 (2018), pp. 71–78. ISSN: 1400-0350. DOI: 10.1007/s11852-016-0469-1.

Holleman, R. C. and Stacey, M. T. “Coupling of Sea Level Rise, Tidal Amplification, and Inundation”. In: *Journal of Physical Oceanography* 44.5 (2014), pp. 1439–1455. ISSN: 0022-3670. DOI: 10.1175/JPO-D-13-0214.1.

Holt, J. T. and James, I. D. “A simulation of the southern North Sea in comparison with measurements from the North Sea Project Part 2 Suspended Particulate Matter”. In: *Continental Shelf Research* 19.12 (1999), pp. 1617–1642. ISSN: 02784343. DOI: 10.1016/S0278-4343(99)00032-1.

Idier, D., Paris, F., Le Cozannet, G., Boulahya, F., and Dumas, F. “Sea-level rise impacts on the tides of the European Shelf”. In: *Continental Shelf Research* 137 (2017), pp. 56–71. ISSN: 02784343. DOI: 10.1016/j.csr.2017.01.007.

Jacob, B. and Stanev, E. V. “Understanding the Impact of Bathymetric Changes in the German Bight on Coastal Hydrodynamics: One Step Toward Realistic Morphodynamic Modeling”. In: *Frontiers in Marine Science* 8 (2021), p. 9293. ISSN: 2296-7745. DOI: 10.3389/fmars.2021.640214.

Jacob, B., Stanev, E. V., and Zhang, Y. J. “Local and remote response of the North Sea dynamics to morphodynamic changes in the Wadden Sea”. In: *Ocean Dynamics* 66.5 (2016), pp. 671–690. DOI: 10.1007/s10236-016-0949-8.

Janssen, F., Schrum, C., and Backhaus, J. O. “A climatological data set of temperature and salinity for the Baltic Sea and the North Sea”. In: *Deutsche Hydrografische Zeitschrift* 51.9 (1999), p. 5. ISSN: 1616-7228. DOI: 10.1007/BF02933676. URL: https://doi.org/10.1007/BF02933676.

Janssen-Stelder, B. “The effect of different hydrodynamic conditions on the morphodynamics of a tidal mudflat in the Dutch Wadden Sea”. In: *Continental Shelf Research* 20.12-13 (2000), pp. 1461–1478. ISSN: 02784343. DOI: 10.1016/S0278-4343(00)00032-7.

Jensen, J., Ebener, A., Bender, J., and Mudersbach, C. *Charakterisierung von Zeitreihen zur historischen Entwicklung der Tidekennwerte in den deutschen Nordseeästuaren sowie Entwicklung von statistischen Modellen zu deren Beschreibung*. Ed. by Bundesanstalt für Gewässerkunde. 2019.

Jordan, C., Visscher, J., and Schlurmann, T. "Projected Responses of Tidal Dynamics in the North Sea to Sea-Level Rise and Morphological Changes in the Wadden Sea". In: *Frontiers in Marine Science* 8 (2021), p. 40171. ISSN: 2296-7745. DOI: 10.3389/fmars.2021.685758.

Jänicke, L. *Assessing changes of tidal dynamics in the North Sea*. Universitätsbibliothek Siegen, 2021. DOI: 10.25819/ubsi/10105.

Jänicke, L. et al. "Assessment of tidal range changes in the North Sea from 1958 to 2014". In: *Journal of Geophysical Research: Oceans* (2020). ISSN: 21699275. DOI: 10.1029/2020JC016456.

Khojasteh, D., Glamore, W., Heimhuber, V., and Felder, S. "Sea level rise impacts on estuarine dynamics: A review". In: *The Science of the total environment* 780 (2021), p. 146470. DOI: 10.1016/j.scitotenv.2021.146470.

Krieger, D. et al. "German Bight storm activity, 1897–2018". In: *International Journal of Climatology* 41.S1 (2021), p. 97. ISSN: 0899-8418. DOI: 10.1002/joc.6837.

Kösters, F. and Winter, C. "Exploring German Bight coastal morphodynamics based on modelled bed shear stress". In: *Geo-Marine Letters* 34.1 (2014), pp. 21–36. ISSN: 0276-0460. DOI: 10.1007/s00367-013-0346-y.

Lee, S. B., Li, M., and Zhang, F. "Impact of sea level rise on tidal range in Chesapeake and Delaware Bays". In: *Journal of Geophysical Research: Oceans* 122.5 (2017), pp. 3917–3938. ISSN: 2169-9275. DOI: 10.1002/2016JC012597.

Lyard, F. H., Allain, D. J., Cancet, M., Carrère, L., and Picot, N. "FES2014 global ocean tide atlas: design and performance". In: *Ocean Science* 17.3 (2021), pp. 615–649. ISSN: 1812-0792. DOI: 10.5194/os-17-615-2021.

Madsen, A. T., Murray, A. S., Andersen, T. J., and Pejrup, M. "Spatial and temporal variability of sediment accumulation rates on two tidal flats in Lister Dyb tidal basin, Wadden Sea, Denmark". In: *Earth Surface Processes and Landforms* 35.13 (2010), pp. 1556–1572. ISSN: 0197-9337. DOI: 10.1002/esp.1999.

Malcherek, A., Piechotta, F., and Knoch, D. *Mathematical Module SediMorph: Validation Document*. Hamburg, 2002.

Meyer, C. and Ragutzki, G. *KFKI Forschungsvorhaben Sedimentverteilung als Indikator für morphodynamische Prozesse: MTK 0591 ; Zwischenbericht 1996*. Vol. 9/1997. Dienstber. Forschungsstelle Küste. Norderney: Forschungsstelle Küste, 1997.

Milbradt, P., Valerius, J., and Zeiler, M. "Das Funktionale Bodenmodell: Aufbereitung einer konsistenten Datenbasis für die Morphologie und Sedimentologie". In: *AufMod* (2015).

Morris, R. and Mitchell, S. B. "Has Loss of Accommodation Space in the Humber Estuary Led to Elevated Suspended Sediment Concentrations?" In: *Journal of Frontiers in Construction Engineering* 2 (1) (2013), pp. 1–9.

Müller, M. "Rapid change in semi-diurnal tides in the North Atlantic since 1980". In: *Geophysical Research Letters* 38.11 (2011), n/a–n/a. ISSN: 00948276. DOI: 10.1029/2011GL047312.

Müller, M. "The influence of changing stratification conditions on barotropic tidal transport and its implications for seasonal and secular changes of tides". In: *Continental Shelf Research* 47 (2012), pp. 107–118. ISSN: 02784343. DOI: 10.1016/j.csr.2012.07.003.

Müller, M., Cherniawsky, J. Y., Foreman, M. G. G., and von Storch, J.-S. "Seasonal variation of the M 2 tide". In: *Ocean Dynamics* 64.2 (2014), pp. 159–177. DOI: 10.1007/s10236-013-0679-0.

Nederhoff, K., Smits, B., and Wang, Z. *KPP Wadden, Data analyse: getij en morfologie*. Ed. by Deltares (Delft) Report 11200521-000-ZKS-0002. 2017.

Nidzieko, N. J. "Tidal asymmetry in estuaries with mixed semidiurnal/diurnal tides". In: *Journal of Geophysical Research* 115.C8 (2010), p. 185. ISSN: 0148-0227. DOI: 10.1029/2009JC005864.

Oppenheimer, M. et al. *Sea level rise and implications for low lying Islands, coasts and communities*. Ed. by IPCC special report on the ocean and cryosphere in a changing climate. Cambridge, UK, 2019.

OSPAR Commission. *Region 2: Greater North Sea*. Vol. region ... / OSPAR Commission for the protection of the marine environment of the North-East Atlantic ; 2. Quality status report 2000. London, 2000. ISBN: 0-946956-48-0.

Otto, L. et al. "Review of the physical oceanography of the North Sea". In: *Netherlands Journal of Sea Research* 26.2-4 (1990), pp. 161–238. ISSN: 00777579. DOI: 10.1016/0077-7579(90)90091-T.

Pelling, H. E., Uehara, K., and Green, J. A. M. "The impact of rapid coastline changes and sea level rise on the tides in the Bohai Sea, China". In: *Journal of Geophysical Research: Oceans* 118.7 (2013), pp. 3462–3472. ISSN: 21699275. DOI: 10.1002/jgrc.20258.

Pelling, H. E., Mattias Green, J. A., and Ward, S. L. "Modelling tides and sea-level rise: To flood or not to flood". In: *Ocean Modelling* 63 (2013), pp. 21–29. ISSN: 14635003. DOI: 10.1016/j.ocemod.2012.12.004.

Peng, D., Hill, E. M., Meltzner, A. J., and Switzer, A. D. "Tide Gauge Records Show That the 18.61-Year Nodal Tidal Cycle Can Change High Water Levels by up to 30 cm". In: *Journal of Geophysical Research: Oceans* 124.1 (2019), pp. 736–749. ISSN: 21699275. DOI: 10.1029/2018JC014695.

Pethick, J. S. "Velocity surges and asymmetry in tidal channels". In: *Estuarine and Coastal Marine Science* 11.3 (1980), pp. 331–345. ISSN: 03023524. DOI: 10.1016/S0302-3524(80)80087-9.

Pickering, M. D., Wells, N. C., Horsburgh, K. J., and Green, J. "The impact of future sea-level rise on the European Shelf tides". In: *Continental Shelf Research* 35 (2012), pp. 1–15. ISSN: 02784343. DOI: 10.1016/j.csr.2011.11.011.

Pickering, M. D. et al. "The impact of future sea-level rise on the global tides". In: *Continental Shelf Research* 142 (2017), pp. 50–68. ISSN: 02784343. DOI: 10.1016/j.csr.2017.02.004.

Plüß, A. *Das Nordseemodell der BAW zur Simulation der Tide in der Deutschen Bucht*. Heide i. Holstein: Boyens Medien, 2003.

Postma, H. "Transport and accumulation of suspended matter in the Dutch Wadden Sea". In: *Netherlands Journal of Sea Research* 1.1-2 (1961), pp. 148–190. ISSN: 00777579. DOI: 10.1016/0077-7579(61)90004-7.

Postma, H. "Exchange of materials between the North Sea and the Wadden Sea". In: *Marine Geology* 40.1-2 (1981), pp. 199–213. ISSN: 00253227. DOI: 10.1016/0025-3227(81)90050-5.

Pritchard, D. and Hogg, A. J. "Cross-shore sediment transport and the equilibrium morphology of mudflats under tidal currents". In: *Journal of Geophysical Research* 108.C10 (2003), p. 1635. ISSN: 0148-0227. DOI: 10.1029/2002JC001570.

Pritchard, D. "Suspended sediment transport along an idealised tidal embayment: Settling lag, residual transport and the interpretation of tidal signals". In: *Ocean Dynamics* 55.2 (2005), pp. 124–136. DOI: 10.1007/s10236-005-0004-7.

Pugh, D. T. *Tides, Surges and Mean Sea-Level*. Chichester: John Wiley and Sons, 1987. ISBN: 047191505X.

Putzar, B. and Malcherek, A. "Entwicklung und Anwendung eines Langfrist-Morphodynamikmodells für die Deutsche Bucht". In: *AufMod* (2015).

M. Quante and F. Colijn, eds. *North Sea Region Climate Change Assessment*. Regional Climate Studies. Cham: Springer International Publishing, 2016. ISBN: 978-3-319-39743-6. DOI: 10.1007/978-3-319-39745-0.

Ragutzki, G. *Verteilung der Oberflächensedimente auf den niedersächsischen Watten*. Norderney, 1980.

Rasquin, C., Seiffert, R., Wachler, B., and Winkel, N. "The significance of coastal bathymetry representation for modelling the tidal response to mean sea level rise in the German Bight". In: *Ocean Science* 16.1 (2020), pp. 31–44. ISSN: 1812-0792. DOI: 10.5194/os-16-31-2020.

H.-E. Reineck and K.-E. Behre, eds. *Das Watt: Ablagerungs- und Lebensraum*. 2., neubearb. u. erw. Aufl. Vol. 50. Senckenberg-Buch. Frankfurt a.M.: Kramer, 1978. ISBN: 3782910672.

Reineck, H.-E. and Siefert, W. "Faktoren der Schlickbildung im Sahlenburger und Neuwerker Watt". In: *Die Küste* 35 (1980) (1980), S. 26–51 : Ill., graph. Darst.

Reistad, M. et al. "A high-resolution hindcast of wind and waves for the North Sea, the Norwegian Sea, and the Barents Sea". In: *Journal of Geophysical Research: Atmospheres* 116.C5 (2011). ISSN: 01480227. DOI: 10.1029/2010JC006402.

Ridderinkhof, H. "The Effect of Tidal Asymmetries on the Net Transport of Sediments in the Ems Dollard Estuary". In: *Journal of Coastal Research* (1997), pp. 41–48. ISSN: 0749-0208. URL: http://www.jstor.org/stable/25736104.

Sassi, M., Duran-Matute, M., van Kessel, T., and Gerkema, T. "Variability of residual fluxes of suspended sediment in a multiple tidal-inlet system: The Dutch Wadden Sea". In: *Ocean Dynamics* 65.9-10 (2015), pp. 1321–1333. DOI: 10.1007/s10236-015-0866-2.

Schindelegger, M., Green, J. A. M., Wilmes, S., and Haigh, I. D. "Can We Model the Effect of Observed Sea Level Rise on Tides?" In: *Journal of Geophysical Research: Oceans* 123.7 (2018), pp. 4593–4609. ISSN: 21699275. DOI: 10.1029/2018JC013959.

Schneggenburger, C., Günther, H., and Rosenthal, W. "Spectral wave modelling with nonlinear dissipation: Validation and applications in a coastal tidal environment". In: *Coastal Engineering* 41.1-3 (2000), pp. 201–235. ISSN: 03783839. DOI: 10.1016/S0378-3839(00)00033-8.

Sehili, A., Lang, G., and Lippert, C. "High-resolution subgrid models: Background, grid generation, and implementation". In: *Ocean Dynamics* 64.4 (2014), pp. 519–535. DOI: 10.1007/s10236-014-0693-x.

Sievers, J., Malte, R., and Milbradt, P. *EasyGSH-DB: Themengebiet - Geomorphologie*. Ed. by Bundesanstalt für Wasserbau. 2020. DOI: 10.48437/02.2020.K2.7000.0001.

Sievers, J., Malte, R., and Milbradt, P. *EasyGSH-DB: Themengebiet - Sedimentologie*. 2020. DOI: 10.48437/02.2020.K2.7000.0005.

Sievers, J. et al. "An integrated marine data collection for the German Bight – Part 1: Subaqueous geomorphology and surface sedimentology (1996–2016)". In: *Earth System Science Data* 13.8 (2021), pp. 4053–4065. ISSN: 1866-3516. DOI: 10.5194/essd-13-4053-2021.

Sindowski, K.-H. *Das ostfriesische Küstengebiet: Inseln, Watten und Marschen : mit 22 Tabellen*. Vol. 57. Sammlung geologischer Führer. Berlin: Borntraeger, 1973. ISBN: 344315011X.

Song, D., Wang, X. H., Kiss, A. E., and Bao, X. "The contribution to tidal asymmetry by different combinations of tidal constituents". In: *Journal of Geophysical Research* 116.C12 (2011), p. 185. ISSN: 0148-0227. DOI: 10.1029/2011JC007270.

Speer, P. E. and Aubrey, D. G. "A study of non-linear tidal propagation in shallow inlet/estuarine systems Part II: Theory". In: *Estuarine, Coastal and Shelf Science* 21.2 (1985), pp. 207–224. ISSN: 02727714. DOI: 10.1016/0272-7714(85)90097-6.

Stanev, E. V. et al. "Extreme westward surface drift in the North Sea: Public reports of stranded drifters and Lagrangian tracking". In: *Continental Shelf Research* 177.11 (2019), pp. 24–32. ISSN: 02784343. DOI: 10.1016/j.csr.2019.03.003.

Stanev, E. V., Dobrynin, M., Pleskachevsky, A., Grayek, S., and Günther, H. "Bed shear stress in the southern North Sea as an important driver for suspended sediment dynamics". In: *Ocean Dynamics* 59.2 (2009), pp. 183–194. DOI: 10.1007/s10236-008-0171-4.

Staneva, J. et al. "Hydrodynamics and sediment dynamics in the German Bight. A focus on observations and numerical modelling in the East Frisian Wadden Sea". In: *Continental Shelf Research* 29.1 (2009), pp. 302–319. ISSN: 02784343. DOI: 10.1016/j.csr.2008.01.006.

Steffelbauer, D. B., Riva, R. E., Timmermans, J. S., Kwakkel, J. H., and Bakker, M. "Evidence of regional sea-level rise acceleration for the north sea". In: *Environmental Research Letters* (2022). DOI: 10.1088/1748-9326/ac753a.

Stive, M. J. F., Roelvink, D. A., and de Vriend, H. J. "Large-Scale Coastal Evolution Concept". In: (1990), pp. 1962–1974. DOI: 10.1061/9780872627765.150.

Turrell, W. R. "New hypotheses concerning the circulation of the northern North Sea and its relation to North Sea fish stock recruitment". In: *ICES Journal of Marine Science* 49.1 (1992), pp. 107–123. ISSN: 1054-3139. DOI: 10.1093/icesjms/49.1.107.

van Maren, D. S., Oost, A. P., Wang, Z. B., and Vos, P. C. "The effect of land reclamations and sediment extraction on the suspended sediment concentration in the Ems Estuary". In: *Marine Geology* 376.Suppl. 1 (2016), pp. 147–157. ISSN: 00253227. DOI: 10.1016/j.margeo.2016.03.007.

van Maren, D. S. and Winterwerp, J. C. "The role of flow asymmetry and mud properties on tidal flat sedimentation". In: *Continental Shelf Research* 60.5 (2013), S71–S84. ISSN: 02784343. DOI: 10.1016/j.csr.2012.07.010.

van Prooijen, B. C. and Winterwerp, J. C. "A stochastic formulation for erosion of cohesive sediments". In: *Journal of Geophysical Research* 115.C1 (2010). ISSN: 0148-0227. DOI: 10.1029/2008JC005189.

van Rijn, L. C., Grasmeijer, B. T., and Ruessink, B. G. *Measurement errors of instruments for velocity, wave heigt, sand concentration and bed levels in field conditions*. Ed. by COAST3D, Dep. of Physical Geography, University of Utrecht WL, Delft Hydraulics. Utrecht, 2000.

van Rijn, L. C. "Unified View of Sediment Transport by Currents and Waves. I: Initiation of Motion, Bed Roughness, and Bed-Load Transport". In: *Journal of Hydraulic Engineering* 133.6 (2007), pp. 649–667. ISSN: 0733-9429. DOI: 10.1061/(ASCE)0733-9429(2007)133:6(649).

Vos, P. C. and Knol, E. "Holocene landscape reconstruction of the Wadden Sea area between Marsdiep and Weser". In: *Netherlands Journal of Geosciences* 94.2 (2015), pp. 157–183. ISSN: 0016-7746. DOI: 10.1017/njg.2015.4.

Wachler, B., Seiffert, R., Rasquin, C., and Kösters, F. "Tidal response to sea level rise and bathymetric changes in the German Wadden Sea". In: *Ocean Dynamics* 70.8 (2020), pp. 1033–1052. DOI: 10.1007/s10236-020-01383-3.

Wang, Z. B. and Townend, I. H. "Influence of the nodal tide on the morphological response of estuaries". In: *Marine Geology* 291-294 (2012), pp. 73–82. ISSN: 00253227. DOI: 10.1016/j.margeo.2011.11.007.

Wang, Z. B., Elias, E. P., van der Spek, A. J., and Lodder, Q. J. "Sediment budget and morphological development of the Dutch Wadden Sea: Impact of accelerated sea-level rise and subsidence until 2100". In: *Netherlands Journal of Geosciences* 97.3 (2018), pp. 183–214. ISSN: 0016-7746. DOI: 10.1017/njg.2018.8.

Ward, S. L., Green, J. A. M., and Pelling, H. E. "Tides, sea-level rise and tidal power extraction on the European shelf". In: *Ocean Dynamics* 62.8 (2012), pp. 1153–1167. DOI: 10.1007/s10236-012-0552-6.

Weisse, R. and Günther, H. "Wave climate and long-term changes for the Southern North Sea obtained from a high-resolution hindcast 1958–2002". In: *Ocean Dynamics* 57.3 (2007), pp. 161–172. DOI: 10.1007/s10236-006-0094-x.

Weisse, R. and Plüβ, A. "Storm-related sea level variations along the North Sea coast as simulated by a high-resolution model 1958–2002". In: *Deutsche Hydrografische Zeitschrift* 56.1 (2006), pp. 16–25. ISSN: 1616-7228. DOI: 10.1007/s10236-005-0037-y.

Willmott, C. J. and Matsuura, K. "Advantages of the mean absolute error (MAE) over the root mean square error (RMSE) in assessing average model performance". In: *Climate Research* 30 (2005), pp. 79–82. DOI: 10.3354/cr030079.

Willmott, C. J. "On the Evaluation of Model Performance in Physical Geography". In: *Spatial Statistics and Models*. Ed. by G. L. Gaile and C. J. Willmott. Dordrecht: Springer Netherlands, 1984, pp. 443–460. ISBN: 978-90-481-8385-2. DOI: 10.1007/978-94-017-3048-8_23.

Winter, C. "On the evaluation of sediment transport models in tidal environments". In: *Sedimentary Geology* 202.3 (2007), pp. 562–571. ISSN: 00370738. DOI: 10.1016/j.sedgeo.2007.03.019.

Winterwerp, J. C., van Kessel, T., van Maren, D. S., and van Prooijen, B. C. *Fine Sediment in Open Water: From Fundamentals to Modeling*. Vol. 55. WORLD SCIENTIFIC, 2021. ISBN: 978-981-12-4361-5. DOI: 10.1142/12473.

Winterwerp, J. C. et al. "SPM response to tide and river flow in the hyper-turbid Ems River". In: *Ocean Dynamics* 67.5 (2017), pp. 559–583. DOI: 10.1007/s10236-017-1043-6.

Woodworth, P. L. and Blackman, D. L. "Evidence for Systematic Changes in Extreme High Waters since the Mid-1970s". In: *Journal of Climate* 17.6 (2004), pp. 1190–1197. ISSN: 0894-8755. DOI: 10.1175/1520-0442(2004)017<1190:EFSCIE>2.0.CO;2.

Zhang, W. et al. "Unravelling the causes of tidal asymmetry in deltas". In: *Journal of Hydrology* 564.3–4 (2018), pp. 588–604. ISSN: 00221694. DOI: 10.1016/j.jhydrol.2018.07.023.

Zhou, Z. et al. "On the stability relationships between tidal asymmetry and morphologies of tidal basins and estuaries". In: *Earth Surface Processes and Landforms* 43.9 (2018), pp. 1943–1959. ISSN: 0197-9337. DOI: 10.1002/esp.4366.

Zijl, F., Verlaan, M., and Gerritsen, H. "Improved water-level forecasting for the Northwest European Shelf and North Sea through direct modelling of tide, surge and non-linear interaction". In: *Ocean Dynamics* 63.7 (2013), pp. 823–847. DOI: 10.1007/s10236-013-0624-2.

Chapter A
Observational Gauge Locations

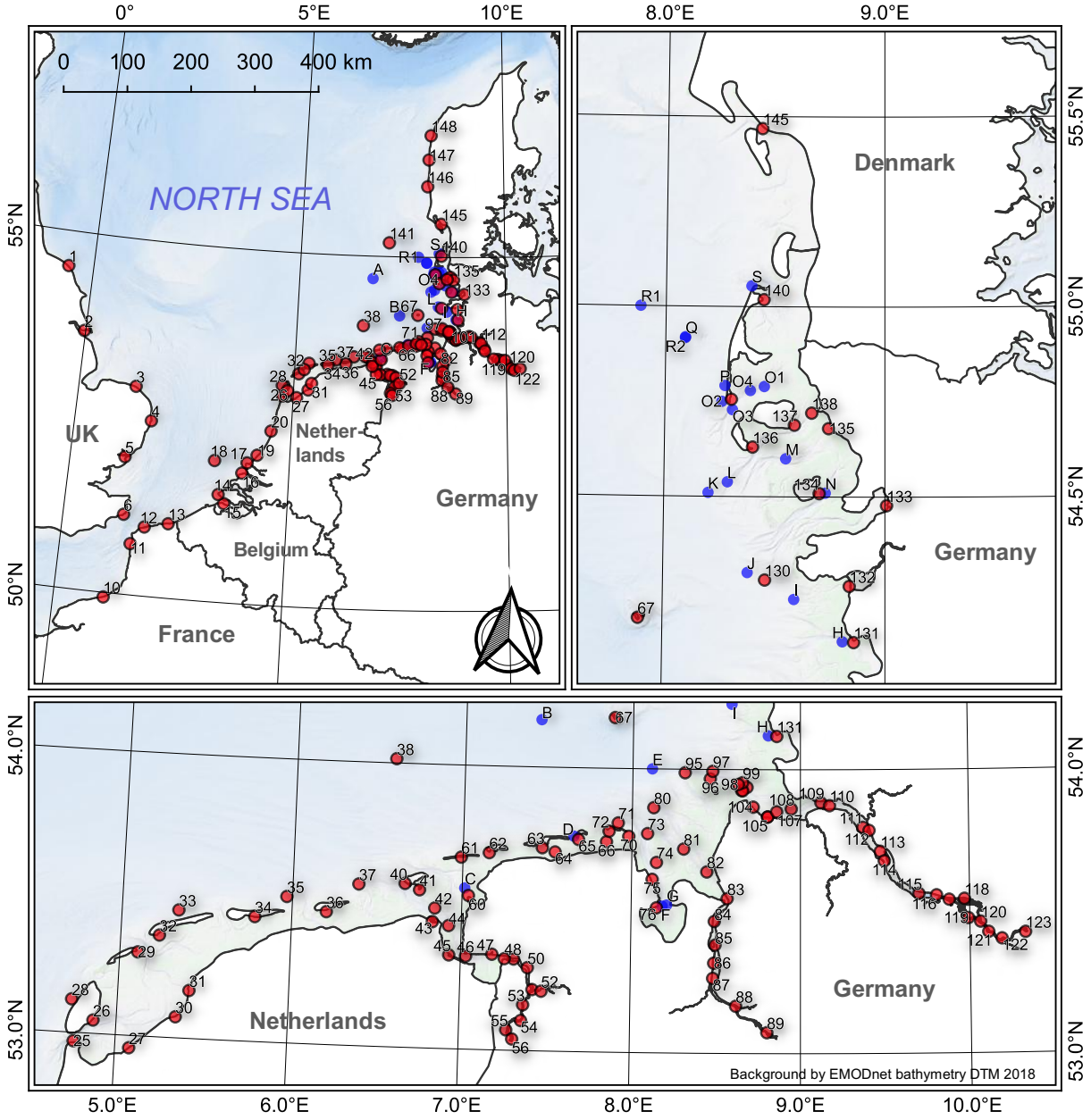

FIGURE A.1: Gauge map showing measurement locations in the southern North Sea. Red dots represent hydrographic and blue dots sea state measurement locations. Gauge names are indicated in the table in Appendix A.

TABLE A.1: Gauge names in Figure A.1.

ID		Short name	Long name
1	UK	WTB_UK	Whitby
2	UK	IMM_UK	Immingham
3	UK	CRO_UK	Cromer
4	UK	LOW_UK	Lowestoft
5	GB	HAW_UK	Harwich
6	UK	DOV_UK	Dover
10	FR	DIE_FR	Dieppe
11	FR	BOU_FR	Boulogne
12	F	CAL_FR	Calais
13	FR	DUN_FR	Dunkerque
14	NL	WEK_NL	Westkapelle
15	NL	VLS_NL	Vlissingen
16	NL	HVL_NL	Haringvliet
17	NL	HVH_NL	Hoek van Holland
18	NL	EUP_NL	Euro Platform
19	NL	SVN_NL	Scheveningen
20	NL	IJB_NL	Ijmuiden
25	NL	DEH_NL	Den Helder
26	NL	OUD_NL	Oudeschild
27	NL	DOE_NL	Den Oever
28	NL	TXN_NL	Texel
29	NL	VLH_NL	Vlieland Haven
30	NL	KOR_NL	Kornwerderzand
31	NL	HAR_NL	Harlingen
32	NL	TSW_NL	Terschelling West
33	NL	TSN_NL	Terschelling
34	NL	NES_NL	Nes
35	NL	WRG_NL	Wierumergronden
36	NL	SMK_NL	Schiermonnikoog
37	NL	HUI_NL	Hubertgat
38	D	FIN1	FINO-I
40	D	BOS	Borkum Suedstrand
41	D	BOF	Borkum Fischerbalje
42	D	EMS	Emshoern
43	NL	EEM	Eemshaven
44	D	DUK	Dukegat
45	NL	DEL	Delfzijl
46	D	KNO	Knock
47	D	EMD	Emden
48	D	POG	Pogum
49	D	GAN	Gandersum
50	D	TER	Terborg
51	D	LEEO	Leer Ort
52	DE	LEL	Leer Leda
53	D	WEE	Weener
54	D	PAP	Papenburg
55	DE	REH	Rhede
56	DE	HER	Herbrum
60		LEY	Leybucht
61		JUI	Juist

ID		Short name	Long name
61		JUI	Juist
62	D	NOY	Norderney Riffgat
63	D	LAN	Langeoog
64	D	BEN	Bensersiel
65	D	SPI	Spiekeroog
66	D	HARS	Harlesiel
67	D	HEL	Helgoland BH
70		WAO	Wangerooge Ost
71	D	WAN	Wangerooge Nord
72		WAW	Wangerooge Wesr
73	D	MPL	Mellumplate
74	D	HOO	Hooksielplate
75	D	VLP	Voslapp
76	D	WAV	Wilhelmshaven
80	D	ALW	LT Alte Weser
81	D	DWG	Dwarsgat
82	D	RSS	Robbensuedsteert
83	D	BAL	Bremerhaven Alter LT
84	D	NUF	Nordenham UF
85	D	RFL	Rechtenfleth
86	D	BRA	Brake
87	D	EFL	Elsfleth
88		VEG	Vegesack
89	D	WBR	Weserbruecke
95	D	BKA	Bake A
96	D	LZ5	Elbe_LZ5
97	D	VOG	G. Vogelsand
98		MGR	Mittelgrund
99	D	ZEH	Zehnerloch
101	D	LZ4	Elbe_LZ4
102	D	LZ4b	Elbe_LZ4b
103	D	LZ4a	Elbe_LZ4a
104	D	CUX	Cuxhaven
105	D	LZ3a	Elbe_LZ3a
106	D	LZ3	Elbe_LZ3
107		OTT	Otterndorf
108	D	LZ2	Elbe_LZ2
109	D	BRUN	Brunsbuettel
110	D	LZ1	Elbe_LZ1
111	D	D4	Elbe_D4
112	D	GLUE	Glueckstadt
113	D	D3	Elbe_D3
114	D	GRAU	Grauerort
115		SLAU	Schula
116	D	BLAN	Blankenese UF
117	D	SEEM	Seemannshoeft
118	D	STP	St. Pauli
119	D	HAR	Harburg
120	D	BUNT	Bunthaus
121		OVER	Over

ID		Short name	Long name
121		OVER	Over
122		ZOLL	Zollenspieker
123		GEH	Geesthacht UP
130		ROC	Rochelsteert
131	D	BUS	Buesum
132	D	EISP	Eidersperrwerk
133	D	HUS	Husum
134		PEL	Pellworm
135	D	SSL	Schluettsiel
136	D	WIT	Wittduen
137	D	WYK	Wyk_Foehr
138	D	DAG	Dagebuell
139	D	HOH	Hoernum_Hafen
140	D	LIH	List
141	D	FIN3	FINO-III
145	DK	ESB_DK	Esbjerk
146	DK	HVI_DK	Hvidesande
147		FER_DK	Ferring
148	DK	THY_DK	Thyboron

ID		Short name	Long name
A	D	NSB-III	Nordseeboje-III
B	D	DB	Deutsche Bucht
C	D	BAN	Bantsbalje
D	D	OTZ	Otzum-I
E	D	ELBE	Elbe
F	D	JAD-I1	Jade-I
G	D	JAD-II	Jade-II
H	D	BUE	Buesum-I
I	D	SUP	Suederpiep
J	D	SUH	Suederhever
K	D	RUE	Ruetgerat
L	D	AMR	Amrum-I
M	D	SUA	Suederaue
N	D	NOH	Norderhever
O1	D	HOR4	Hoernum-I
O2	D	HOR3	Hoernum Loch-I
O3	D	HOR1	Hoernum Tief-I
O4	D	HOR2	Hoernum Tief-II
P	D	BUN	Bunkerhill
Q	D	SYLT	Sylt
R1	D	WES	Westerland
R2	D	WES-II	Westerland-II
S	D	LST	List-I

Chapter B
Error Metrics, Statistics, and Regression

An error e (see Equation B.1) at a time t is defined as the difference between a reference (i.e., observation o) and a variant scenario (i.e., prediction p). Observations (often field measurements) represent the reference and modeling data the variant state. A comparison of variant and reference results in a number of errors which can be expressed as error metrics. Error metrics may either describe a time series of errors or errors along a number of gauges.
I used the widely accepted mean error (ME) μ and the root mean square error (RMSE) in my dissertation (Equations B.2 to B.4). The index of agreement R^2 (in Equation B.5) and its square root were applied to estimate the statistical significance of nonlinear multiple regression.

$$e_t = o_t - p_t \tag{B.1}$$

$$\mu = \frac{1}{n}\sum_{t=1}^{n} e_t \tag{B.2}$$

$$\sigma = \sqrt{\frac{1}{n-1}\sum_{t=1}^{n} |e_t - \mu|} \tag{B.3}$$

$$RMSE = \sqrt{\frac{1}{n}\sum_{t=1}^{n} (e_t)^2} \tag{B.4}$$

$$R^2 = \sqrt{\frac{\frac{1}{n}\sum_{t=1}^{n}(o_t - \overline{o})(p_t - \overline{p})}{\sigma_p \sigma_o}} \tag{B.5}$$

n	number of samples
e_t	error at the time t
o_t	observed sample at the time t
$\overline{o}$	mean of all observed samples
p_t	predicted sample at the time t
$\overline{p}$	mean of all predicted samples
μ	mean error (ME)
σ	standard deviation
MAE	mean absolute error (MAE)
RMSE	root mean square error (RMSE)
R^2	index of agreement
σ_o	standard deviation of observation
σ_p	standard deviation of prediction

A mix of positive and negative error residuals may lead to a ME close to 0 which is why the ME was always interpreted with the standard deviation σ (Equation B.3). The RMSE weights error samples towards larger error residuals through error squaring (Willmott and Matsuura, 2005; Willmott, 1984).
In trend analysis, different regression measures were applied (following Hagen et al., 2022). Trend analyses includeded simple linear regression (MATLABs `fitlm()`, last access 13.12.2021), second order polynomials, or multiple, non-linear curve fitting (MATLABS `fit`, last access 14.03.2022). All results were evaluated for statistical significance with an F-test at a 5 % significance level or by evaluating the index of agreement $R^2 > 0.5$. An F-Test results in either the

acceptance (insignificance) or the decline of a h_0 hypothesis (significance). The h_0 hypothesis was rejected if samples of two data sets came from normal distributions with unequal variance consequently indicating a dissimilar sample distribution between analysis and regression. It must be noted that statistical testing procedures assume normally distributed samples.
Some analyses deployed a simple outlier check (MATLABs `isoutlier()`, last access 13.12.2021) which I established to improve regression robustness, e.g., for morphologically averaged tidal asymmetry descriptors or bathymetry parameters. Samples which departed more than three scaled, median, absolute deviations from the sample median were then rejected in trend analysis.

Chapter C

Supplement: The Quantification of Recent Coastal Siltation

C.1 The Variability of the Tidal High and Low Water

Observed annual tidal characteristic values and MSL vary by several centimeters (Table C.1).

TABLE C.1: Mean of the annual 95^{th} quantile of the morphologically averaged tidal high water (upper intertidal boundary) and the 5^{th} quantile of the tidal low water (lower intertidal boundary) in the period of 1996 and 2016 in all morphological subunits from Figure 3.10 and their standard deviation over time σ.

#	unit ID	95^{th} q. HW $\pm\sigma$ in m	5^{th} q. LW $\pm\sigma$ in m
1	HUI	1.69 ± 0.08	-1.63 ± 0.06
2	BOS	1.73 ± 0.08	-1.71 ± 0.07
3	DEL	1.97 ± 0.09	-1.99 ± 0.08
4	EMD	2.15 ± 0.10	-2.10 ± 0.08
5	NOY	1.75 ± 0.07	-1.67 ± 0.07
6	LAN	1.84 ± 0.06	-1.73 ± 0.07
7	SPI	1.90 ± 0.07	-1.79 ± 0.07
8	WAN_W	1.96 ± 0.07	-1.86 ± 0.07
9	WAN_O	1.99 ± 0.07	-1.97 ± 0.08
10	MPL	2.17 ± 0.07	-2.23 ± 0.08
11	WAV	2.54 ± 0.07	-2.50 ± 0.07
12	ALW	2.09 ± 0.07	-2.06 ± 0.08
13	DWG	2.34 ± 0.07	-2.24 ± 0.08
14	BAL	2.53 ± 0.08	-2.33 ± 0.07
15	NEUW_S	2.08 ± 0.07	-2.04 ± 0.08
16	NEUW_N	2.09 ± 0.07	-1.98 ± 0.10
17	BKA	2.07 ± 0.08	-1.99 ± 0.09
18	CUX	2.21 ± 0.08	-1.95 ± 0.11
19	BRUN	2.24 ± 0.09	-1.85 ± 0.12
20	MEL	2.07 ± 0.08	-2.00 ± 0.09
21	EISP	2.01 ± 0.08	-1.99 ± 0.09
22	HUS	2.00 ± 0.09	-2.09 ± 0.09
23	PELL	1.82 ± 0.09	-1.88 ± 0.09
24	LANG	1.89 ± 0.09	-1.94 ± 0.09
25	DAG	1.80 ± 0.09	-1.86 ± 0.09
26	HOH	1.64 ± 0.09	-1.58 ± 0.10
27	LIST	1.45 ± 0.09	-1.41 ± 0.10

C.2 Subtidal Area

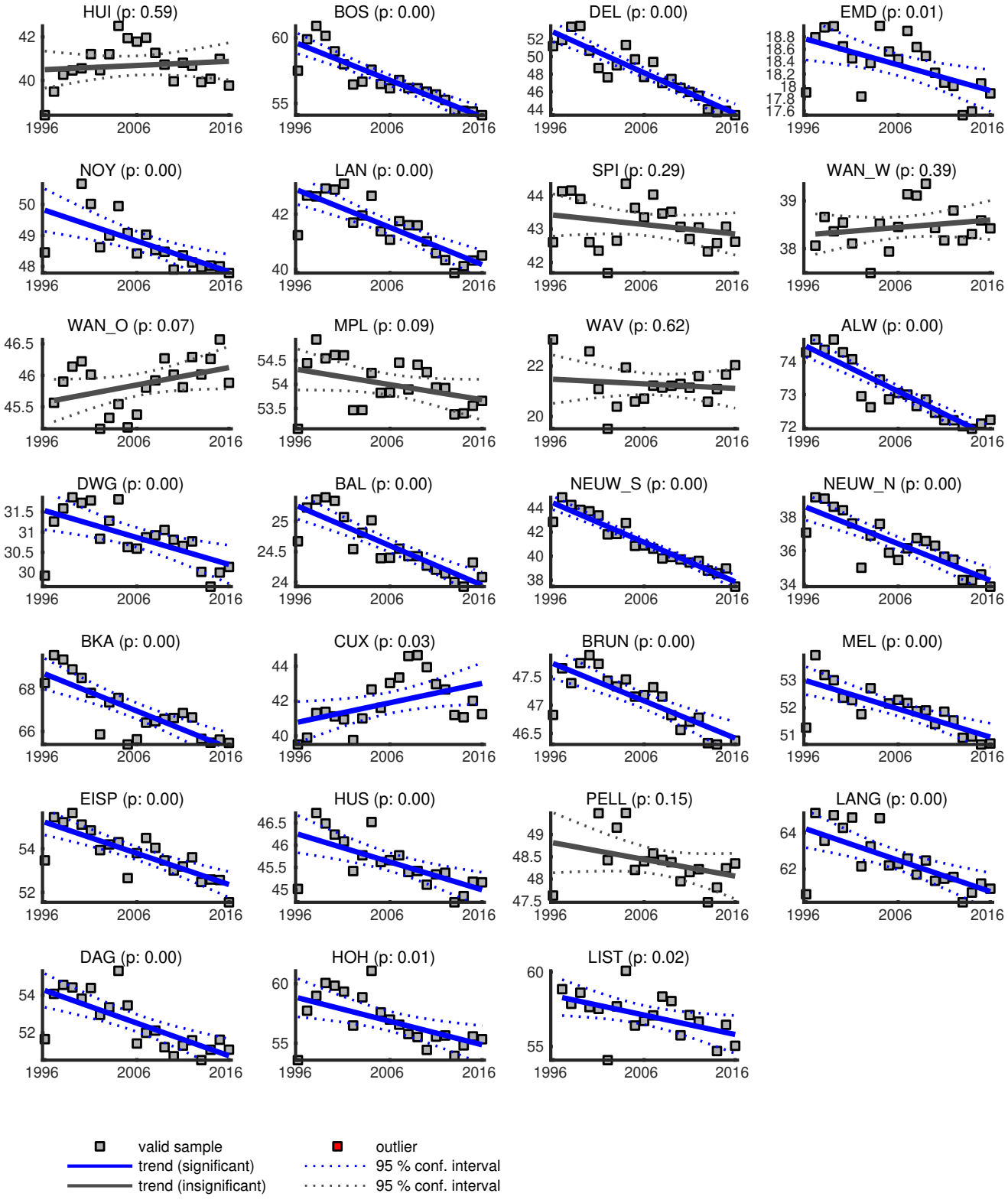

FIGURE C.1: Linear regression of the normalized subtidal area for morphological units from Figure 3.10. Blue lines indicate significant ($p < 0.05$) trends and their 95 % confidence intervals (dashed). Gray lines represent insignificant fitting with their 95 % confidence intervals (dashed). Valid samples are represented by gray squares and outliers by red squares. Outliers are not considered in trend estimation and significance testing.

C.3 Mean Subtidal and Intertidal Height

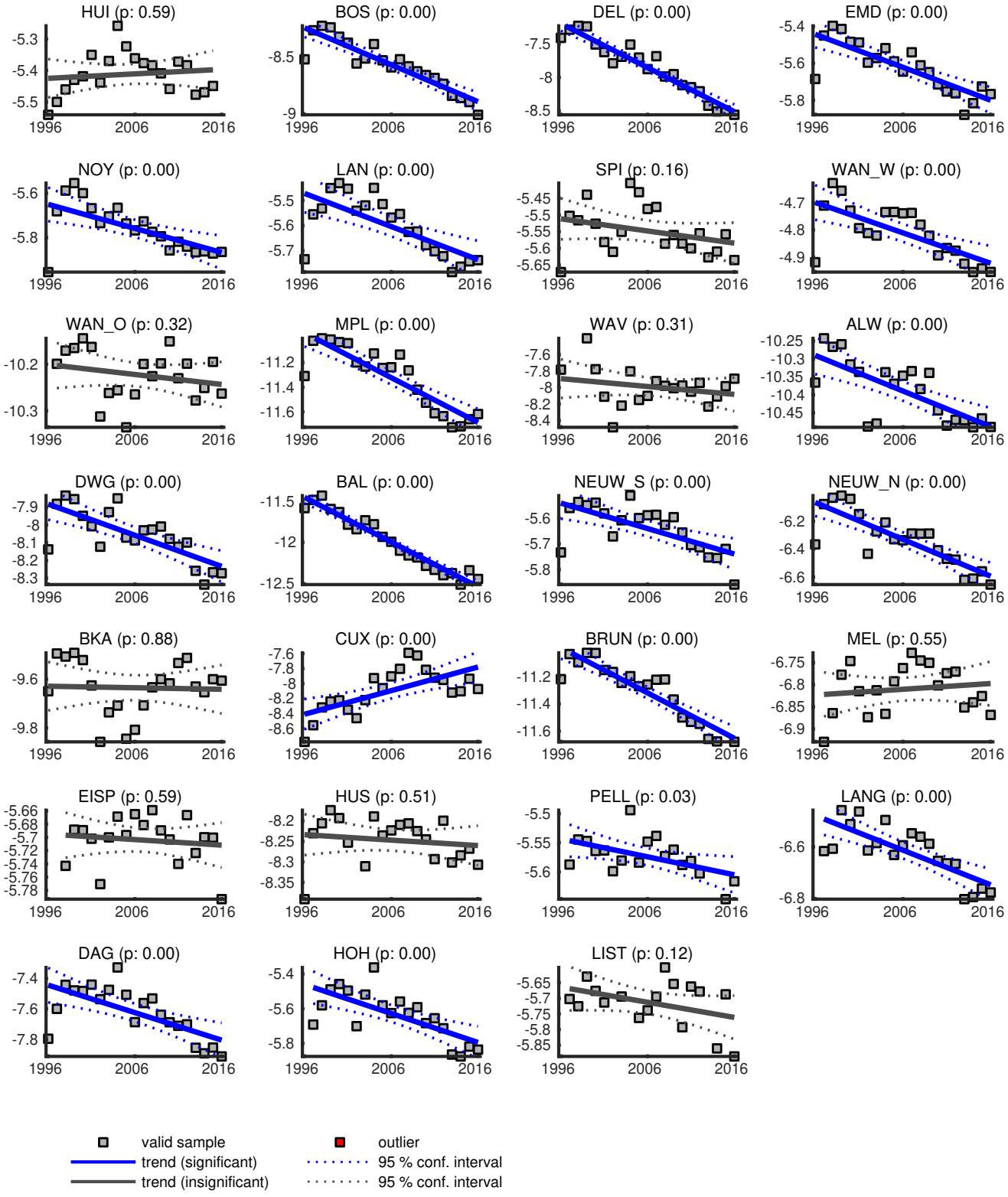

FIGURE C.2: Linear regression of subtidal mean height for morphological units from Figure 3.10. Blue lines indicate significant ($p < 0.05$) trends and their 95 % confidence intervals (dashed). Gray lines represent insignificant fitting with their 95 % confidence intervals (dashed). Valid samples are represented by gray squares and outliers by red squares. Outliers are not considered in trend estimation and significance testing.

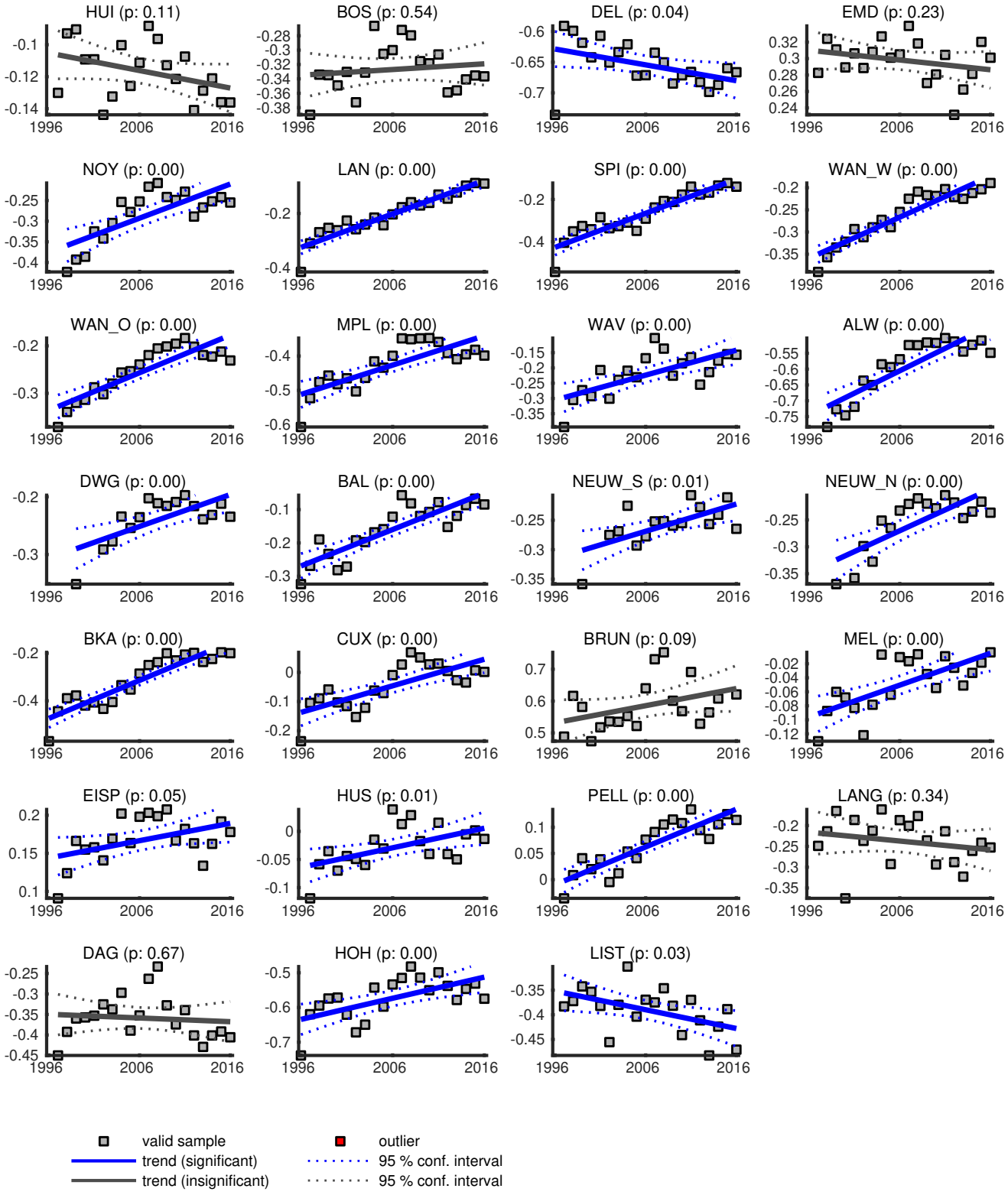

FIGURE C.3: Linear regression of the mean intertidal height for morphological units from Figure 3.10. Blue lines indicate significant ($p < 0.05$) trends and their 95 % confidence intervals (dashed). Gray lines represent insignificant fitting with their 95 % confidence intervals (dashed). Valid samples are represented by gray squares and outliers by red squares. Outliers are not considered in trend estimation and significance testing.

C.4 Intertidal Storage and Subtidal Channel Volume

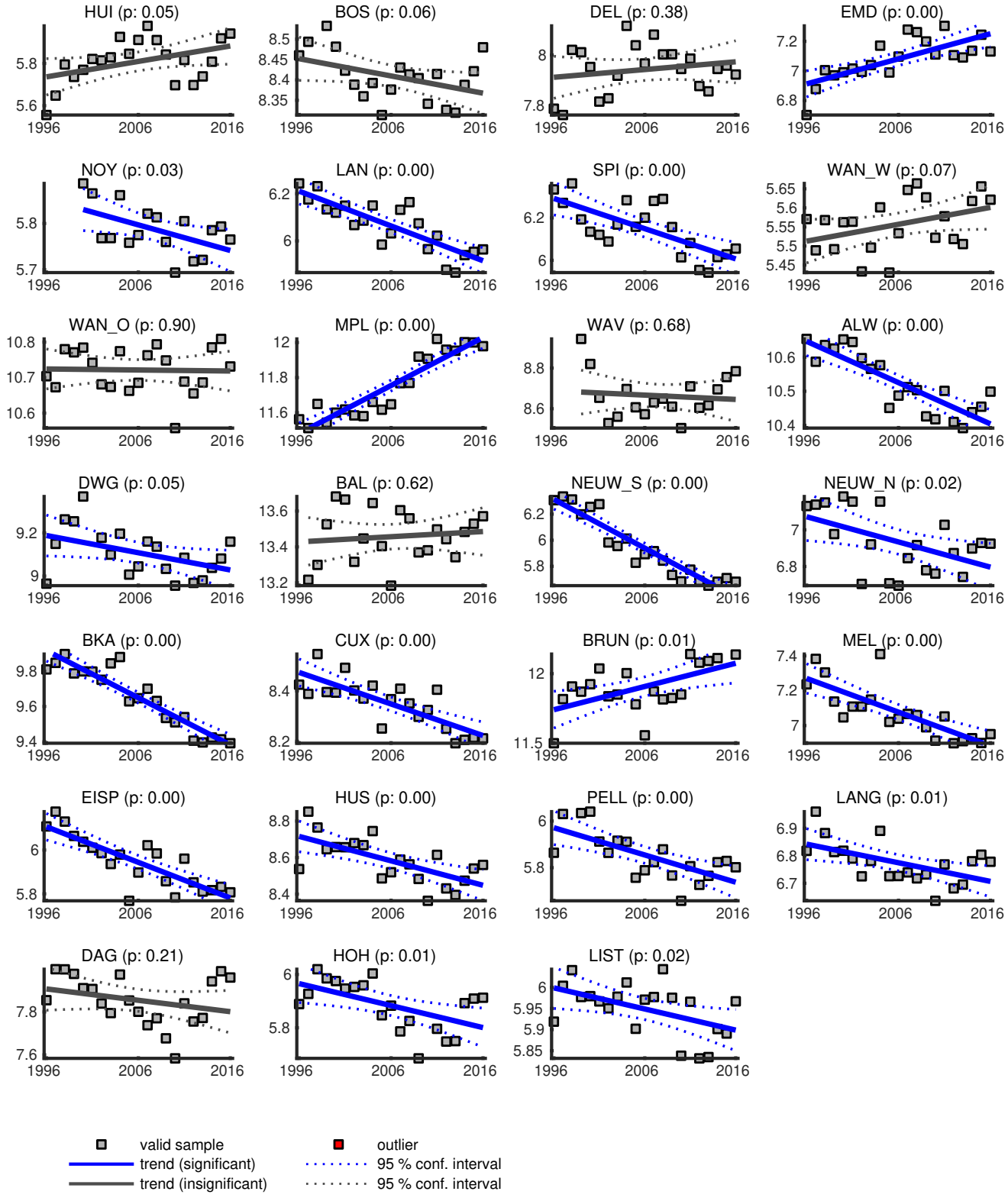

FIGURE C.4: Linear regression of the normalized subtidal channel volume V_c for morphological units from Figure 3.10. Blue lines indicate significant ($p < 0.05$) trends and their 95 % confidence intervals (dashed). Gray lines represent insignificant fitting with their 95 % confidence intervals (dashed). Valid samples are represented by gray squares and outliers by red squares. Outliers are not considered in trend estimation and significance testing.

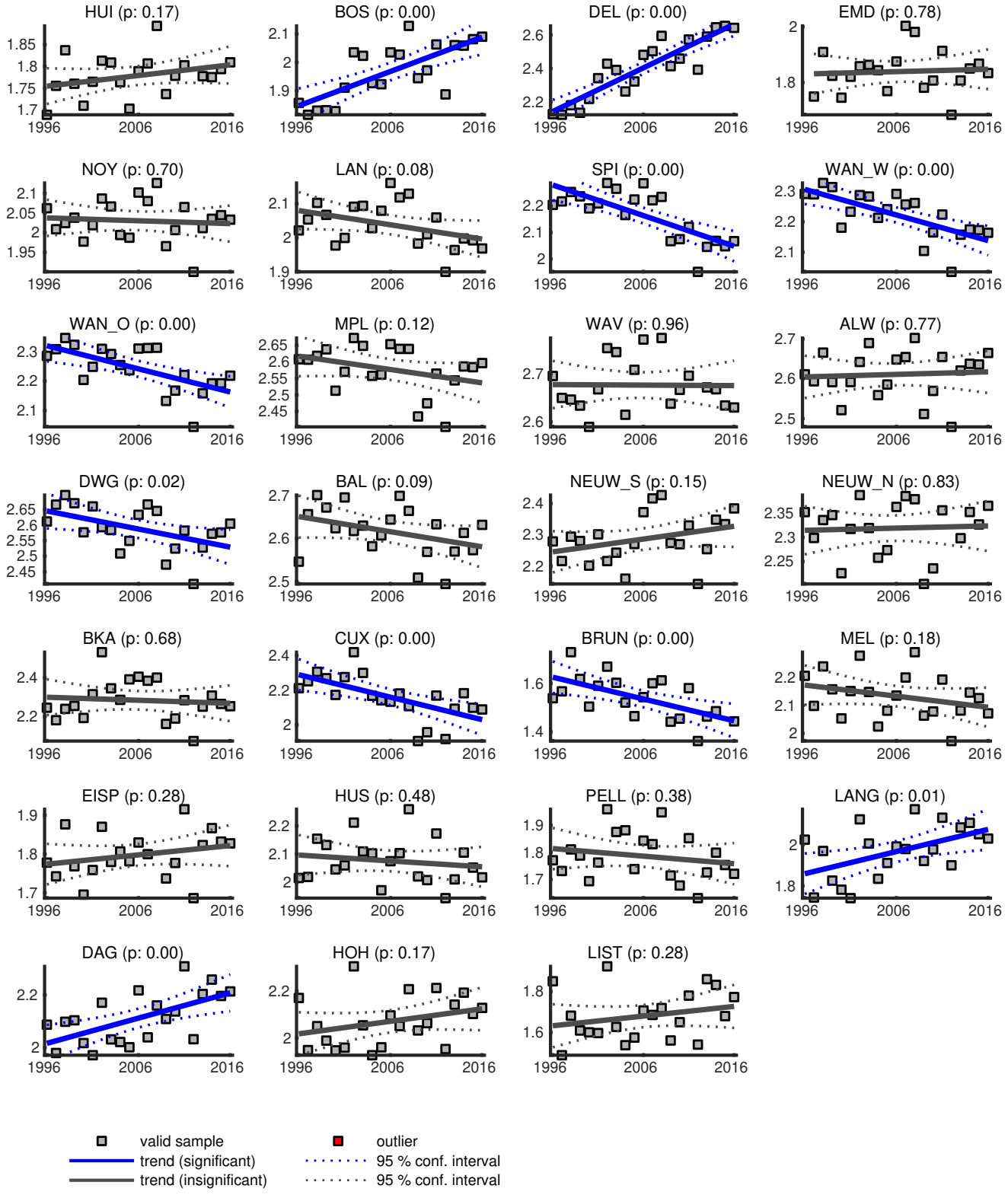

FIGURE C.5: Linear regression of the normalized intertidal storage volume V_s for morphological units from Figure 3.10. Blue lines indicate significant ($p < 0.05$) trends and their 95 % confidence intervals (dashed). Gray lines represent insignificant fitting with their 95 % confidence intervals (dashed). Valid samples are represented by gray squares and outliers by red squares. Outliers are not considered in trend estimation and significance testing.

C.5 Subtidal, Intertidal, and Total Sediment Budget

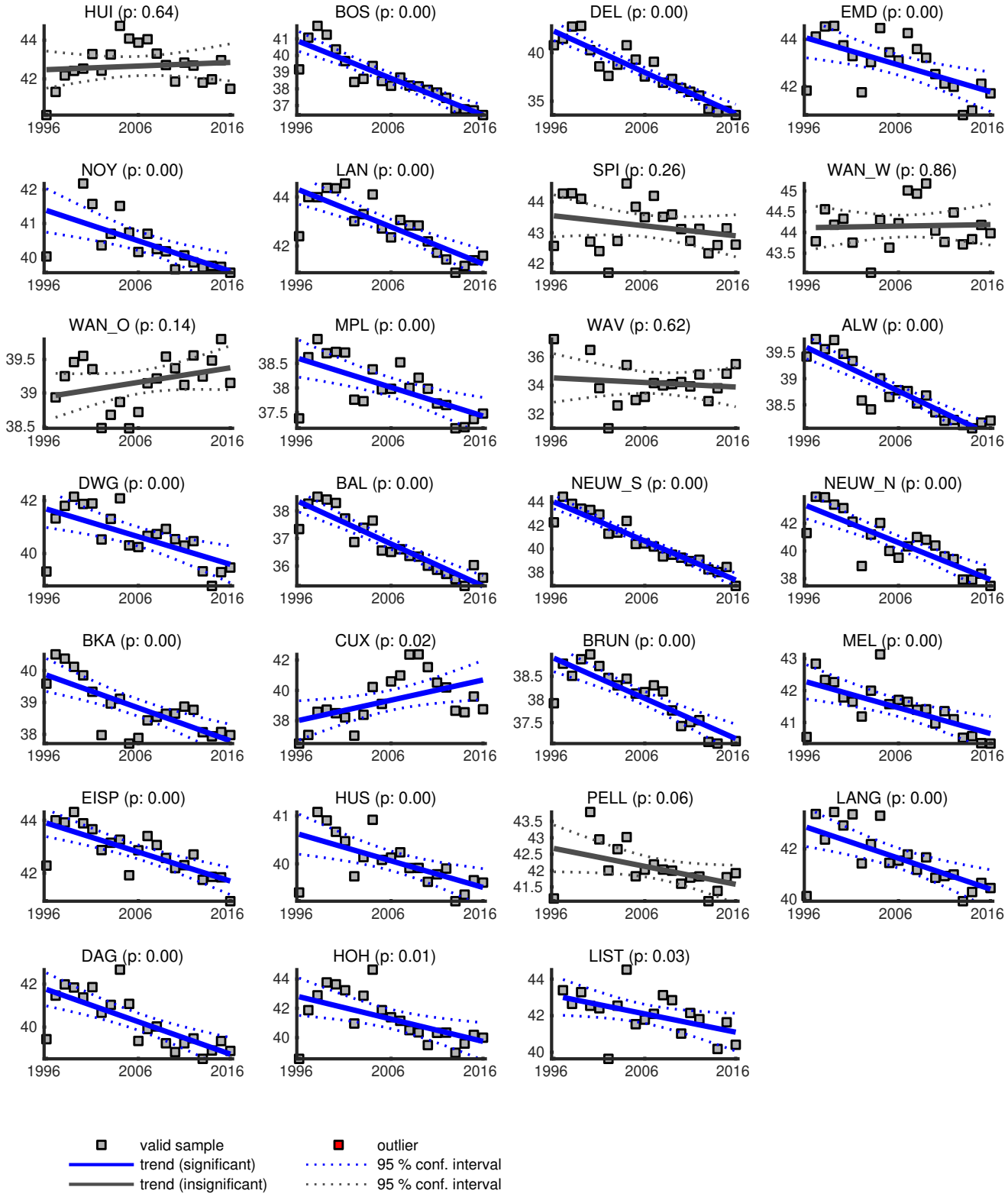

FIGURE C.6: Linear regression of the normalized subtidal sediment volume for morphological units from Figure 3.10. Blue lines indicate significant ($p < 0.05$) trends and their 95 % confidence intervals (dashed). Gray lines represent insignificant fitting with their 95 % confidence intervals (dashed). Valid samples are represented by gray squares and outliers by red squares. Outliers are not considered in trend estimation and significance testing.

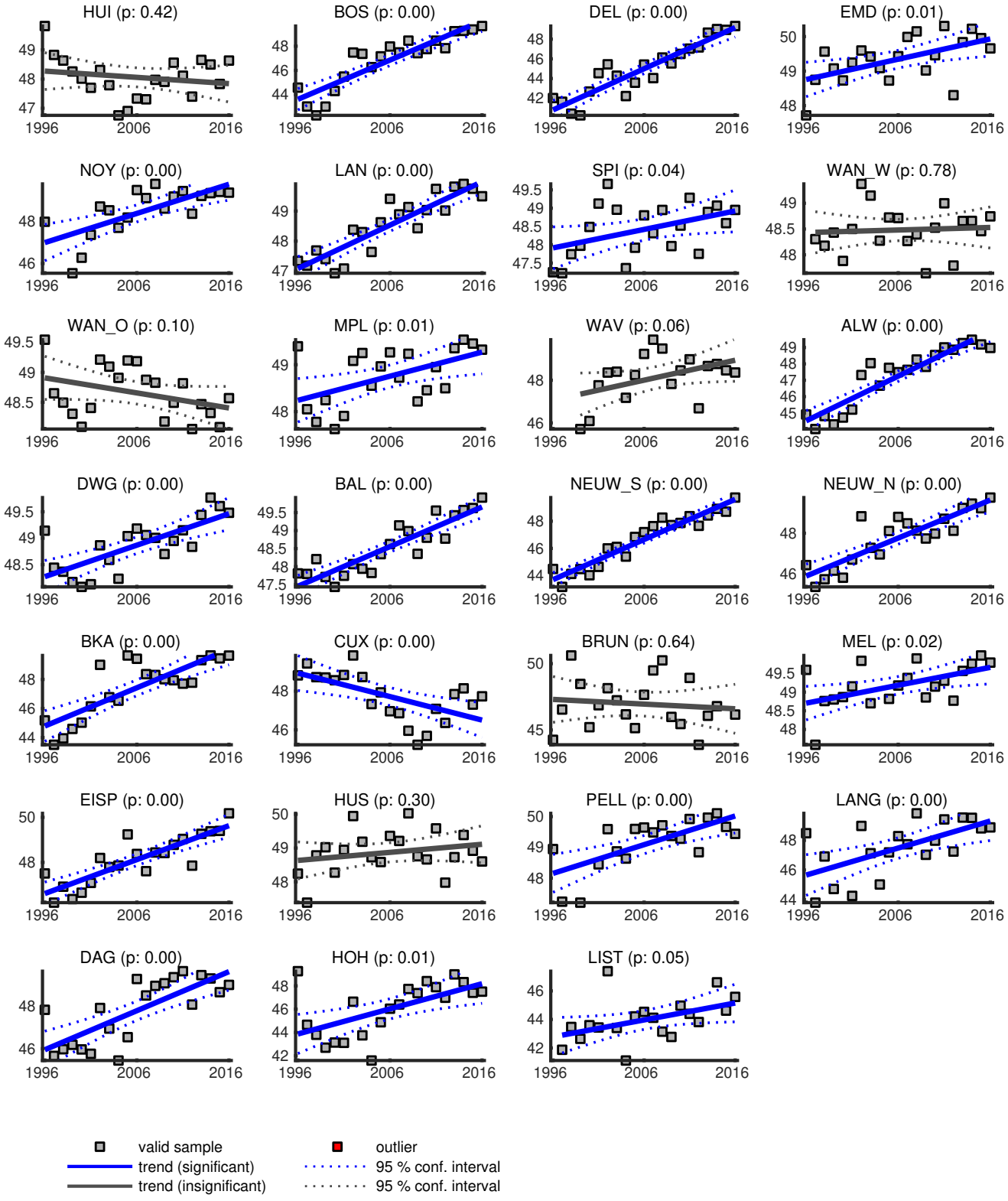

FIGURE C.7: Linear regression of the normalized intertidal sediment volume for morphological units from Figure 3.10. Blue lines indicate significant ($p < 0.05$) trends and their 95 % confidence intervals (dashed). Gray lines represent insignificant fitting with their 95 % confidence intervals (dashed). Valid samples are represented by gray squares and outliers by red squares. Outliers are not considered in trend estimation and significance testing.

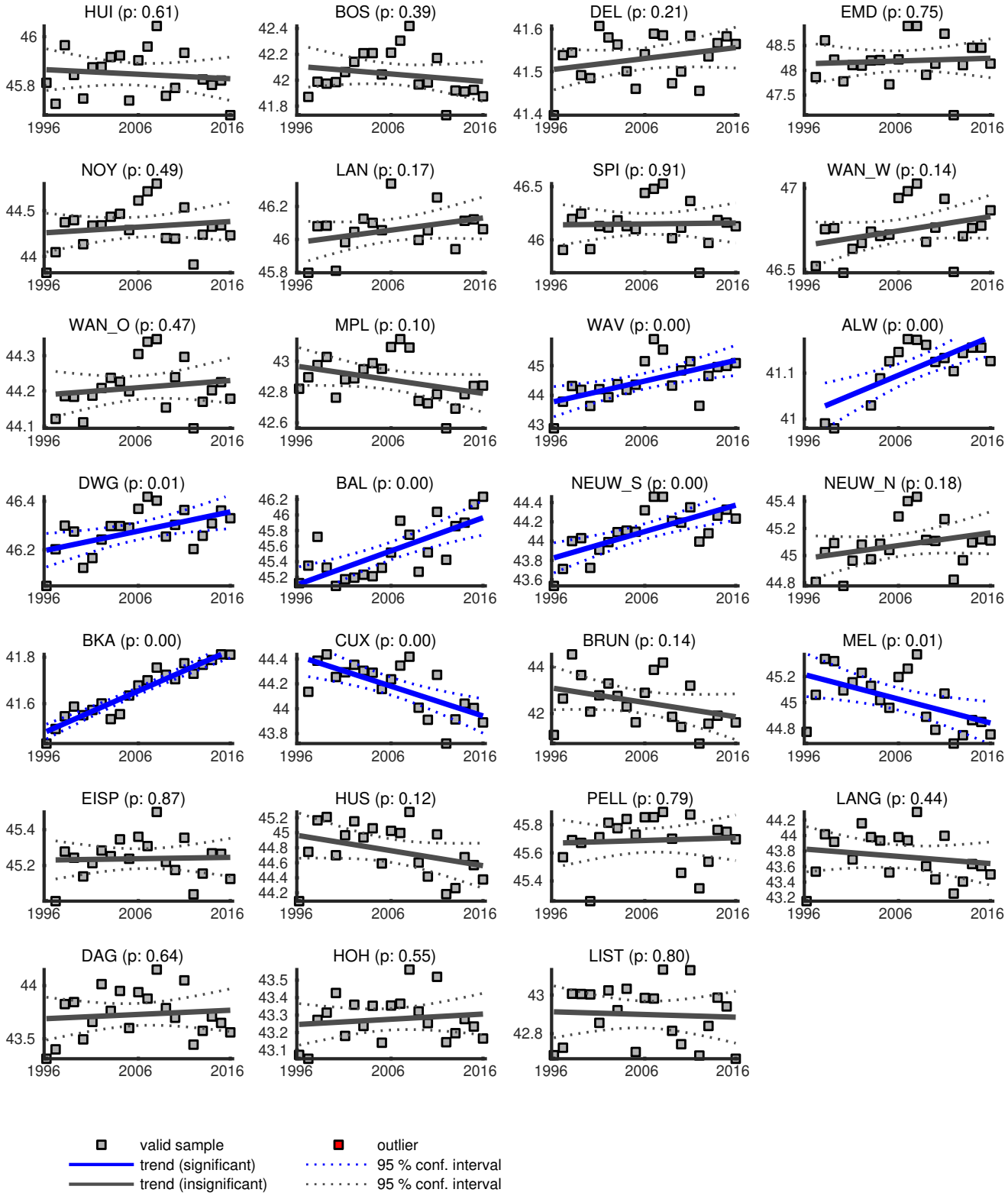

FIGURE C.8: Linear regression of the normalized total sediment volume for morphological units from Figure 3.10. Blue lines indicate significant ($p < 0.05$) trends and their 95 % confidence intervals (dashed). Gray lines represent insignificant fitting with their 95 % confidence intervals (dashed). Valid samples are represented by gray squares and outliers by red squares. Outliers are not considered in trend estimation and significance testing.

Chapter D

Supplement: Finding Changes in Tidal and Non-Tidal Forcing

D.1 Changes in Significant Wave Height

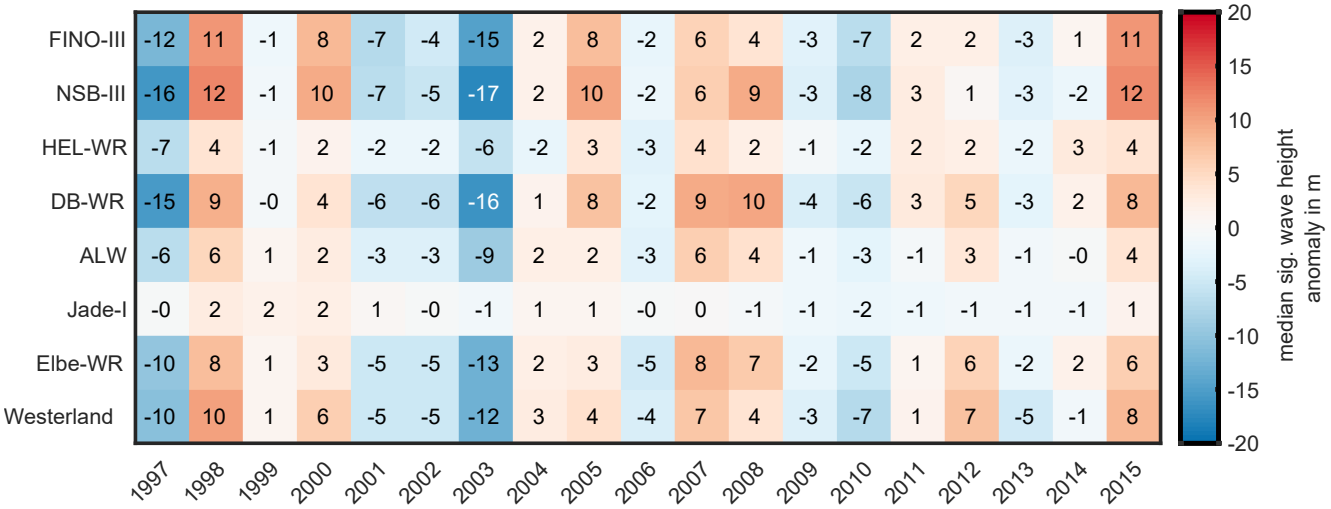

FIGURE D.1: Median modeled significant wave height anomaly at selected gauges in the German Bight in the period of 1996 to 2018.

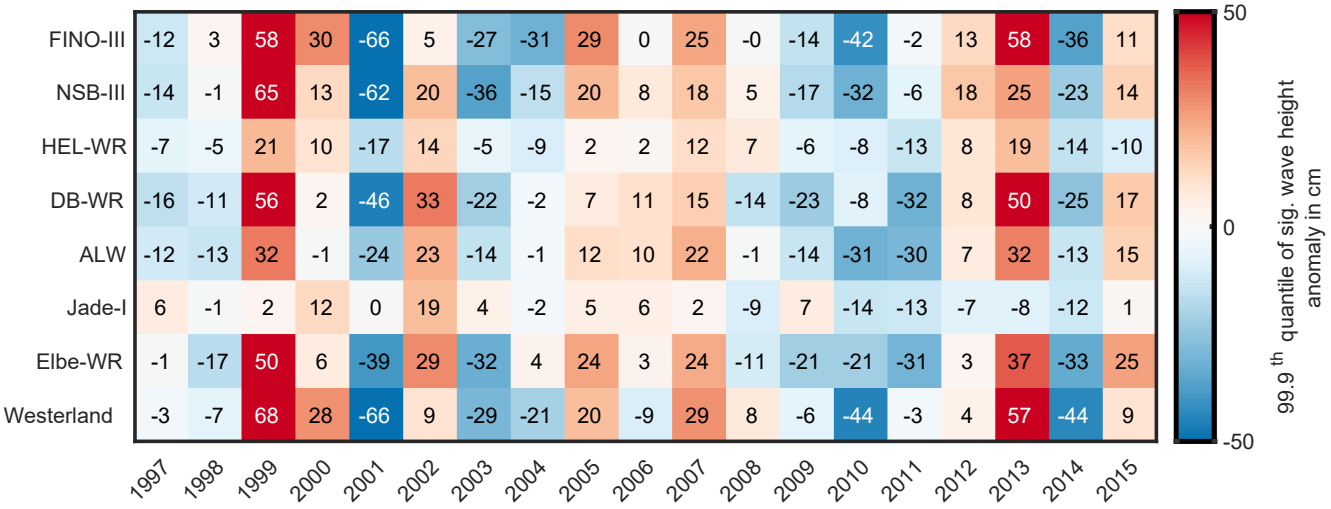

FIGURE D.2: 99.9^{th} quantile of modeled significant wave heights at selected gauges in the German Bight in the period of 1996 to 2018.

D.2 Flood and Ebb Slack Duration

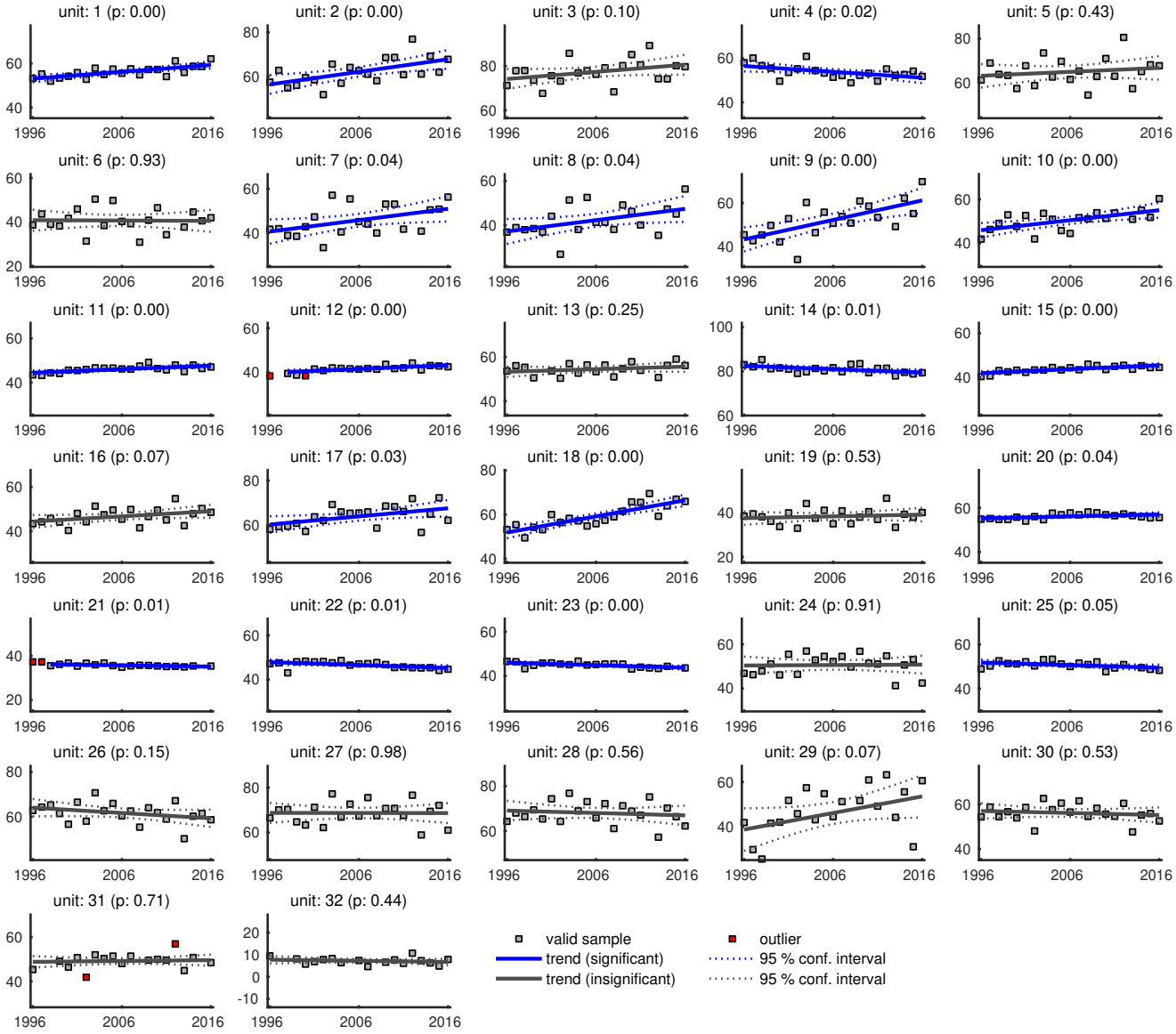

FIGURE D.3: Linear regression of the mean flood slack duration for morphological units from Figure 5.7. Blue lines indicate significant ($p < 0.05$) trends and their 95 % confidence intervals (dashed). Gray lines represent insignificant fitting with their 95 % confidence intervals (dashed). Valid samples are represented by gray squares and outliers by red squares. Outliers are not considered in trend estimation and significance testing.

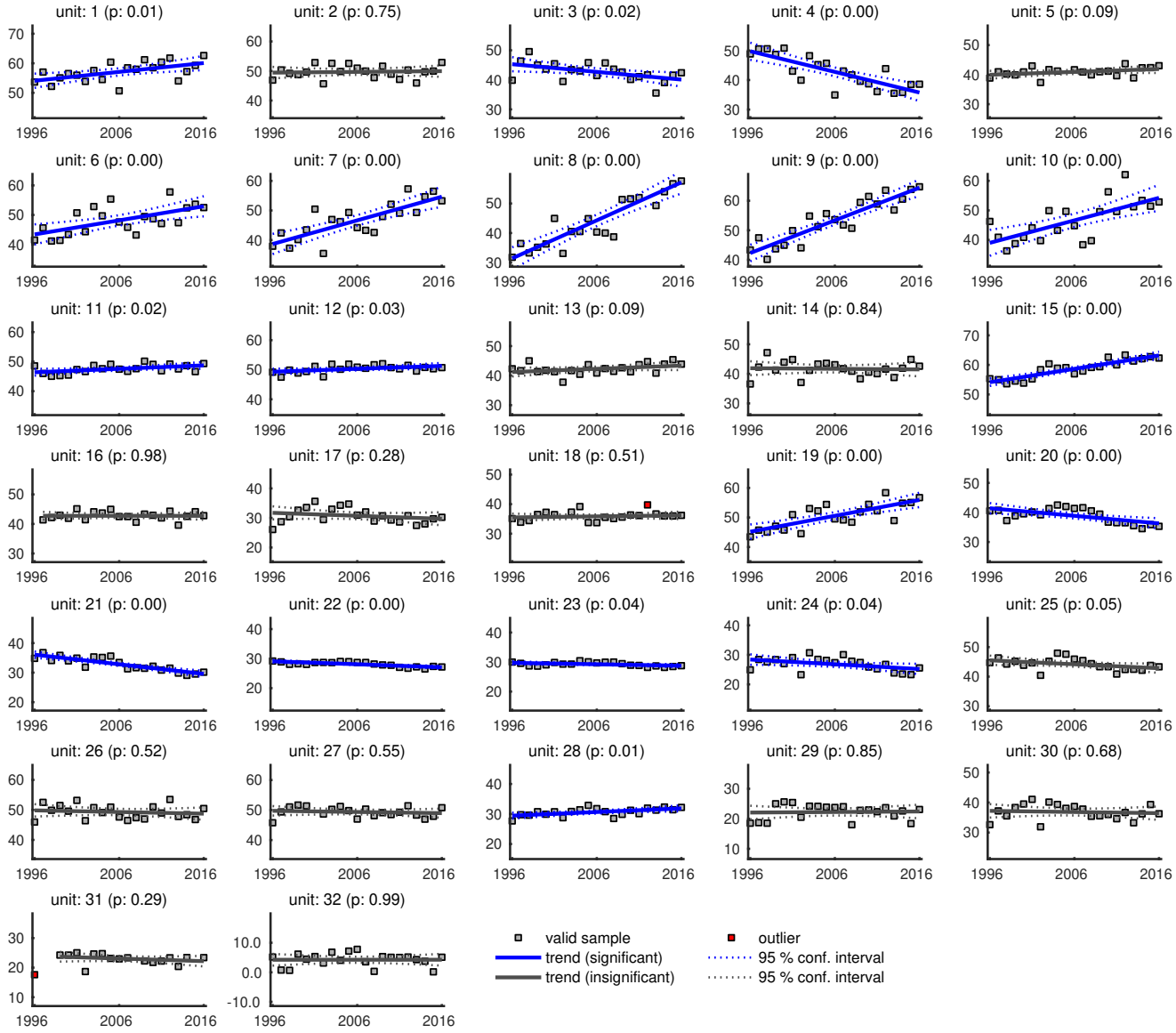

FIGURE D.4: Linear regression of the mean ebb slack duration for morphological units from Figure 5.7. Blue lines indicate significant ($p < 0.05$) trends and their 95 % confidence intervals (dashed). Gray lines represent insignificant fitting with their 95 % confidence intervals (dashed). Valid samples are represented by gray squares and outliers by red squares. Outliers are not considered in trend estimation and significance testing.

25

WASSERBAU
River and Coastal Engineering

DOI: 10.15480/882.8712

TUHH
Hamburg
University of
Technology